Distributed formation control for autonomous robots

Garcia de Marina Peinado, Hector Jesús

Distributed formation control for autonomous robots

Héctor Jesús García de Marina Peinado

university of groningen

The research described in this dissertation has been carried out at the Faculty of Mathematics and Natural Sciences, University of Groningen, the Netherlands.

disc

The research reported in this dissertation is part of the research program of the Dutch Institute of Systems and Control (DISC). The author has successfully completed the educational program of DISC.

This work was supported by the EU INTERREG program under the auspices of the SMARTBOT.

Cover by: www.lovebird-design.com

Printed by Eikon Plus
Krakow, Poland

ISBN (book): 978-90-367-8902-8
ISBN (e-book): 978-90-367-8901-1

2nd Edition

university of groningen

Distributed formation control for autonomous robots

PhD thesis

to obtain the degree of PhD at the
University of Groningen
on the authority of the
Rector Magnificus Prof. E. Sterken
and in accordance with
the decision by the College of Deans.

This thesis will be defended in public on

Friday 24 June 2016 at 9.00 hours

by

Héctor Jesús García de Marina Peinado

born on 18th February 1980
in Madrid, España

Supervisors
Prof. M. Cao
Prof. B. Jayawardhana
Prof. J.M.A. Scherpen

Assessment committee
Prof. B.D.O. Anderson
Prof. M.B. Egerstedt
Prof. A.J. van der Schaft

Acknowledgments

My special admiration to my advisors Ming Cao, Bayu Jayawardhana and Jacquelien Scherpen. I would also like to thank my assessment committee, professors Brian D.O. Anderson, Magnus B. Egerstedt and Arjan van der Schaft. I was really honored by having your time and feedback for enhancing this thesis.

I am really thankful to all the team forming the Discrete Technology & Production Automation department at RUG[1]. The results in this thesis would not have been possible without all the discussions (technical or not) held with you guys!

[1] Special thanks to Tobias Van Damme for translating the summary of this thesis to Dutch.

Contents

1 Introduction **1**
- 1.1 Distributed formation control in practice . . . 2
- 1.2 Manipulation of the formation . . . 4
- 1.3 Outline and main contributions of this thesis . . . 5
  - 1.3.1 List of publications . . . 7

2 Theoretical preliminaries **9**
- 2.1 Notation . . . 9
- 2.2 Graphs and frameworks . . . 10
- 2.3 Distance and bearing rigid formations . . . 10
  - 2.3.1 Realization of infinitesimally and minimally rigid formations 14
  - 2.3.2 Frames of coordinates . . . 15
- 2.4 Modelling the agents, first and second-order dynamics . . . 16
- 2.5 Gradient formation control . . . 17
- 2.6 Mismatches and robustness issues in gradient formation control . . 22
- 2.7 Illustrative experiments . . . 23

3 Estimation and compensation of measurement inconsistencies in formations **27**
- 3.1 Modeling measurement inconsistency and estimating agents . . . 28
- 3.2 Estimator-based gradient control I . . . 29
  - 3.2.1 Selecting the estimating agents . . . 33
  - 3.2.2 Stabilizing a large class of infinitesimally and minimally rigid formations in $\mathbb{R}^2$ . . . 34
  - 3.2.3 Stabilizing a special class of infinitesimally and minimally rigid formations in $\mathbb{R}^3$ . . . 36
  - 3.2.4 Experimental results . . . 37
- 3.3 Estimator-based gradient control II . . . 38

3.3.1 Controlling the shape-distortion . . . 43
3.3.2 Experimental results . . . 44
3.4 Concluding remarks . . . 44

4 Distributed rotational and translational motion control of formations 47
4.1 Mismatches as distributed motion parameters . . . 49
4.2 Stability analysis . . . 58
4.3 Translational motion with controlled heading . . . 61
4.3.1 Experimental results . . . 64
4.4 Tracking and enclosing a target . . . 66
4.4.1 Experimental results . . . 71
4.5 Concluding remarks . . . 73

5 Scaling-control of formations 75
5.1 Scaling-control by controlling one edge . . . 77
5.1.1 Distributed scaling-control without a common frame of coordinates . . . 80
5.1.2 Experimental results . . . 82
5.2 Distributed changing-motion-control of rigid formations . . . 85
5.2.1 Design of the controller for precise morphing and motion of the formation . . . 86
5.2.2 Stability analysis . . . 88
5.2.3 Periodic scaling and spinning of a rigid formation . . . 90
5.2.4 Avoiding obstacles by a precise change of the shape while keeping the formation heading . . . 91
5.3 Concluding remarks . . . 94

6 Formation motion-control of second-order agents 97
6.1 Gradient control in formations of second-order agents . . . 97
6.2 Robustness issues caused by mismatches . . . 101
6.3 Estimators-based gradient control . . . 104
6.4 Distributed formation-motion control . . . 108
6.5 Concluding remarks . . . 112

7 Formation control of a team of quadcopters 113
7.1 The quadcopter . . . 114
7.1.1 Frames of coordinates . . . 114
7.1.2 Physical model . . . 117
7.1.3 Motors and propellers models . . . 119
7.2 Controllers . . . 120
7.2.1 Attitude controller . . . 121
7.2.2 Altitude controller . . . 122

7.2.3 Velocity controller 123
7.2.4 Experimental results 125
7.3 Formation control results 126
7.3.1 Square formation with biased range sensors 128
7.3.2 Flying in formation with controlled heading 129
7.3.3 Tracking and enclosing a target 131
7.4 Concluding remarks 133

8 Conclusions **135**
8.1 Contributions 135
8.2 Further research 138

A Mobile robots setup **141**

B Flight simulator X-Plane and employed quadcopter **143**
B.1 X-Plane 143
B.2 Technical details of the quadcopter 144

Bibliography **145**

Summary **153**

Samenvatting **155**

Chapter 1
Introduction

My name's Guybrush Threepwood, and I want to be a PhirateD.
The secret of Monkey Island.

SWARM robotics consist of mostly simple robots with a desired collective behavior that emerges from the local interactions among individual robots and the environment. An exhaustive survey about swarm robotics can be found in [12, 14, 66], where it is shown how the *swarm engineering*[1] is an emergent discipline with numerous practical applications. The usage of robots in a coordinated fashion is a reality in many tasks such as the transportation of objects [83], area exploration & surveillance [86], vehicle platooning for energy efficiency [71] or tracking and enclosing a target [51]. All these tasks have practical applications in the society such as rescue missions in disaster areas or in the more controversial military field.

In other fields such as precision agriculture, deployment of communication networks or coverage of sport/art events, among others, a large set of problems shows up. For example, we have the early identification of diseases in cultivations, the temporary increase of the local capacity of a cellphone network or the real time acquisition of 3-D images and video. The usage of micro aerial vehicles offers potential solutions in these areas that can be enhanced by swarm engineering. Nowadays, the study of swarms of flying robots is not only limited to controlled laboratories which employ precise motion capture systems [49]. On the contrary, the development of low-cost high accuracy outdoor localization systems [29, 65] makes employment of aerial swarms in outdoors scenarios possible and in an affordable and safe way. Indeed, small autonomous robots facilitate cheaper designs and easy maintenance, opening their usage and experimentation to a broader range.

[1] Swarm engineering [14] is the systematic application of scientific and technical knowledge, to model and specify requirements, design, realize, verify, validate, operate and maintain a swarm intelligence system.

In order to accomplish many of the swarm missions we find in the *formation control* an important and useful tool. The purpose of this tool is to help to achieve the goal of keeping a desired shape of a multi agent[2] formation.

There are tasks that simply would not be accomplished by working with a single robot. On the other hand, a controlled formation can be employed in order to offer novel functionality. One class of examples is the enhanced sensing instrumentation, which includes the outstanding jointed ESA's and NASA's eLISA (evolved Laser Interferometer Space Antenna) mission forecasted for 2034 for the detection of gravitational waves [25]. In this mission, three spacecrafts are deployed in the space for flying along an Earth-like heliocentric orbit. These spacecrafts are arranged in an equilateral triangle with a side-length of five million kilometers but aiming at an accuracy close to the atomic level. Another example is the ESA's PROBA 3 (Project for On-Board Autonomy) mission for the investigation of the Sun [24] that is scheduled to 2018. Here the two spacecrafts will fly in formation separated by hundred meters with an accuracy of millimeters.

This thesis is mainly focused in the field of formation control for autonomous robots.

1.1 Distributed formation control in practice

Considerable research efforts have been made in the past few years in order to design distributed control laws that stabilize the shapes of formations of autonomous agents [32, 50, 52, 79]. In particular, within the research area of developing cooperative control theory for multi-agent systems, a sequence of theoretical investigations have been made to design formation control laws using the notion of graph rigidity [4, 19, 48, 85]. Such control laws are usually based on the gradients of the potential functions [78] closely related to the graphs describing the distance constraints between the neighboring agents. The latter is what characterizes a distributed strategy, that is to say the agents rely their autonomy and behaviour on only local information, mostly relative quantities with respect to their neighbors. The benefits of using such distributed systems is as follows:

- Scalability: The resources needed by a single autonomous agent do not grow with the increase of the total number of agents in the system.
- Fault tolerance: There is not a single/central unit of control/failure.
- Concurrency: The process of (local) information is performed in a parallel and independent fashion in order to achieve a global goal.

[2] Sometimes in this book we will employ the broader term *agent*. We mean by an agent something whose behaviour fits within a set of mathematical models. We will see that a robot is an example of agent.

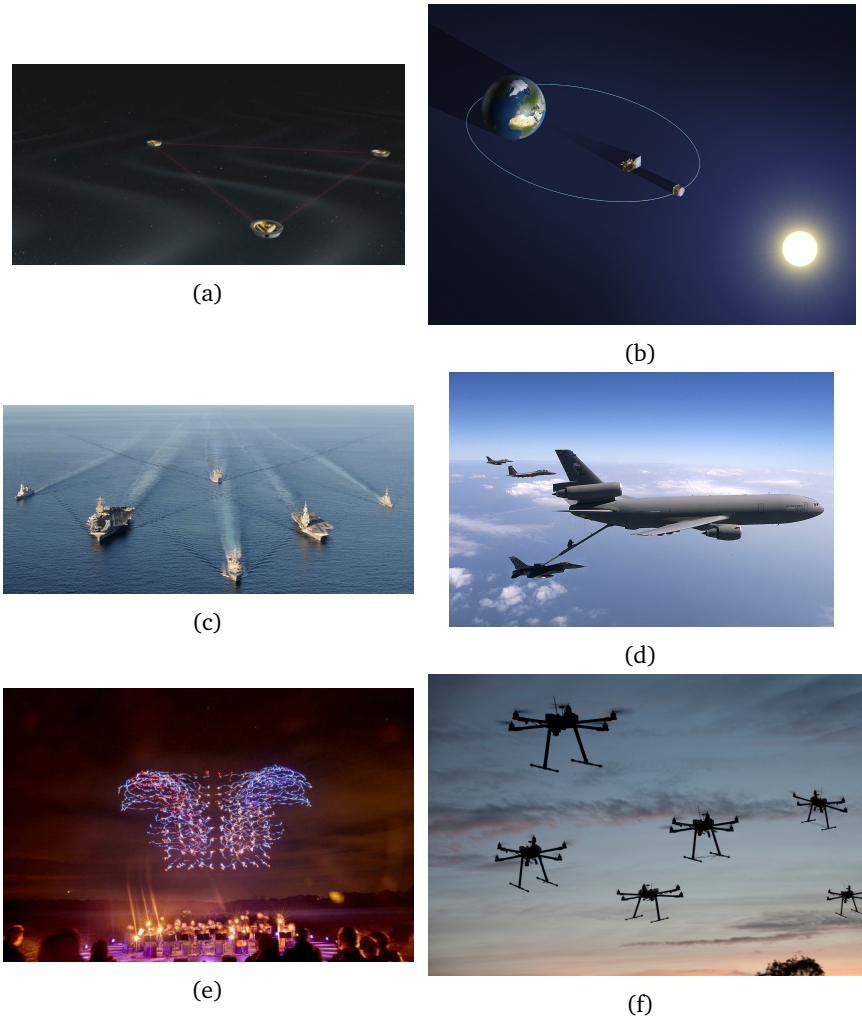

(a) (b) (c) (d) (e) (f)

Figure 1.1: a) ESA's and NASA's eLISA mission (planned for 2034) for detecting gravitational waves where the spacecrafts fly in a triangular formation with a side-length of five million kilometers; b) ESA's PROBA3 (planned for 2018) mission for studying the Sun, where the two spacecrafts fly in a coordinated formation in order to be in eclipse all the time; c) and d) typical coordinated motion of military vehicles; e) one hundred coordinated drones employed in INTEL's musical/visual performance at the end of 2015; f) team of quadcopters flying in formation. Photos courtesy of ESA, NASA, US. Army and Intel.

However, during the implementation and execution of the solutions available in the published literature about formation control to actual autonomous agents one has to face some practical and common problems that degrade the expected performance of the distributed system. When one uses gradient control laws, it has been recently reported in [10, 73] that if agents disagree with their neighboring peers on the measured (e.g., biased range sensors) or prescribed distances between them, two main undesired effects occur: an unknown distorted final shape and a steady-state group motion. While the former effect can be expected due to the change in the system equilibrium point caused by a constant disturbance, the latter seems somehow surprising. Such inconsistency induced motions take peculiar forms: in $\mathbb{R}^2$, the agents move collectively in a distorted but rigid formation following a closed orbit that is determined by a single sinusoidal signal; in $\mathbb{R}^3$, the orbit becomes helical that is determined by a single sinusoidal signal and a constant drift.

This undesired group motion is rather unexpected especially when knowing the robustness property as a consequence of the *exponential* convergence of gradient control; after all, exponential convergence of a dynamic system usually implies its robustness against small disturbances. With the hindsight gained from [10, 73], one realizes that the exponential convergence takes place for the error signals determined by the differences of the real and prescribed distances between neighboring agents, but this does not prevent the ill behavior of the position or velocity signals of the agents when measurement inconsistency exists. Such an observation is by no means trivial, but may affect the application of robotic formations because robustness issue is particularly relevant in practice, where distance disagreements may arise for several reasons. Firstly, robots may have different guidance systems, which may differ in their setting points; secondly, sensors equipped on robots may not return the same reading even if they are measuring the same distance due to heterogeneity in manufacturing processes; and thirdly, the same sensor can produce different readings for the same distance in face of random measurement noises.

These mentioned issues and their practical consequences motivate us to study how to address and solve them but without adding extra requirements, e.g., no extra sensing or communication, or without loosing the nice features from the original system, such as its distributed nature or exponential convergence properties.

1.2 Manipulation of the formation

Keeping and maintaining a formation is usually not the only task for the swarm of agents. It is a pretty common scenario to demand from a formation to maintain a prescribed shape and to travel without breaking it. Furthermore, the formation may interact with the surrounding environment by changing its desired trajectory

or by morphing its shape in the presence of an obstacle or by changing the covered area.

The formation and the group motion control problems are usually tackled separately, namely by using the gradient-based strategies for formation control and by leader-follower coordination for motion control, where for the latter the leader moves according to a desired trajectory and the followers simply track the leader [9]. But when the separately designed different controllers (formation, motion, scaling for avoiding obstacles, etc) are jointly in force as in the common scenario in practice, conflict often occurs: the shape of the formation is distorted when an agent compromises between the demands from formation and motion controls as to where and how it needs to move [6, 69]. Furthermore, in order to achieve a coordinated motion of the whole formation, global information is required such as a common frame of coordinates for the agents or the position of the centroid of the formation, or extra sensing such as neighboring agents measuring their relative velocities.

This issue is addressed in this thesis by studying how to accomplish, simultaneously and in a distributed fashion, the tasks of *scale-free* shape keeping, group motion and controlled scaling of the shape. We show that the proposed technique is potentially compatible with different agent's dynamics and that it allows us to make the study of more difficult problems easier, such as the interception, tracking and enclosing a free target with an unknown velocity. Moreover, the practical implementation of the presented algorithms in this thesis is computationally inexpensive, making the proposed algorithms attractive for autonomous robots with limited computational power.

1.3 Outline and main contributions of this thesis

In Chapter 2 we briefly introduce the notation used in this thesis and review the basics of gradient-based formation control together with the robustness issues caused by the presence of inconsistent measurements or mismatches in the prescribed distances of neighboring agents.

We start with the main results in Chapter 3 where we focus on dealing with the tricky robustness issue by the use of an estimator-based gradient control. We are able to show that under mild assumptions, the proposed control strategy stabilizes formations in the presence of measurement inconsistency eliminating all the reported undesirable steady-state collective motions and distortion in the formations' final shapes. It takes full advantage of the strength of the existing gradient control, especially the exponential convergence speed, and at the same time preserves the distributed nature of the local cooperative control laws. Furthermore, we show that we can deal with inconsistencies in the form of a combination of a constant

bias and a finite number of sinusoidal noise, which often arises from resonance vibrations from motors, or in marine robotic tasks when sea waves perturb sensing [18] [11]. The main results regarding this matter have been published in [34, 35].

We address the formation-motion control problem in Chapter 4 by introducing distributed parameter pairs in the gradient-based formation control law for steering the whole formation; in particular, for each prescribed distance constraint, we introduce a pair of motion parameters, mimicking the mismatches. By a systematic design of such motion parameters, we show that we can steer the entire formation in rotation and/or translation in a distributed manner. The proposed gradient-based formation-motion joint controller using the motion parameters has several advantages. First, one can achieve precisely the desired steady-state formation shape and the group motion simultaneously, including rotational motion, in a distributed fashion. To the best of our knowledge, no such result has been reported in the literature. For single-integrator agent dynamics, we relate analytically the magnitude of the motion parameters to the speed of the group motion. Second, our proposed approach enables us to align the formation with respect to a global coordinate frame by adding a simple control term to an arbitrary agent when guiding the group in motion. In comparison, in the literature such an alignment is usually obtained by assigning a leader who knows the global frame and letting the other agents (followers) estimate the leader's velocity employing a distributed estimator [9]. Obviously in our approach, such estimators are not needed at all. Third, one can easily use our method to address the target tracking and enclosing problem both in $\mathbb{R}^2$ and $\mathbb{R}^3$ where one assigns the formation shape to specify how the target is enclosed and tracked by the pursuers. In comparison to the solution of such problems in [43, 54] among other works, we do not confine our formation to follow the same circular trajectory nor require *all* enclosing agents to measure their relative positions with respect to the target. The main results regarding this matter have been published in [36].

The surprisingly simple structure of our proposed control law opens possibilities to solve other difficult problems, such as controlling the scaling of a formation as we show in Chapter 5. The proposed distributed controller even allows to control the change between two different shapes or to vary periodically the scale of a given *scale-free* shape, e.g., the family of regular squares. The results regarding this matter have been summarized in the papers [38, 39].

We will also address the formation coordination task for agents governed by second-order dynamics addressed in Chapter 6. We analyze the robustness issue by the inconsistent measurement or mismatches and show that exactly the same non-desired consequences take place as in the first-order case. We further extend the estimators for removing these issues and the group-motion controllers from the first-order case. Finally we show how to apply these findings in a practical case where the agents are quadcopters in Chapter 7. The results regarding this matter

have been summarized in the submitted paper [37, 40].

In Chapter 8, we reemphasize the common thread of this thesis and summarize our contributions. We also highlight some topics that may become interesting for a future research.

Finally, the experimental setups[3] employed in this thesis with actual mobile robots and a flight simulator are explained in Appendices A and B.

1.3.1 List of publications

Journal papers:

- H. Garcia de Marina, Ming Cao, and B. Jayawardhana. Controlling rigid formations of mobile agents under inconsistent measurements. Robotics, IEEE Transactions on, 31(1):31–39, Feb 2015.
- H. Garcia de Marina, B. Jayawardhana, and Ming Cao. Distributed rota- tional and translational maneuvering of rigid formations and their applications. Robotics, IEEE Transactions on, 32(3):684-696, Jun 2016.
- H. Garcia de Marina, B. Jayawardhana, and Ming Cao. Taming inter-distances mismatches for formation-motion control of rigid formations in second-order agents. 2016. Under review. Automatic Control, IEEE Transactions on.
- H. Garcia de Marina, B. Jayawardhana, and Ming Cao. Precise scaling with motion control for teams of robots in rigid formations. 2016. In preparation.

Conference papers:

- H. Garcia de Marina, M. Cao, and B Jayawardhana. Controlling formations of autonomous agents with distance disagreements. In Proc. of the 4th IFAC Workshop on Distributed Estimation and Control in Networked Systems, 2013.
- H. Garcia de Marina, B. Jayawardhana, and Ming Cao. On the Role and Compensation of Distance Mismatches in Rigid Formation Control for Second-Order Agents. In Proc. of the 10th IFAC Symposium on Nonlinear Control Systems, NOLCOS 2016.
- H. Garcia de Marina, B. Jayawardhana, and Ming Cao. Distributed scaling control of rigid formations. In Proc. of the 55th IEEE Conference on Decision and Control, 2016.

[3]The raw footage of the experiments reported in this thesis can be found in the playlist Robotics at `http://www.youtube.com/c/HectorGarciadeMarina`

Chapter 2
Theoretical preliminaries

A beginning is the time for taking the most delicate care that the balances are correct. Knowing where the trap is– that's the first step in evading it.

Bernard: I'm sure Dr. Fred wouldn't start this if it weren't safe!
Laverne: After all, he IS a doctor.
Bernard: Has anyone ever been hurt reading this thing?
Dr. Fred: Of course not! This is the first time I've ever tried it on people.
The day of the tentacle.

In this chapter, we first introduce the general notation that will be used throughout the thesis. Some basic knowledge of graph theory, in particular rigidity graph theory, is reviewed. Rigidity graph theory plays an important role in the design of a *desired shape* for the formation of the agents. In order to achieve such desired shape by the agents we will cover the popular gradient-based technique for formation-control in both of the two popular variants: *position-based* and *distance-based*. In the position-based strategy the agents control the relative positions (vector quantities) between them, whereas in distance-based strategy the agents just control the distances (scalar quantities) between them. We will see how in the distance-based approach the *exponential* stability does not provide protection for the formation against some classes of disturbances and biases in the range sensors of the agents. We will show how these biases are mathematically equivalent to assume perfect measurements by neighboring agents but having different understanding about the distance that they want to maintain between each other, i.e., there is a mismatch in the desired distance. As a practical illustration, we finish this chapter by showing some lab experiments covering realistic situations with mobile robots in order to validate the theoretical findings.

2.1 Notation

Let us introduce some notation employed throughout the thesis. For a given matrix $A \in \mathbb{R}^{n\times p}$, define $\overline{A} \triangleq A \otimes I_m \in \mathbb{R}^{nm\times pm}$, where the symbol $\otimes$ denotes the Kronecker product, $m = 2$ for $\mathbb{R}^2$ or otherwise $m = 3$ for $\mathbb{R}^3$, and I_m is the

m-dimensional identity matrix. We denote by $|\mathcal{X}|$ the cardinality of the set $\mathcal{X}$, by $||x||$ the Euclidean norm of a vector x and by $\hat{x} \triangleq \frac{x}{||x||}$ the unit vector of x. We denote by $\mathrm{col}(\cdot)$ the column vector by collecting all its arguments as the vector's components. For a stacked vector/matrix $x \triangleq \begin{bmatrix} x_1^T & x_2^T & \dots & x_k^T \end{bmatrix}^T$ with $x_i \in \mathbb{R}^{n\times l}, i \in \{1,\dots,k\}$, we define the block diagonal matrix $D_x \triangleq \mathrm{diag}\{x_i\}_{i\in\{1,\dots,k\}} \in \mathbb{R}^{kn\times kl}$. We define the orthogonal projector operator as $P_{\hat{x}}^{\perp} \triangleq \left(I_m - \hat{x}_k \hat{x}_k^T\right)$. Finally we use $\mathbf{1}_{n\times m}$ and $\mathbf{0}_{n\times m}$ to denote the all-one and all-zero vector/matrix in $\mathbb{R}^{n\times m}$ respectively and we will drop the subscripts if the dimensions are clear from the context.

2.2 Graphs and frameworks

We consider a formation of $n \geqslant 2$ autonomous agents whose positions are denoted by $p_i \in \mathbb{R}^m$ with $i \in \{1,\dots,n\}$. The agents are able to sense the relative positions of its neighboring agents. The neighbor relationships are described by an undirected graph $\mathbb{G} = (\mathcal{V}, \mathcal{E})$ with the vertex set $\mathcal{V} = \{1,\dots,n\}$ and the ordered edge set $\mathcal{E} \subseteq \mathcal{V}\times\mathcal{V}$. The set $\mathcal{N}_i$ of the neighbors of agent i is defined by $\mathcal{N}_i \triangleq \{j \in \mathcal{V} : (i,j) \in \mathcal{E}\}$. We define the elements of the incidence matrix $B \in \mathbb{R}^{|\mathcal{V}|\times|\mathcal{E}|}$ for $\mathbb{G}$ by

$$b_{ik} \triangleq \begin{cases} +1 & \text{if} \quad i = \mathcal{E}_k^{\text{tail}} \\ -1 & \text{if} \quad i = \mathcal{E}_k^{\text{head}} \\ 0 & \text{otherwise} \end{cases}, \tag{2.1}$$

where $\mathcal{E}_k^{\text{tail}}$ and $\mathcal{E}_k^{\text{head}}$ denote the tail and head nodes, respectively, of the edge $\mathcal{E}_k$, i.e., $\mathcal{E}_k = (\mathcal{E}_k^{\text{tail}}, \mathcal{E}_k^{\text{head}})$. For undirected graphs in this thesis, as we will see, how one sets the direction of the edges is not relevant for the stability results.

A *framework* is defined by the pair $(\mathbb{G}, p)$, where p is the stacked vector of the agents' positions p_i with $i \in \{1,\dots,n\}$. The stacked vector of the sensed relative positions by the agents can then be described by

$$z = \overline{B}^T p. \tag{2.2}$$

Note that each vector $z_k = p_i - p_j$ in z corresponds to the relative position associated with the edge $\mathcal{E}_k = (i,j)$.

2.3 Distance and bearing rigid formations

A *distance rigid formation* or simply a *rigid formation* of autonomous agents is simply a formation whose corresponding framework $(\mathbb{G}, p)$ is *distance rigid* or simply *rigid*.

But to define rigid frameworks, we need some other basic concepts and definitions.

Definition 2.1. The *edge function* $f_{\mathbb{G}} : \mathbb{R}^{mn} \to \mathbb{R}^{|\mathcal{E}|}$ is defined by

$$f_{\mathbb{G}}(p) \triangleq \underset{\forall k \in \{1,\ldots,|\mathcal{E}|\}}{\text{col}}(||z_k||^2) = D_z^T z = D_{\overline{B}^T p}^T \overline{B}^T p.$$

Definition 2.2. [8] A framework $(\mathbb{G}, p)$ is *locally rigid* if for every $p \in \mathbb{R}^{mn}$, there exists a neighborhood $\mathcal{P}$ of p such that $f_{\mathbb{G}}^{-1}(f_{\mathbb{G}}(p)) \cap \mathcal{P} = f_{\mathbb{K}}^{-1}(f_{\mathbb{K}}(p)) \cap \mathcal{P}$, where $\mathbb{K}$ is the complete graph with the same vertex set $\mathcal{V}$ of $\mathbb{G}$.

Definition 2.3. [8] A framework $(\mathbb{G}, p)$ is *globally rigid* if $f_{\mathbb{G}}^{-1}(f_{\mathbb{G}}(p)) = f_{\mathbb{K}}^{-1}(f_{\mathbb{K}}(p))$ for all $p \in \mathbb{R}^{mn}$.

Roughly speaking a framework $(\mathbb{G}, p)$ is rigid if it is not possible to smoothly move one node of the framework without moving the rest while maintaining the inter-agent distances given by $f_{\mathbb{G}}(p)$. We are interested in a particular class of rigid formations that are *infinitesimally rigid*. Take the approximation of $f_{\mathbb{G}}(p)$ given by

$$f_{\mathbb{G}}(p + \delta p) = f_{\mathbb{G}}(p) + df_{\mathbb{G}}(p)\delta p + O(\delta p^2),$$

where δp is an infinitesimal displacement of p and compute the Jacobian matrix

$$df_{\mathbb{G}}(p) = \frac{\partial f_{\mathbb{G}}(p)}{\partial p} = 2D_z^T \overline{B}^T = 2R(z),$$

where $R(z) \in \mathbb{R}^{|\mathcal{E}| \times m|\mathcal{V}|}$ is the *rigidity matrix* [4] of the framework $(\mathbb{G}, p)$. The nontrivial kernel of $R(z)$ includes the translation and rotation of the whole framework in the Cartesian space. An infinitesimally rigid framework $(\mathbb{G}, p)$ is a rigid framework that is invariant under and only under such infinitesimal transformations using $R(z)$, i.e., $f_{\mathbb{G}}(p + \delta p) = f_{\mathbb{G}}(p)$ for all p. Equivalently and more precisely,

Definition 2.4. [8] We say that p is a *regular point of* $f_{\mathbb{G}}$ if $\operatorname{rank} R(\overline{B}^T p) = \max\left\{ \operatorname{rank} R(\overline{B}^T q) : q \in \mathbb{R}^{m|\mathcal{V}|} \right\}$.

Definition 2.5. [8] A framework $(\mathbb{G}, p)$ is *infinitesimally rigid* in $\mathbb{R}^2$ (resp. $\mathbb{R}^3$) if $\operatorname{rank} R(z) = 2n - 3$ (resp. $3n - 6$).

Theorem 2.6. *[8] A framework $(\mathbb{G}, p)$ is infinitesimally rigid in $\mathbb{R}^m$ if and only if p is a regular point of $f_{\mathbb{G}}$ and $(\mathbb{G}, p)$ is rigid in $\mathbb{R}^m$.*

Note that with Theorem 2.6 some nongeneric sets such as the set of all collinear agents in 2D or all coplanar agents in 3D are not infinitesimally rigid.

Definition 2.7. [8] A framework $(\mathbb{G}, p)$ is *minimally rigid* if it has exactly $2n - 3$ (resp. $3n - 6$) edges in $\mathbb{R}^2$ (resp. $\mathbb{R}^3$).

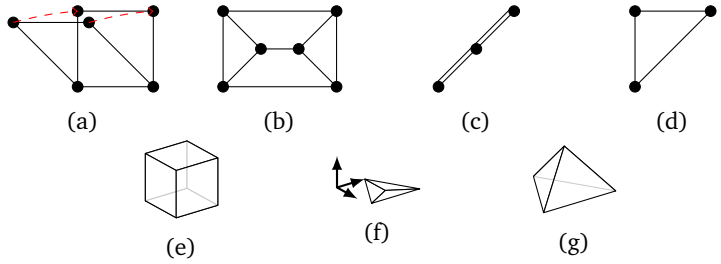

Figure 2.1: a) The square without an inner diagonal is not rigid since we can smoothly move the top two nodes keeping the other two fixed without breaking the distance constraints; b) A rigid but not infinitesimally rigid framework. If we rotate the left inner triangle, then the right inner triangle can be counter-rotated in order to keep $f_{\mathbb{G}}(p)$ constant; c) A rigid but not infinitesimally rigid framework. Although the graph is complete, the nodes' positions are collinear leading to $\operatorname{rank} R(z) = 1 < 3$; d) The triangle is infinitesimally and minimally rigid. The only possible transformations in order to keep $f_{\mathbb{G}}(p)$ constant are the translation or rotation of the whole framework; e) The cube formed by squares without diagonals is not rigid; f) The zero-volume tetrahedron is rigid but not infinitesimally rigid in $\mathbb{R}^3$, since all the nodes are co-planar; and g) The tetrahedron in $\mathbb{R}^3$ is infinitesimally and minimally rigid.

The last definition is due to the fact that if we remove one edge from a minimally rigid framework, then the framework is not rigid anymore. One special property of $R(z)$ in infinitesimally and minimally rigid frameworks is that it is full row rank [8]. We illustrate in Figure 2.1 some examples in $\mathbb{R}^2$ and $\mathbb{R}^3$ of rigid and non-rigid frameworks.

We see clearly that the concept of *infinitesimal rigidity* is associated to the definition of a particular shape by only setting some inter-distances between the nodes of the framework, therefore by controlling only these inter-distances we can achieve, at least locally, the specific desired shape. It is locally since the same set of inter-distances for an infinitesimally rigid formation can define more than one (but finite number) shape at once, e.g., a mirrored one.

Let the following stacked vector of relative positions $z^* = \left[{z_1^*}^T \; {z_2^*}^T \; \dots \; {z_{|\mathcal{E}|}^*}^T \right]^T$ define a desired infinitesimally and minimally rigid shape with $||z_k^*|| = d_k$ for all $k \in \{1, \dots, |\mathcal{E}|\}$ where d_k is the desired inter-distance. The resulting set $\mathcal{Z}$ of the possible formations with the same shape is defined by

$$\mathcal{Z} \triangleq \left\{ \left(I_{|\mathcal{E}|} \otimes \mathcal{R} \right) z^* \right\}, \tag{2.3}$$

where $\mathcal{R}$ is the set of all rotational matrices in 2D or 3D. Roughly speaking, $\mathcal{Z}$ consists of all formation positions that are obtained by rotating z^*. Note that if we

define the set

$$\mathcal{D} \triangleq \Big\{ z \,:\, ||z_k|| = d_k, k \in \{1, \ldots, |\mathcal{E}|\} \Big\},$$

in general it holds that $\mathcal{Z} \subseteq \mathcal{D}$. This is usually one of the reasons why distance-based gradient control can only achieve $\mathcal{Z}$ locally, since the potential function where the gradient is taken from has a local minimum at all the shapes defined by $\mathcal{D}$.

Consider a scale-free shape *based on* an infinitesimally and minimally rigid shape, for example the collection of all regular squares with an internal diagonal. This collection can be distinguished from other (infinitesimally and minimally rigid) scale-free shapes by checking its inner angles or equivalently by looking at all the scalar products $\hat{z}_l^T \hat{z}_n$ where l and n are two edges sharing a node; this fact has been explained in more detail in [87]. Bearing-based rigid frameworks are related to the distance-based ones where the bearing-based shape can be defined by the inner angles, instead of the distances. Let us review some fundamental concepts in bearing rigidity.

Definition 2.8. [88] Frameworks $(\mathcal{G}, p)$ and $(\mathcal{G}, p')$ are *bearing equivalent* if $P_{z_k}^{\perp} z_k' = 0$ for all $k \in \{1, \ldots, |\mathcal{E}|\}$.

Definition 2.9. [88] Frameworks $(\mathcal{G}, p)$ and $(\mathcal{G}, p')$ are *bearing congruent* if $P_{(p_i - p_j)}^{\perp}(p_i' - p_j') = 0$ for all $i, j \in \mathcal{V}$.

Definition 2.10. [88] The *bearing function* is defined by $f_{B_{\mathbb{G}}}(p) \triangleq \hat{z} \in \mathbb{R}^{m|\mathcal{E}|}$, where[1] $\hat{z}$ is the stacked vector of $\hat{z}_k$ for all $k \in \{1, \ldots, |\mathcal{E}|\}$.

Analogous to the rigidity matrix we can define the *bearing rigidity matrix* by computing the Jacobian matrix of the bearing function

$$R_B(z) = \frac{\partial f_{B_{\mathbb{G}}}(p)}{\partial p} = \overline{D}_{\tilde{z}}^T D_{P_{\hat{z}}^{\perp}}^T \overline{B}^T,$$

where $P_{\hat{z}}^{\perp} \in \mathbb{R}^{m|\mathcal{E}| \times m}$ is the stacked matrix of operators $P_{\hat{z}_k}^{\perp}$ and $\tilde{z} \in \mathbb{R}^{|\mathcal{E}|}$ is the stacked vector of $\frac{1}{||z_k||}$ for all $k \in \{1, \ldots, |\mathcal{E}|\}$. The non-trivial kernel of $R_B(z)$ includes the scalings and translations of the framework [88], leading to the following definition.

Definition 2.11. [88] A framework is *infinitesimally bearing rigid* if the kernel of its bearing rigidity matrix only corresponds to scalings and translations.

In order words if a scale-free shape can be determined uniquely by its inner angles, then it belongs to the *infinitesimally bearing rigid* framework. It is important

[1] In order not to overload the notation, here by $\hat{z}$ we exclusvely mean the vector-element wise normalization of z.

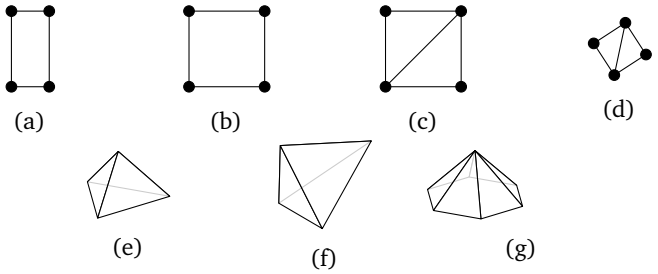

Figure 2.2: The square and the rectangle without an inner diagonal in (a) and (b) are bearing equivalent but not bearing congruent. The square (c) has been rotated and scaled in (d) and both are infinitesimally and minimally congruent. The tetrahedron in (e) is infinitesimally and minimally rigid in $\mathbb{R}^3$ and it is infinitesimally and minimally congruent with its scaled and rotated version in (f). In $\mathbb{R}^2$ all the infinitesimmaly minimally rigid shapes are also infinitesimally bearing rigid, however in $\mathbb{R}^3$ this is not true, for example, the pyramid in with a hexagonal base in (g).

to highlight the following relevant result in $\mathbb{R}^2$ (unfortunately for higher dimensions it is not true) connecting both distance and bearing rigidity theories.

Lemma 2.12. *[88] In $\mathbb{R}^2$ a framework is infinitesimally bearing rigid if and only if it is infinitesimally rigid.*

Consider a given a shape defined by $\mathcal{Z}$, we define the scale-free $\mathcal{Z}_\mathcal{S}$ by taking $\mathcal{Z}$ rescaled by all the possible scale factors $s \in \mathbb{R}^+$ such that $||z_k|| = sd_k$ for all $k \in \{1, \dots, |\mathcal{E}|\}$. This leads to the following definition

Definition 2.13. The shapes defined by $\mathcal{Z}$ within the set $\mathcal{Z}_\mathcal{S}$ are *infinitesimally and minimally congruent* rigid.

The name comes from the fact that all the scales of an infinitesimally and minimally rigid shape are bearing congruent. Note that obviously $\mathcal{Z}_\mathcal{S} \subseteq \mathcal{D}_\mathcal{S}$, where $\mathcal{D}_\mathcal{S}$ is defined in the same way as $\mathcal{D}$ but with $||z_k|| = sd_k$ for all $k \in \{1, \dots, |\mathcal{E}|\}$. We define $\mathcal{Z}_s$ as $\mathcal{Z}$ for a fixed s. We provide examples of the introduced concepts about bearing rigidity in Figure 2.2.

2.3.1 Realization of infinitesimally and minimally rigid formations

For a desired shape, one can always design $\mathbb{G}$ to make the formation infinitesimally and minimally rigid. In fact in $\mathbb{R}^2$, an infinitesimally and minimally rigid framework with two or more vertices can always be constructed through the Henneberg

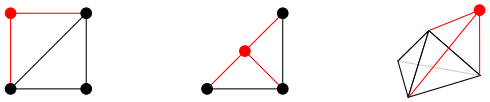

(a) (b) (c)

Figure 2.3: In (a) and (b) we illustrate the two operations for the Henneberg insertion in $\mathbb{R}^2$ taking as a starting point a triangular framework with three nodes. These two operations can construct any infinitesimally and minimally rigid framework in $\mathbb{R}^2$. Although there is not (yet) a collection of operations for constructing any infinitesimally and minimally rigid framework in $\mathbb{R}^3$, we illustrate in (c) how to construct a set of them by taking as a starting point a tetrahedron with four nodes.

construction [45], starting from a single edge, by a sequence of the following operations:

1. Add a new vertex to the graph, together with edges connecting it to two previously existing vertices.

2. Subdivide an edge of the graph, and add an edge connecting the newly formed vertex to a third previously existing vertex.

Unfortunately there is no known corresponding systematic operations in $\mathbb{R}^3$ yet. Nevertheless in $\mathbb{R}^3$ one can always obtain an infinitesimally and minimally rigid framework by following analogous steps as in the $\mathbb{R}^2$ case. For example, starting from a tetrahedron, add a new vertex and form another tetrahedron with three other vertices that forms a triangle in the existing framework. These algorithms in $\mathbb{R}^2$ and $\mathbb{R}^3$ are graphically illustrated in Figure 2.3.

2.3.2 Frames of coordinates

In order to describe and design motions for a desired formation defined by $\mathcal{Z}$ it will be useful to attach a frame of coordinates to the centroid of the shape. We denote by O_g the *global frame* of coordinates fixed at the origin of $\mathbb{R}^m$ with some arbitrary fixed orientation. In a similar way, we denote by O_b the *body frame* fixed at the centroid p_c of the desired scale-free rigid formation. Furthermore, if we rotate the scale-free rigid formation with respect to O_g, then O_b is also rotated in the same manner. Note that p_c is invariant with respect to $\mathcal{Z}_{\mathcal{S}}$. Let ${}^b p_i$ denote the position of agent i with respect to O_b. In order to simplify notation whenever we represent an agent's variable with respect to O_g, the superscript is omitted, e.g., $p_i \triangleq {}^g p_i$.

2.4 Modelling the agents, first and second-order dynamics

The dynamical model of the agents plays a fundamental role in the formation control problem. In this thesis we will mainly use two kinds of dynamical models for the agents: the first-order and the second-order dynamics. In addition to defining the behaviour of the agents themselves, how we model the dynamics of the agents has further consequences on the behaviour of the formation such as its stability, rate of convergence and transient behaviors.

A simple approach is to consider just to actuate over the velocities of the agents or, equivalently, to model them employing the first-order dynamics

$$\dot{p} = u, \tag{2.4}$$

where u is the stacked vector of control inputs $u_i \in \mathbb{R}^m$ for $i = \{1, \dots, n\}$. This model might represent the commanded velocity to a more complex system, e.g., quadrotors or ocean vehicles. Indeed one can employ the signal generated by (2.4) as the desired 3D-velocity for the proposed tracking controllers of the quadrotor in [13, 41, 46, 56] or vessels in [30], which have been widely employed in experimental setups in formation and motion control [28, 31, 55].

A more realistic dynamical model for actual vehicles is the so-called second-order dynamics given by

$$\begin{cases} \dot{p} = v \\ \dot{v} = u \end{cases}, \tag{2.5}$$

where v is the stacked vector of agents' velocities $v_i \in \mathbb{R}^m$ for $i = \{1, \dots, n\}$. It is more realistic in the sense that the control input in (2.5) is actuating over the accelerations of the system, i.e., we consider Newtonian dynamics where the actuators of the system produce a desired force or torque. In practice this means that we can by-pass the generated velocity reference in (2.4) and command directly the corresponding motors with the control signal in (2.5). However the analysis, design and other aspects, such as guaranteeing the stability of the system, become more complex for second-order in comparison to first-order dynamics. It is up to the designer to consider and analyze first the characteristics of the actual agents in order to choose the better approach. In this thesis we first derive the main results considering the first-order dynamics and in Chapter 6 we will extend them to the second-order case.

2.5 Gradient formation control

Consider a formation of n agents governed by the first-order dynamics (2.4) and associated with the neighbor relationship graph $\mathbb{G}$. For each edge $\mathcal{E}_k$ one can construct a potential function V_k with its minimum at the desired distance $||z_k^*||$ so that the gradient of such functions can be used to control inter-agent distances distributively. Then the function V_k should satisfy the following conditions

$$V_k : \mathbb{R}^m \to \mathbb{R}_{\geqslant 0} \tag{2.6}$$

$$V_k(z_k) = 0 \iff ||z_k|| = d_k \tag{2.7}$$

$$\nabla_{z_k} V_k(z_k) = 0 \iff ||z_k|| = d_k, \tag{2.8}$$

where we define $\nabla_x \triangleq [\frac{\partial}{\partial x_1}, \ldots, \frac{\partial}{\partial x_m}]^T$ for the calculation of the vector gradient along $x \in \mathbb{R}^m$. We take as a potential function

$$V\left(\overline{B}^T p\right) = V(z) = \sum_{k=1}^{|\mathcal{E}|} V_k(z_k),$$

and apply to each agent i in (2.4) the following gradient descent control

$$u_i = -\nabla_{p_i} \sum_{k=1}^{|\mathcal{E}|} V_k(z_k). \tag{2.9}$$

One can then show straightforwardly that the multi-agent formation will converge locally to the desired shape employing the following known results.

Theorem 2.14. *[1, 60] If $V(z)$ satisfies (2.6), (2.7) and (2.8) and is real analytic, i.e., it possesses derivatives of all orders and agrees with its Taylor series in the neighborhood of every point, then the system (2.4) under the distributed (2.9) will converge locally asymptotically to the desired shape $\mathcal{Z}$.*

The authors of [1, 60] have shown that for a real analytic potential function V, system (2.4) with the control law (2.9) is locally asymptotically stable about the point corresponding to the local minima of $V(z)$. In order to achieve $\mathcal{D}$ we can employ the following family of quadratic[2] potential functions

$$V_k(z_k) = \frac{1}{2l}(||z_k||^l - d_k^l)^2, \quad l \in \mathbb{N}, \tag{2.10}$$

[2]Any analytic potential functions, including the ones for collision avoidance [80], can be approximated by a quadratic function in a small neighborhood about their local minima, and for this reason such quadratic potentials are of special interest of study.

with the following gradient along z_k

$$\begin{aligned}\nabla_{z_k} V_k(z_k) &= (\nabla_{z_k}||z_k||)\left(\frac{\partial V_k(z_k)}{\partial||z_k||}\right)\\ &= z_k||z_k||^{l-2}(||z_k||^l - d_k^l).\end{aligned} \tag{2.11}$$

One immediate observation is that when $l = 1$ we have that (2.10) is the classical *elastic potential function* and the right-hand side of (2.11) becomes the unit vector $\hat{z}_k$ multiplied by the distance error $(||z_k|| - d_k)$.

Let $\mathcal{Z}_R$ be the set $\mathcal{Z}$ where $\mathcal{R}$ in (2.3) has been substituted by a desired rotational matrix R with respect to O_g. Then define the set $\hat{\mathcal{Z}}_R$ as the collection of unit vectors $\hat{z}_k$ for all $k \in \{1, \ldots, |\mathcal{E}|\}$ taken from $\mathcal{Z}_R$. Note that $\hat{\mathcal{Z}}_R$ and $\mathcal{Z}_S$ are intimately related to the same scale-free shape. For achieving $\hat{\mathcal{Z}}_R$ we can employ the following potential function

$$V(z) = \sum_{k=1}^{|\mathcal{E}|} V_k(z_k) = \frac{1}{2}\sum_{i=1}^{|\mathcal{E}|} ||\hat{z}_k - \hat{z}_k^*||^2, \tag{2.12}$$

where the desired unit vector $\hat{z}_k^*$ encodes the desired orientation with respect to O_g and the collection $\hat{z}_k^*$ for all $k \in \{1, \ldots, |\mathcal{E}|\}$ defines a family of infinitesimally and minimally congruent rigid shapes and therefore it is infinitesimally bearing rigid. Finally for controlling orientation, position and scale, i.e., the prescribed shape given by $\mathcal{Z}_R$, we use the standard potential function

$$V(z) = \sum_{k=1}^{|\mathcal{E}|} V_k(z_k) = \frac{1}{2}\sum_{i=1}^{|\mathcal{E}|} ||z_k - z_k^*||^2. \tag{2.13}$$

For obvious reasons, in the literature about formation control, the usage of (2.10) is regarded as a distance-based control strategy, while those of (2.12) and (2.13) are considered as position-based control strategy where the potential function (2.12) involves vectorial orientation which is a piece of position-based information. Distance-based control has the advantage over position-based since all robots can work in their own local coordinate system, with the main drawback of losing the control on the final orientation of the formation. In addition, the position-based control usually requires fewer number of edges than in the distance-based one, see [9, 88] for more details.

Remark 2.15. If a *desired shape* given by a collection of z_k^*'s is not geometrically feasible, then there is not exist a p^* such that $\bar{B}^T p^* = z^*$. Hence the minimum of $V(z)$ in practice will be impossible to reach. For example, a formation consisting of three agents in $\mathbb{R}^2$ where the desired d_1, d_2 and d_3 do not satisfy the triangular inequality or the desired $z_1^* + z_2^* + z_3^* \neq 0$. A study about *impossible desired shapes*

in distance-based control is given in [75].

For the mentioned potentials (2.10)-(2.13) it is straightforward to check that for every edge $\mathcal{E}_k = (i,j)$ one has $\nabla_{p_i} V_k = -\nabla_{p_j} V_k = \nabla_{z_k} V_k$, and obviously $\nabla_{p_h} V_k = \mathbf{0}_{m\times 1}$ for all $h \neq i,j$. Thus the agent dynamics (2.4) under (2.9) can be written in the following compact form

$$\dot{p} = -\overline{B}\nabla_z V(z). \tag{2.14}$$

In this thesis we will mainly focus on the distance-based strategy. Denoting the distance error for edge k by

$$e_k = ||z_k||^l - d_k^l, \tag{2.15}$$

it follows that

$$\nabla_{z_k} V_k(||z_k||) = z_k ||z_k||^{l-2} e_k.$$

By substituting it into (2.14) and noting that

$$\dot{e}_k = l\,||z_k||^{l-1} \frac{d}{dt}||z_k|| = l\,||z_k||^{l-2} z_k^T \dot{z}_k,$$

we can write down the closed-loop system dynamics in the compact form

$$\dot{p} = -\overline{B} D_z D_{\tilde{z}} e = -R(z)^T D_{\tilde{z}} e \tag{2.16}$$

$$\dot{z} = \overline{B}^T \dot{p} = -\overline{B}^T R(z)^T D_{\tilde{z}} e \tag{2.17}$$

$$\dot{e} = l D_{\tilde{z}} D_z^T \dot{z} = -l D_{\tilde{z}} R(z) R(z)^T D_{\tilde{z}} e, \tag{2.18}$$

where $e, \tilde{z} \in \mathbb{R}^{|\mathcal{E}|}$ are the stacked vectors of e_k's and $||z_k||^{l-2}$'s respectively for all $k \in \{1,\dots,|\mathcal{E}|\}$. In the following proposition, we establish the local exponential convergence of the error (2.15) to zero for arbitrary $l \in \mathbb{N}$. This fact is a straightforward extension of the result in [59] for the case when $l = 2$, and we provide the proof below for completeness.

Proposition 2.16. *Consider the closed-loop system (2.16)-(2.18) with graph $\mathbb{G}$ driven by the gradient of the potential function $V = \sum_k V_k$ where V_k is defined in (2.10) for a fixed $l \in \mathbb{N}$. If the formation in the desired shape $\mathcal{D}$ is infinitesimally and minimally rigid, then the error signal e goes to zero locally exponentially fast.*

Proof. First we prove that the error system (2.18) is autonomous. The elements of $R(z)R(z)^T = D_z^T \overline{B}^T \overline{B} D_z$ are products of the form $z_i^T z_j$, $i,j \in \{1,\dots,|\mathcal{E}|\}$. It has been shown in [44] that for any infinitesimally and minimally rigid framework, there exists a neighborhood $\mathcal{U}_z$ about this framework such that any $z_i^T z_j$, $z_i, z_j \in \mathcal{U}_z$, can be written as a smooth function $g_{ij}\left(\mathrm{col}(||z_k||^2)\right)$, and since $||z_k|| = (e_k + d_k^l)^{\frac{1}{l}}$,

we can write

$$z_i^T z_j = g_{ij}(e). \tag{2.19}$$

Thus the vector $\tilde{z}$ and the matrix $R(z)R(z)^T$ can be rewritten as smooth functions depending locally only on e about the origin. This shows that the error system (2.18) is at least locally an autonomous system.

Now to prove the stability of $e = \mathbf{0}$ for (2.18), we choose as a Lyapunov function $V = \frac{1}{2l}||e||^2$ which satisfies

$$\frac{\mathrm{d}V}{\mathrm{d}t} = \frac{1}{l} e^T \dot{e} = -e^T D_{\tilde{z}} R(z) R(z)^T D_{\tilde{z}} e.$$

Since $R(z)R(z)^T$ and $D_{\tilde{z}}$ are positive definite matrices at the desired formation shape as $R(z)$ has full row rank at $z \in \mathcal{D}$ [59], the matrix

$$Q(e) = D_{\tilde{z}} R(z) R(z)^T D_{\tilde{z}}, \tag{2.20}$$

is positive definite at $e = \mathbf{0}$. Since the eigenvalues of $Q(e)$ are smooth functions of e, there exists a compact set

$$\mathcal{Q} \triangleq \{e : ||e||^2 \leqslant \rho\}, \tag{2.21}$$

for some positive constant ρ where $Q(e)$ is positive definite. Define $\lambda_{\min}$ to be the smallest eigenvalue of $Q(e)$ in $\mathcal{Q}$. Then

$$\frac{\mathrm{d}V}{\mathrm{d}t} \leqslant -\lambda_{\min} ||e||^2, \tag{2.22}$$

which immediately implies the local exponential convergence of e to zero. □

We want to emphasize that $e(t) \to \mathbf{0}$ as $t \to \infty$ does not imply $z(t) \to \mathcal{Z}$ but instead $z(t) \to \mathcal{D}$. As pointed out by Theorem 2.14, $z(t)$ is guaranteed to converge to $\mathcal{Z}$ only when the initial condition $z(0)$ is sufficiently close to $\mathcal{Z}$.

Another interesting property of employing the kind of potential functions (2.10)-(2.13) is that we have the following fact.

Lemma 2.17. *The centroid defined by $p_c(t) = \frac{1}{|\mathcal{V}|} \sum_{i=1}^{|\mathcal{V}|} p_i(t)$ is invariant for all t and it is equal to $p_c(0)$.*

Proof. From system (2.14) the proof comes directly from the fact that $\mathbf{1}_{1\times|\mathcal{V}|}$ is a left eigenvector of B fot its zero eigenvalue. □

Therefore we can determine the position of the centroid of the resulting formation given the initial conditions.

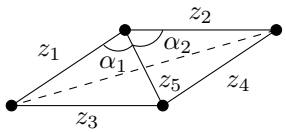

Figure 2.4: In this infinitesimally rigid formation the dashed vector "z_6" is missing in $\mathbb{G}$. Therefore the computations $z_1^T z_2$ and $z_3^T z_4$ are not straightforward anymore just employing (2.24). Nevertheless, $||z_6||^2 = ||z_1||^2 + ||z_2||^2 + 2||z_1||||z_2|| \cos(\alpha_1 + \alpha_2)$, where α_1 and α_2 can be determined employing the law of cosines with the norms $||z_1||$, $||z_3||$ and $||z_5||$ and $||z_2||$, $||z_4||$ and $||z_5||$ respectively. Therefore $z_1^T z_2 = g_{12}(e)$ and $z_3^T z_4 = g_{34}(e)$.

Example 2.1. As an illustrative example throughout the thesis we consider a generic triangular formation consisting of three agents whose $\mathbb{G}$ has the following incidence matrix

$$B = \begin{bmatrix} 1 & 0 & -1 \\ -1 & 1 & 0 \\ 0 & -1 & 1 \end{bmatrix}. \tag{2.23}$$

For this example, (2.16) becomes

$$\left.\begin{aligned} \dot{p}_1 &= -z_1||z_1||^{l-2}e_1 + z_3||z_3||^{l-2}e_3 \\ \dot{p}_2 &= -z_2||z_2||^{l-2}e_2 + z_1||z_1||^{l-2}e_1 \\ \dot{p}_3 &= -z_3||z_3||^{l-2}e_3 + z_2||z_2||^{l-2}e_2 \end{aligned}\right\}.$$

Let us now provide the computation of (2.19). First in view of the law of cosine for this triangle

$$2z_i^T z_j = ||z_k||^2 - ||z_i||^2 - ||z_j||^2, \tag{2.24}$$

where $i, j, k \in \{1, 2, 3\}$ are different, we can compute trivially the three $g_{ij}(e)$. The computation of g_{ij} for a general formation is not as easy as in this triangular formation, see for example a particular case in Figure 2.4. In order to compute $\lambda_{\min}$ as in (2.22), which requires implicitly the knowledge of $\mathcal{Q}$ that is not easy to obtain, we calculate the minimum eigenvalues of (2.20) evaluated in the neighborhood $\mathcal{U}_z$ of the desired shape $\mathcal{Z}$. Note that $\mathcal{Q}$ is the neighborhood of $\mathcal{D}$.

Although Theorem 2.14 and Proposition 2.16 have provided local asymptotic and exponential stability of the closed-loop systems respectively, there are inherent robustness issues associated with the gradient-based formation control as reported recently in [10, 44, 59]. The cause is rooted in the possible mismatches in the prescribed inter-agent distances.

2.6 Mismatches and robustness issues in gradient formation control

It is clear from (2.9) with V_k as in (2.10) that both agents i and j share the same potential V_k in the implementation of the gradient formation control. Let us focus on agent i whose control is

$$u_i = -\sum_{k=1}^{|\mathcal{E}|} u_i^k,$$

where u_i^k is the corresponding gradient $\nabla_{p_i} V_k$. More precisely, for the edge $\mathcal{E}_k = (i, j)$, we have

$$u_i^k = \nabla_{p_i} V_k = z_k ||z_k||^{l-2} (||z_k||^l - d_k^l) \tag{2.25}$$
$$u_j^k = \nabla_{p_j} V_k = -z_k ||z_k||^{l-2} (||z_k||^l - d_k^l). \tag{2.26}$$

However, when the two agents disagree on the desired distance d_k in between, namely

$$d_k^{\text{tail}} = d_k^{\text{head}} - \mu_k, \tag{2.27}$$

the applied control input, with $l = 1$, corresponding to $\mathcal{E}_k$ for agent i becomes

$$\begin{aligned} u_i^k &= \hat{z}_k (||z_k|| - d_k^{\text{head}} + \mu_k) \\ &= \hat{z}_k (||z_k|| - d_k^{\text{head}}) + \hat{z}_k \mu_k. \end{aligned} \tag{2.28}$$

In other words, mismatched prescribed distances lead to mismatched potential functions, and agents i and j do not share anymore the same V_k for $\mathcal{E}_k = (i, j)$ and so

$$V_k^i = \frac{1}{2l} (||z_k||^l - d_k^l + \mu_k)^2$$
$$V_k^j = \frac{1}{2l} (||z_k||^l - d_k^l)^2.$$

Remark 2.18. The control law (2.28) is equivalent to the situation where agent i measures precisely the relative direction $\hat{z}_k$ with respect to its neighbor j, but their range sensors giving $||z_k||$ are biased with respect to each other by μ_k.

It is obvious that for a general distance-based formation control problem with $n = 2$, if the two agents do not share the same prescribed distance to maintain, then an eventual steady-state motion will happen regardless of the dynamics of the agents since the agent with a smaller prescribed distance will chase the other one. Therefore, for $n > 2$ it would not be surprising to observe some collective motion in the steady-state of the formation if the neighboring agents do not share the same

prescribed distance to maintain. The scenario of having one mismatch per edge in its prescribed distance d_k^l with $l = 2$ has been studied rigorously in [44, 59] with the following two identified consequences for the formation:

1. *Unknown distorted final shape.* When the mismatches are small, due to the exponential decay of the error system, the errors $e_k(t)$ converge to some unknown small but non-zero values, and thus the shape of the formation becomes distorted even as t goes to infinity.

2. *Steady-state collective motion induced by the mismatches.* In $\mathbb{R}^2$, the agents move collectively in formation following a closed orbit that is determined by a single sinusoidal signal; in $\mathbb{R}^3$, the orbit becomes helical that is determined by a single sinusoidal signal and a constant drift.

Remark 2.19. For the sake of simplicity and clarity in the notation, if it is not otherwise explicitly stated, from this point onwards we will consider the case for $l = 2$ in (2.10) and the main results can be easily extended to any $l \in \mathbb{N}$. Then $\tilde{z} = \mathbf{1}_{|\mathcal{E}|\times 1}$ and thus $D_{\tilde{z}}$ is the identity matrix.

2.7 Illustrative experiments

In this section we validate and illustrate the findings of the chapter using the E-pucks mobile robots described in Appendix A. We first show the effectiveness of the control (2.9) employing the distance-based potential (2.10) with $l = 1$ for a formation of four robots with sensing topology defined by

$$B = \begin{bmatrix} 1 & 0 & -1 & 0 & -1 \\ -1 & 1 & 0 & 0 & 0 \\ 0 & -1 & 1 & -1 & 0 \\ 0 & 0 & 0 & 1 & 1 \end{bmatrix}, \tag{2.29}$$

where the desired shape defined by $\mathcal{Z}$ is a square with side-length of 250 pixels and we set the edge $\mathcal{E}_2$ to be the diagonal as in the Figure 2.2c. In addition we apply a control gain $c = 3.5 \times 10^{-1}$ to (2.9) in order to shape the exponential transitory, i.e., making it slower for not reaching the saturation levels of the robots' motors. The experimental results are shown in Figure 2.5.

So far we have considered that all the robots have the same perfect calibrated sensors. Now we are going to add a bias of -20 pixels to the range sensor of the robot 1 in the edge $\mathcal{E}_1 = (1, 2)$, i.e., it measures precisely the relative direction $\hat{z}_1$ but not the range $||z_1||$. According to (2.28) this is equivalent to have a mismatch $\mu_1 = -20$. The consequences are depicted in Figure 2.6.

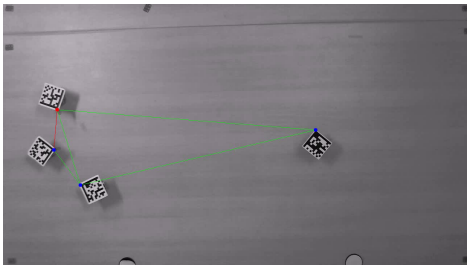

(a) Time $t = 0$ secs.

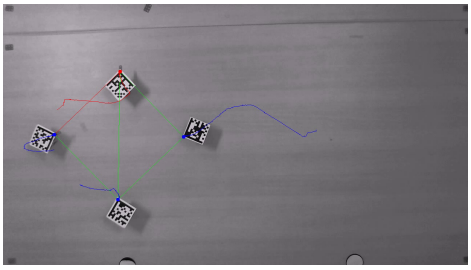

(b) Time $t = 25$ secs.

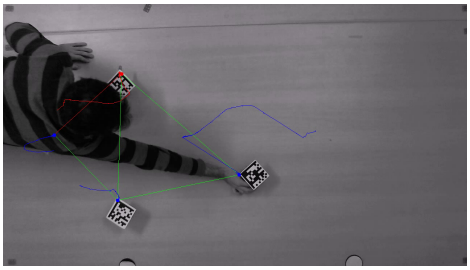

(c) Time $t = 29$ secs.

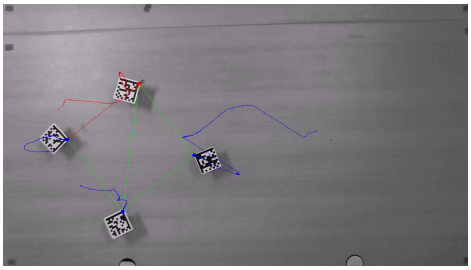

(d) Time $t = 59$ secs.

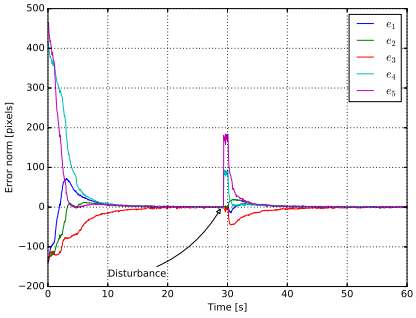

(e)

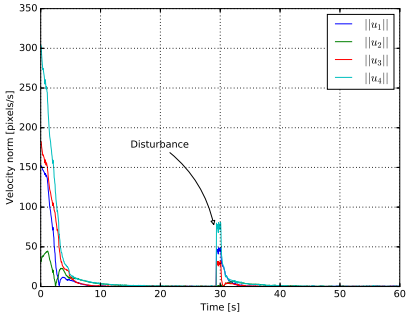

(f)

Figure 2.5: Experimental results of a team of four robots forming a regular square with sensing topology as given in (2.29). The robot 1 and the edge $\mathcal{E}_1$ have been marked in red. All the distances errors e_k for all $k \in \{1, \dots, 5\}$ and velocities v_i for $i \in \{1, \dots, 4\}$ converge to zero as it can be checked in plots (e) and (f) with $z(t) \to \mathcal{Z}$ as $t \to \infty$. Since we are employing a distance-based control strategy, the final orientation of $\mathcal{Z}$ is not under control and it is determined by the initial conditions $p_i(0)$ for all $i \in \{1, \dots, 4\}$.

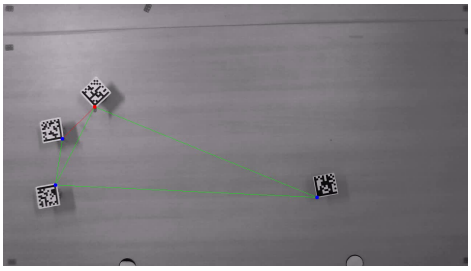

(a) Time $t = 0$ secs.

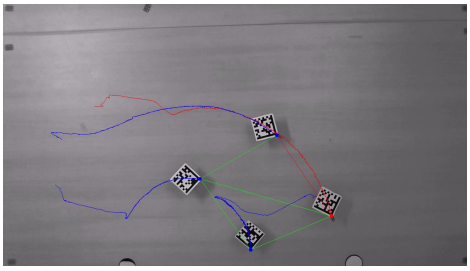

(b) Time $t = 76$ secs.

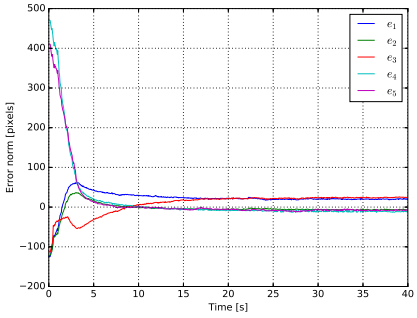

(c)

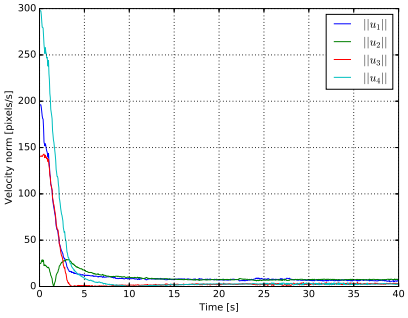

(d)

Figure 2.6: Experimental results of a team of four robots forming a regular square with sensing topology as given in (2.29). The robot 1 and the edge $\mathcal{E}_1$ have been marked in red. We have also added a bias of -20 pixels in the sensor of robot 1 for measuring the inter-distance $||z_1||$. According to Remark 2.18, this is equivalent for robot 1 to have a prescribed distance $d_1^{tail} = 270$, whereas robot 2 has a prescribed distance of $d_1^{head} = 250$ pixels for the same edge $\mathcal{E}_1$. In the steady-state, robot 1 wants to be further from robot 2 and vice versa. This misbehavior leads to a distorted shape and to a stationary collective motion as observed in (c) and (d). The collective motion has the form of a closed-orbit, whose radius (which can be infinity) is determined by the mismatches, $\mathcal{Z}$.

Chapter 3

Estimation and compensation of measurement inconsistencies in formations

T.W.: It is not the tools we use which make us good, but rather how we employ them? You see this bit of wall there? Well, I can't patch it with air.
RdY: I'm beginning to see why they made you the engineer.

Icewind Dale.

MEASUREMENT inconsistencies, or equivalently mismatches, are a source of undesired effects in a formation, hence, it makes sense to try to eliminate such misbehaviors but without adding too much extra requirements or complexity to the whole networked system. A straightforward solution would be to allow communication among neighboring agents, if they exchange at the time instant t_0 their information about the desired inter-distance to maintain and the actual measured inter-distance between them, then a simple calculation can determine the mismatch at time t_0, e.g.

$$d_k^{\text{tail}} - d_k^{\text{head}} = \mu_k.$$

Unfortunately, this task cannot usually be solved in a simple way by just one-round communication or transmission. For example, we have already mentioned that agents' sensors may not return the same reading about the same physical quantity, e.g., they are biased or miscalibrated, and this bias can be slowly time-varying due to other factors such as the sensor's temperature. Second, agents may have different guidance systems, which may differ in their setting points about a prescribed distance to maintain during the time. Third, the same sensor can produce different readings for the same physical distance in face of random measurements noises. Fourth, a continuous communication among agents may not be possible or desired. And last but not least, the agents may have different clocks complicating the data comparison in a possible communication.

In this chapter we will present in detail how local estimators can be designed for a set of chosen agents, called *the estimating agents*, such that the measurement inconsistencies can be estimated and compensated distributively. Three main

challenges are worth pointing out. First, the estimators' dynamics should not, if possible, affect the exponential convergence that is associated with the gradient control. Second, compensation should be done locally and different estimating agents should not give rise to conflicting compensation goals. Third, the class of discrepancies should be broad enough to contain at least constant signals. In view of these challenges, one soon realizes that the design task is not easy at all. In what follows, we propose two different estimator-based gradient controllers. The first one presented in Section 3.2 is based on the well-known internal model principle that has been used for solving tracking and disturbance rejection problems [17, 23], and more recently for cooperative control of multi-agents systems [84]. This solution requires to select the estimating agents in a particular way and a lower bound to a gain in the estimator must be satisfied in order to guarantee the convergence. On the other hand the second estimator-based gradient controller presented in Section 3.3 does not need such requirements for removing the undesired collective motion, however the desired steady-state shape can only be guaranteed for the special cases of triangles and tetrahedrons.

3.1 Modeling measurement inconsistency and estimating agents

We assume that the mismatches μ_k as in (2.27) are in the form of the superposition of a constant signal and $q_k \in \mathbb{N}$ sinusoidal signals with known frequencies $\{\omega_1, \omega_2, \ldots, \omega_{q_k}\}$, namely

$$\mu_k(t) = \alpha_k + \sum_{f=1}^{q_k} \beta_f \sin(\omega_f t + \phi_f), \tag{3.1}$$

where α_k, β_f and ϕ_f are fixed but unknown offset, amplitude and phase respectively. This noise model is widely used for formation control when the robots are known to work in the environment with periodic background noises. For example, short-term sea waves can be described by a superposition of periodic waves whose frequencies can be accurately estimated [11], and thus the measurement noise for underwater marine vehicles using floating buoys [18] can be treated as the superposition of a finite number of sinusoidal signals with known frequencies.

The system (2.16) including the mismatches as in (2.27) can be written in the following compact form[1]

$$u = -\overline{B} D_z e - \overline{S}_1 D_z \mu, \tag{3.2}$$

[1]Recall that for the sake of clarity in the analyses we have set $l = 2$ by default in the quadratic potential (2.10), hence we have that $d_k^{2\,\text{tail}} = d_k^{2\,\text{head}} - \mu_k$.

where $\mu \in \mathbb{R}^{|\mathcal{E}|}$ is the stacked column vector of μ_k for all $k \in \{1, \ldots, |\mathcal{E}|\}$ and the elements of $S_1 \in \mathbb{R}^{|\mathcal{V}| \times |\mathcal{E}|}$ are derived from $\mathbb{G}$ as follows

$$s_{1_{ik}} \triangleq \begin{cases} 1 & \text{if} \quad i = \mathcal{E}_k^{\text{tail}} \\ 0 & \text{if} \quad i = \mathcal{E}_k^{\text{head}} \\ 0 & \text{otherwise} \end{cases} . \tag{3.3}$$

In the sensing topology given by the graph $\mathbb{G}$, for each edge $\mathcal{E}_k = (\mathcal{E}_k^{\text{tail}}, \mathcal{E}_k^{\text{head}}) \in \mathcal{E}$ we implement a local estimator to the agent $\mathcal{E}_k^{\text{tail}}$, defined as an *estimating agent*. Therefore we are encoding the estimating agents in S_1 as well. We can change the estimating agent $\mathcal{E}_k^{\text{tail}}$ in the edge $\mathcal{E}_k$ by just changing the direction of the corresponding arrow in $\mathbb{G}$, which is perfectly safe for the gradient-based controllers presented in Chapter 2 since $\mathbb{G}$ is an undirected graph. The mission of the estimating agents will be to estimate and compensate the mismatch μ_k in (2.28), but considering the case $l = 2$, by the output $\hat{\mu}_k \in \mathbb{R}$ of an estimator in the following way

$$u_i^k = z_k(e_k + \mu_k - \hat{\mu}_k), \tag{3.4}$$

noting that agent $\mathcal{E}_k^{\text{tail}}$ is measuring $(e_k + \mu_k)$ as a whole since it does not know how biased or mismatched its actual error distance e_k is. It is clear that the main goal of the estimating agent in view of (3.4) is to achieve $\hat{\mu}_k = \mu_k$. Now we are ready to include the output of the estimators in (3.2) as follows

$$u = -\overline{B} D_z e - \overline{S}_1 D_z (\mu - \hat{\mu}), \tag{3.5}$$

where $\hat{\mu} \in \mathbb{R}^{|\mathcal{E}|}$ is the stacked column vector of $\hat{\mu}_k$ for all $k \in \{1, \ldots, |\mathcal{E}|\}$.

As it was mentioned in the introduction of this chapter, in the following sections we are going to propose two different estimators for generating $\hat{\mu}$.

3.2 Estimator-based gradient control I

This first estimator will be designed for estimating and then compensating the mismatches of the form of (3.1). We propose the following estimator's dynamics described by

$$\begin{cases} \dot{\xi}_k &= \Lambda_k \xi_k + \kappa \Upsilon_k (e_k + \mu_k - \hat{\mu}_k) \\ \hat{\mu}_k &= \Upsilon_k^T \xi_k \end{cases} \tag{3.6}$$

where $\xi_k \in \mathbb{R}^{1+2q_k}$ is the state of the estimator k and it can be initialized arbitrarily,

$$\Lambda_k = \begin{bmatrix} 0 & \mathbf{0} & \mathbf{0} \\ \mathbf{0} & \mathbf{0} & -D_\Omega \\ \mathbf{0} & D_\Omega & \mathbf{0} \end{bmatrix}, \quad \Upsilon_k = \begin{bmatrix} b_1 \\ b_2 \end{bmatrix}, \tag{3.7}$$

where Ω is the stacked column vector of ω_f for all $f \in \{1, \dots, q_k\}$ from the mismatch μ_k as in (3.1), the constants $b_1 \in \mathbb{R}$ and $b_2 \in \mathbb{R}^{2q_k}$ are such that the pair (Υ_k, Λ_k) is observable, and $\kappa > 0$ is a gain to be designed.

Now we are ready to present the state-space model for the closed-loop n-agent system derived from (2.4), (3.5) and (3.6) in the following compact form

$$\mathbf{P}: \begin{cases} \dot{e} &= -2R(z)R(z)^T e - 2R(z)S_1(z)^T(\mu - \hat{\mu}) \\ y &= e \end{cases} \tag{3.8}$$

$$\mathbf{C}: \begin{cases} \dot{\xi} &= D_\Lambda \xi + \kappa D_\Upsilon (y + \mu - \hat{\mu}) \\ \hat{\mu} &= D_\Upsilon^T \xi \end{cases} \tag{3.9}$$

$$\mathbf{W}: \begin{cases} \dot{w} &= D_\Lambda w \\ \mu &= D_\Upsilon^T w \end{cases}, \tag{3.10}$$

where $S_1(z) = D_z^T \overline{S}_1^T$, $\xi \in \mathbb{R}^{|\mathcal{E}|+2\sum_1^{|\mathcal{E}|} q_k}$ as the stacked column vector of ξ_k's is the state of $\mathbf{C}$, $\Lambda \in \mathbb{R}^{(|\mathcal{E}|+2\sum_1^{|\mathcal{E}|} q_k)\times(|\mathcal{E}|+2\sum_1^{|\mathcal{E}|} q_k)}$ and $\Upsilon \in \mathbb{R}^{|\mathcal{E}|+2\sum_1^{|\mathcal{E}|} q_k}$ are the stacked matrices of Λ_k and Υ_k and $w \in \mathbb{R}^{|\mathcal{E}|+2\sum_1^{|\mathcal{E}|} q_k}$ as the stacked column vector of w_k's is the state of the exosystem $\mathbf{W}$ whose output is the discrepancy signal given in (3.1). For all the defined signals we have that $k \in \{1, \dots, |\mathcal{E}|\}$. Note that the state equations (3.8)-(3.10) define an autonomous system by using (2.19). The initial estimates of the offset, phase and amplitude of μ_k are encoded in the initial condition $w(0)$. We recall that the estimating agents are measuring $e + \mu$ as a whole, while the unknown mismatch μ appears in (3.8) and (3.9). The signal flow of the closed-loop system is shown in the block diagram in Figure 3.1.

Using the standard framework in robust output regulation problem, one can take the inconsistency μ to be the disturbances that directly influence the input and the output signals of the plant $\mathbf{P}$, and the controller $\mathbf{C}$ must contain internal models that are copies of the exosystem $\mathbf{W}$. One can check that in this case the Byrnes-Isidori regulator equation [16] is solvable with the trivial solution $\xi = w$ and $e = \mathbf{0}$.

After setting up the mathematical descriptions of the estimator-based control and the corresponding state-space system model, we are ready to show that the n-agent system under mismatches is exponentially stabilized by our proposed distributed control.

Theorem 3.1. *For the closed-loop n-agent formation (3.8) and (3.9) with the measurement inconsistency vector μ driven by the exosystem (3.10) and unknown initial*

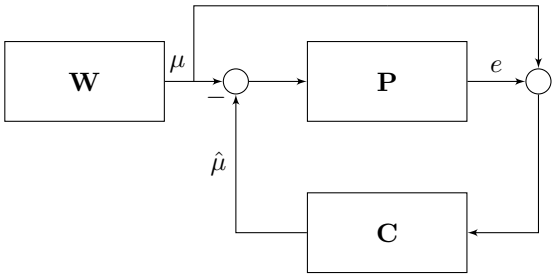

Figure 3.1: The plant $\mathbf{P}$ corresponds to the error system e, where its input and output are perturbed by the discrepancy μ generated by the exosystem $\mathbf{W}$ as in (3.10). The disturbance rejection is achieved by using the internal controller $\mathbf{C}$ that contains a copy of the exosystem.

condition $w(0) \in \mathbb{R}^{|\mathcal{E}|+2\sum_1^{|\mathcal{E}|} q_k}$*, if the matrix*

$$Z \triangleq -R(z^*)R(z^*)^T + R(z^*)S_1(z^*)^T \tag{3.11}$$

is Hurwitz at the desired shape $z^* \in \mathcal{Z}$ *corresponding to* $e = \mathbf{0}$*, then there exist* $\kappa^* > 0$ *and* $b^* > 0$ *such that for any* $\kappa||D_\Upsilon||^2 > \kappa^*$ *and* $||b_2|| < b^*$*, the system admits a locally exponentially attractive invariant manifold* $\mathcal{Q} \triangleq \{(w, p, \xi) \,|\, e = \mathbf{0}, \xi = w\}$*, and thus the shape of the formation converges exponentially to the desired shape defined by* $e = \mathbf{0}$ *with* $z \in \mathcal{Z}$*, the estimation* $\hat{\mu}$ *converges exponentially to* μ *and the velocity* $\dot{p}$ *converges exponentially to zero (i.e., the formation eventually stops).*

Proof. We take the coordinate transformation $\alpha = e + \mu - D_\Upsilon^T \xi$ and $\theta = w - \xi$, and then the equations (3.8)-(3.10) can be rewritten into

$$\begin{bmatrix} \dot{e} \\ \dot{\alpha} \\ \dot{\theta} \end{bmatrix} = \begin{bmatrix} -2R(z)S_2(z)^T & -2R(z)S_1(z)^T & \mathbf{0} \\ -2R(z)S_2(z)^T & -2R(z)S_1(z)^T - \kappa D_\Upsilon^T D_\Upsilon & D_\Upsilon^T D_\Lambda \\ -\kappa D_\Upsilon & \mathbf{0} & D_\Lambda - \kappa D_\Upsilon D_\Upsilon^T \end{bmatrix} \begin{bmatrix} e \\ \alpha \\ \theta \end{bmatrix}, \tag{3.12}$$

where $S_2(z) = R(z) - S_1(z)$. We then calculate its Jacobian matrix L at the equilibrium point $e = \mathbf{0}$, $\alpha = \mathbf{0}$ and $\theta = \mathbf{0}$. Although the system matrix of (3.12) is state dependent, several of its components are functions of the inner products $z_i^T z_j$ and thus their partial derivatives can be computed straightforwardly. In fact, the Jacobian matrix is

$$L = \begin{bmatrix} L_1 & L_2 \\ L_3 & L_4 \end{bmatrix}, \tag{3.13}$$

where

$$L_1 = \begin{bmatrix} -2R(z^*)S_2(z^*)^T & -2R(z^*)S_1(z^*)^T \\ -2R(z^*)S_2(z^*)^T & -2R(z^*)S_1(z^*)^T - \kappa D_\Upsilon^T D_\Upsilon \end{bmatrix}$$

$$L_2 = \begin{bmatrix} \mathbf{0} \\ D_\Upsilon^T M \end{bmatrix}, \quad L_3 = \begin{bmatrix} -\kappa D_\Upsilon & \mathbf{0} \end{bmatrix}, \quad L_4 = D_\Lambda - \kappa D_\Upsilon D_\Upsilon^T.$$

We now prove that L_1 is Hurwitz, and this is equivalent to prove the system

$$\dot{e} = -2R(z)S_2(z)^T e - 2R(z)S_1(z)^T \alpha \tag{3.14}$$

$$\dot{\alpha} = -2R(z)S_2(z)^T e - 2R(z)S_1(z)^T \alpha - \kappa D_\Upsilon^T D_\Upsilon \alpha \tag{3.15}$$

is asymptotically stable at the origin $e = \mathbf{0}$ and $\alpha = \mathbf{0}$ in which case $\hat{\mu} = \mu$. Let $f(e, \alpha) \triangleq -2R(z)S_2(z)^T e - 2R(z)S_1(z)^T \alpha$, and we compute

$$F_0 \triangleq \frac{\partial f(e, \mathbf{0})}{\partial e}|_{e=\mathbf{0}} = 2Z, \tag{3.16}$$

which is Hurwitz since Z is in view of the condition in the theorem. Therefore, there exists a positive definite matrix $P = P^T$ such that

$$F_0^T P + P F_0 = -2I. \tag{3.17}$$

Then for system (3.14)-(3.15) consider the candidate Lyapunov function

$$V(e, \alpha) = e^T P e + \frac{1}{2}\alpha^T \alpha, \tag{3.18}$$

whose time derivative along the system's solution is

$$\begin{aligned} \dot{V}(e, \alpha) &= 2e^T P f(e, \alpha) + \alpha^T f(e, \alpha) - \kappa ||D_\Upsilon||^2 ||\alpha||^2 \\ &= 2e^T P f(e, \mathbf{0}) + 2e^T P \left(f(e, \alpha) - f(e, \mathbf{0}) \right) \\ &\quad + \alpha^T f(e, \alpha) - \kappa ||D_\Upsilon||^2 ||\alpha||^2 \\ &= 2e^T P (F_0 e + g(e) + \bar{f}(e)\alpha) + \alpha^T f(e, \alpha) \\ &\quad - \kappa ||D_\Upsilon||^2 ||\alpha||^2, \end{aligned} \tag{3.19}$$

where $g(e)$ is the Taylor-series residue that satisfies

$$\lim_{||e|| \to 0} \frac{||g(e)||}{||e||} = 0, \tag{3.20}$$

and $\bar{f}(e) = -2R(z)S_1(z)^T$. In particular, (3.20) implies that for any $\epsilon > 0$, there exists a δ such that $||e|| \leqslant \delta \implies ||g(e)|| \leqslant \epsilon ||e||$. Taking $\epsilon = \frac{1}{2||P||}$ with the

corresponding δ, since $\bar{f}(e)$ is locally Lipschitz, we know that for all $||e|| \leqslant \delta$, $||\alpha|| \leqslant \delta$, there exist $p, q > 0$ such that

$$\dot{V}(e,\alpha) \leqslant -2||e||^2 + 2||e||||P||\frac{1}{2||P||}||e|| + p||e||||\alpha|| + \\ + q||\alpha||^2 - \kappa||D_\Upsilon||^2||\alpha||^2, \tag{3.21}$$

where the third and fourth terms on the right-hand side are due to the boundedness of $\bar{f}(e)$ in an open ball. Hence, by choosing $\kappa||D_\Upsilon||^2 > 0$ such that

$$q + \frac{p^2}{2} - \kappa||D_\Upsilon||^2 \leqslant -\frac{1}{2}, \tag{3.22}$$

we have, in view of Young's inequality, that

$$\dot{V}(e,\alpha) \leqslant -\frac{1}{2}(||e||^2 + ||\alpha||^2), \tag{3.23}$$

and thus system (3.14)-(3.15) converges exponentially to the origin for all the initial conditions $e(0), \alpha(0)$ starting in the compact set $\mathcal{C} := \{p, \hat{\mu}, \mu \,|\, \lambda_{\min}(P)||e||^2 + \frac{1}{2}||e + \mu - \hat{\mu}||^2 \leqslant \delta^2\}$, where $\lambda_{\min}(P)$ is the minimum eigenvalue of P. So we have proved that L_1 is Hurwitz.

We further observe that L_4 is Hurwitz for any $\kappa > 0$, which follows from the asymptotic stability of $\dot{\theta} = L_4\theta$ since $L_4 + L_4^T = -2\kappa D_\Upsilon D_\Upsilon^T$ and the pair (D_Υ, D_Λ) is observable. Thus, if L_2 is zero, i.e., $b_2 = \mathbf{0}$ since $\Upsilon_k^T = \begin{bmatrix} b_1 & \mathbf{0} \end{bmatrix}$ is a left eigenvector for the single zero eigenvalue of Λ_k, then the eigenvalues of L are the eigenvalues of L_1 and L_4. Therefore, for a sufficiently small D_Υ such that $0 < ||b_2|| < b^*$, L is still Hurwitz. Hence, system (3.12) is locally exponentially stable, which implies that (w, p, ξ) locally exponentially converges to $\mathcal{Q}$. Since $\dot{p} = \mathbf{0}$ in the invariant manifold $\mathcal{Q}$, we conclude also that $\dot{p}(t) \to \mathbf{0}$ exponentially as $t \to \infty$, i.e., the formation eventually stops. □

Remark 3.2. Note that we have not only removed all undesired effects induced by the presence of inconsistency, but with the estimation of $\mu(t)$, Theorem 3.1 provides a systematic method to calibrate the offset of the sensors in the estimating agents with respect to the sensors in the non-estimating agents.

In the next section, we explain how to choose the estimating agents systematically to guarantee the conditions in Theorem 3.1 to hold.

3.2.1 Selecting the estimating agents

The condition of Z being Hurwitz in Theorem 3.1 is a sufficient condition for the local exponential stability of system (3.8)-(3.9). To check this condition, one needs

(a) (b)

Figure 3.2: A triangular formation associated with a cyclic and acylic estimating-agent graph where the tails of the arrows indicate the corresponding estimating agents.

to calculate the eigenvalues of an $|\mathcal{E}| \times |\mathcal{E}|$ square matrix. Such computations can be burdensome and in this section we are going to show that for a large class of infinitesimally and minimally rigid formations one can still guarantee the admissibility of the condition by choosing smartly the estimating agents and thus avoid computing the eigenvalues.

3.2.2 Stabilizing a large class of infinitesimally and minimally rigid formations in $\mathbb{R}^2$

In this subsection we study a class of infinitesimally and minimally rigid formations in $\mathbb{R}^2$ that are generated by a sequence of Henneberg insertion operations (see Section 2.3.1) starting from triangular formations, for which we present two ways of picking the estimating agents. Then we introduce a systematic way of choosing the estimating agents based on such a Henneberg insertion.

Proposition 3.3. *For any undirected triangular formation, where each agent acts as an estimating agent for only one edge, then its associated Z matrix is Hurwitz.*

Proof. One can check that in this case $R(z)S_2(z)^T + S_2(z)R(z)^T = R(z)R(z)^T$. In addition, $R(z^*)R(z^*)^T$ is a positive definite matrix since undirected triangular formations are infinitesimally and minimally rigid. So $-R(z)S_2(z)^T$ is Hurwitz at $z \in \mathcal{Z}$ or equivalently $e = \mathbf{0}$, and this in turn is equivalent to Z is Hurwitz. □

Proposition 3.4. *For any undirected triangular formation, where one agent is the estimating agent for both of the two edges that it is associated with and exactly one other agent is the estimating agent for the remaining edge, then its Z matrix is Hurwitz.*

Proof. In this case, we have

$$R(z)S_2^T(z) = \begin{bmatrix} ||z_1||^2 & 0 & 0 \\ -z_2^T z_1 & ||z_2||^2 & -z_2^T z_3 \\ 0 & -z_3^T z_2 & ||z_3||^2 \end{bmatrix}, \tag{3.24}$$

which can be rewritten into the block lower-triangular form

$$R(z)S_2^T(z) = \begin{bmatrix} A_{11} & \mathbf{0} \\ A_{12} & A_{22} \end{bmatrix}. \tag{3.25}$$

Here, $A_{11} = ||z_1||^2$ is always positive; the characteristic polynomial of A_{22} is quadratic and thus it is easy to compute that both of its two eigenvalues live in the open left half-plane when z_2 and z_3 are not parallel, which has to be true since the formation is infinitesimally rigid. So the Z matrix itself is Hurwitz. □

The two situations of choosing estimating agents for triangular formations are illustrated in Fig. 3.2.

Proposition 3.5. *For any infinitesimally and minimally rigid formation in $\mathbb{R}^2$ that is generated by the Henneberg insertion operation, its associated Z matrix is Hurwitz if one chooses the estimating agents following exactly the sequence of the Henneberg insertions and in addition: (i) for the first three agents, pick the estimating agents as in Proposition 3.3 or Proposition 3.4; (ii) for any new insertion operation that has just added two edges from a new agent to two existing agents, pick those two existing agents to be the estimating agents for the newly added two edges. Note that only those two chosen estimating agents are involved and the other agents are not affected at all.*

Proof. It suffices to prove that for an n-agent, $n \geqslant 3$, infinitesimally and minimally rigid formation in $\mathbb{R}^2$ whose Z matrix is Hurwitz with its chosen estimating agents, the new $(n+1)$-agent formation obtained from the n-agent formation by the Henneberg insertion operation still has a Hurwitz Z matrix if its estimating agents are chosen according to the rule stipulated in the proposition.

Let the n-agent formation's Z matrix be $R(z)S_2^T(z)$ and the Z matrix for the $(n+1)$-agent formation be $\bar{R}(z)\bar{S}_2^T(z)$. Then

$$\bar{R}(z)\bar{S}_2^T(z) = \begin{bmatrix} R(z)S_2^T(z) & \mathbf{0} \\ \divideontimes & C(z) \end{bmatrix}, \tag{3.26}$$

where "$\divideontimes$" denotes the submatrix of less importance and

$$C(z) = \begin{bmatrix} ||z_l||^2 & -z_l^T z_{l+1} \\ -z_{l+1}^T z_l & ||z_{l+1}||^2 \end{bmatrix}, \tag{3.27}$$

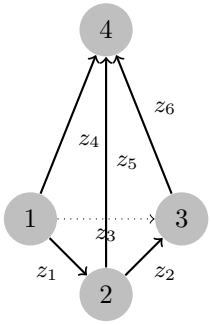

Figure 3.3: Tetrahedron formation where the tails of the arrows indicate the corresponding estimating agents.

where z_l and z_{l+1} are the two vectors pointing from the two chosen estimating agents' positions to the $(n+1)th$ agent's position. Then using the similar argument as proving Proposition 3.4, one can show that $\bar{R}(z)\bar{S}_2^T(z)$ is also Hurwitz. □

3.2.3 Stabilizing a special class of infinitesimally and minimally rigid formations in $\mathbb{R}^3$

Now we look at undirected rigid formations in $\mathbb{R}^3$. We start with simple tetrahedron formations.

Proposition 3.6. *For an undirected tetrahedron formation in $\mathbb{R}^3$, if its estimating agents are chosen as shown in Figure 3.3, then its Z matrix is Hurwitz.*

Proof. The Z matrix for the tetrahedron formation with the estimating agents chosen as shown in Figure 3.3 is

$$R(z)S_2^T(z) = \begin{bmatrix} A(z) & \mathbf{0} \\ * & G(z) \end{bmatrix}, \tag{3.28}$$

where $A(z)$ is the same matrix as in (3.24), $G(z)$ is the Grammian matrix $\bar{z}^T\bar{z}$ and $\bar{z}$ is the stacked column vector of z_4, z_5, and z_6. Since the tetrahedron formation is infinitesimally and minimally rigid at z^*, all the vectors in $\bar{z}$ are linearly independent. Therefore, $G(\bar{z})$ is positive definite at z^* and thus the Z matrix is Hurwitz. □

Since there is no necessary and sufficient combinatorial conditions for formations' rigidity properties in $\mathbb{R}^3$ yet, we can only look at a special class of rigid formations in $\mathbb{R}^3$.

Proposition 3.7. *Consider the class of infinitesimally and minimally rigid formation in $\mathbb{R}^3$ that can be generated by adding in sequence new agents to a tetrahedron formation such that every time the new agent is connected to three existing agents that form a triangular formation. If in each insertion operation, the three estimating agents for the three newly added edges are exactly the three associated existing agents, then the Z matrix for the overall formation is Hurwitz.*

The proof for this proposition is very similar to that of Proposition 3.5 and then we omit it.

3.2.4 Experimental results

We have already shown an experiment in Section 2.7 where the robots use directly the standard gradient control strategy but a single bias in robot 1 makes the formation to drift away with a distorted shape.

We then validate the result in Theorem 3.1 for the same team of four robots, where their desired shape $\mathcal{Z}$ is a square with side-length of 250 pixels and we have set the edge $\mathcal{E}_2$ to be the diagonal as in Figure 2.2c. The robots follow the modified gradient control law (3.5) including the output of the local estimators but with $l = 1$ for the quadratic potential function (2.10), therefore D_z is substituted by $D_{\hat{z}}$ in (3.5). In addition we have added a control gain $c = 3.5 \times 10^{-1}$ to all the robots in order to prevent saturations in their motors. The sensing topology of the formation is given by the following incidence matrix

$$B = \begin{bmatrix} 1 & 0 & 1 & 0 & 1 \\ -1 & 1 & 0 & 0 & 0 \\ 0 & -1 & -1 & 1 & 0 \\ 0 & 0 & 0 & -1 & -1 \end{bmatrix}, \tag{3.29}$$

Assuming that robots $2, 3$ and 4 have a well calibrated range sensor, we have introduced a bias of 20 pixels to the range sensor of robot 1 or equivalently we set the following vector of mismatches

$$\mu = \begin{bmatrix} 20 & 0 & 20 & 0 & 20 \end{bmatrix}. \tag{3.30}$$

In order to estimate and compensate the mismatches we implement a local estimator of the form of (3.6) to the estimating agents defined by Propositions 3.4 and 3.5, namely

$$S_1 = \begin{bmatrix} 1 & 0 & 1 & 0 & 1 \\ 0 & 1 & 0 & 0 & 0 \\ 0 & 0 & 0 & 1 & 0 \\ 0 & 0 & 0 & 0 & 0 \end{bmatrix}. \tag{3.31}$$

Note that robots 2 and 3 are also running an estimator for the edges $\mathcal{E}_2$ and $\mathcal{E}_4$ respectively. We have set the estimator control gain to $\kappa = 1 \times 10^{-1}$, where numerical computations show that this value is smaller than the bound given in Theorem 3.1, so the condition about κ^* in Theorem 3.1 is just a sufficient condition. The experimental results are discussed in Figure 3.4

In order to validate the results of Theorem 3.1 for a 3D formation under the time varying mismatches as in (2.27) we set a numerical simulation. We consider a formation of five agents in $\mathbb{R}^3$. The measurement inconsistency takes the form of the superposition of a constant random offset and a sine wave with a known frequency. Each inconsistency μ_k has different frequencies and offsets. We implement the control law (3.5) in the agents with the local estimators as in (3.6) and choose the estimating agents according to Proposition 3.6. The five agents are prescribed to maintain two regular tetrahedrons sharing the same base where all the edge lengths are $d = 5$ units. The five agents are placed randomly within a volume of 50 cubic units. We choose $\kappa = 1$, $\Upsilon_k^T = \begin{bmatrix} 1 & 1 & 0 \end{bmatrix}$, and the estimators ξ_k's are initialized to be zero. In Figure 3.5 it is clear that the agents' velocities converge to zero and the formation shape converges to the desired one. Moreover, $\hat{\mu}(t)$ converges to the periodic inconsistency $\mu(t)$.

3.3 Estimator-based gradient control II

Although the proposed distributed estimator (3.6) estimates and compensates effectively all the mismatches, it is gain dependent and the estimating agents have to be chosen carefully. In this section we are going to show an alternative estimator which is gain independent and the estimating agents can be chosen arbitrarily. Unfortunately, although this new estimator removes the undesired collective motion in the steady-state, it can only guarantee the desired shape in the steady-state for the particular cases of triangles and tetrahedrons. Nevertheless, we will see that by choosing the estimating agents in a particular way, we can focus the final distortion on chosen edges.

Consider only constant mismatches, i.e., $\mu(t) = \mu$, and the following dynamics for the estimator $\hat{\mu}$ in (3.5)

$$\dot{\hat{\mu}} = -D_z^T \overline{S}_1^T \left(\overline{B} D_z e + \overline{S}_1 D_z (\mu - \hat{\mu}) \right), \tag{3.32}$$

where as in Section 3.2 the matrix S_1 has encoded the estimating agents. Analyzing the right hand side of (3.32) we have that each estimator installed at the estimating

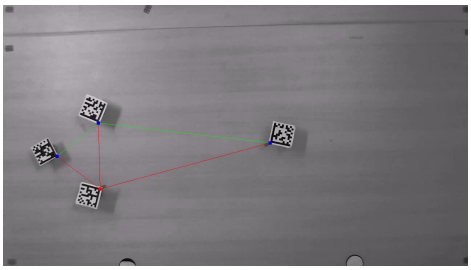

(a) Time $t = 0$ secs.

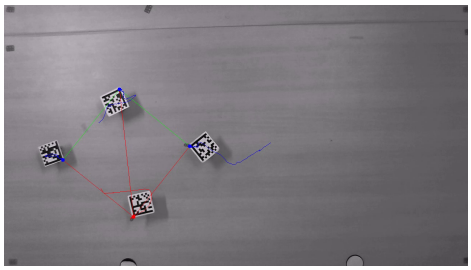

(b) Time $t = 60$ secs.

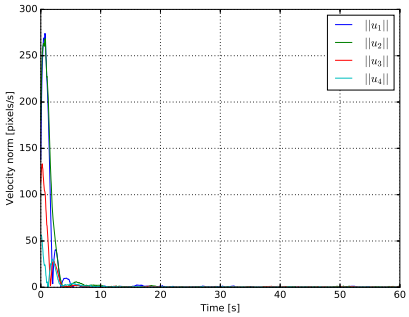

(c)

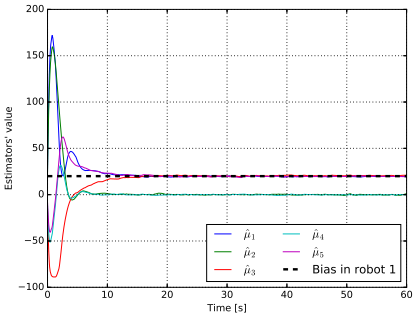

(d)

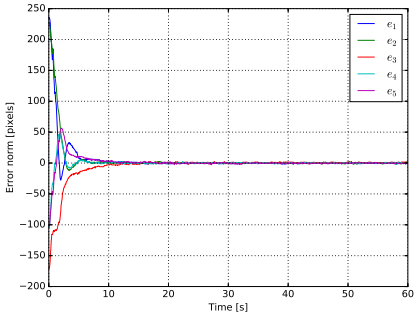

(e)

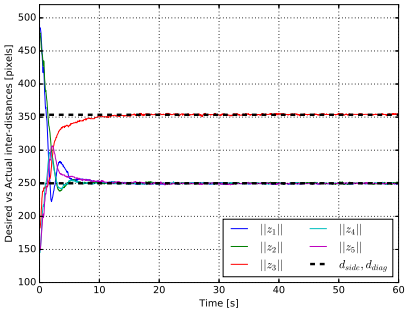

(f)

Figure 3.4: Experimental results of a team of four robots forming a regular square with sensing topology as given in (3.29). We have added a bias of 20 pixels to the range sensor of robot 1, therefore there will be a mismatch in the edges $\mathcal{E}_1, \mathcal{E}_3$ and $\mathcal{E}_5$. The biased robot and its edges have been marked in red in the video caps. In order to remove the undesired effects caused by the mismatches, we have chosen the estimating agents according to (3.31) for running the proposed local estimators in (3.6). Indeed the undesired collective motion is removed as it is shown in (c). Furthermore, the robot 1 estimates its bias as shown in (d) and $\hat{\mu}_2$ and $\hat{\mu}_4$ converge to zero since the rest of robots do not have any biases. Hence, the mismatches can be effectively compensated and the shape of the formation converges to the desired one as shown in (b), (e) and (f).

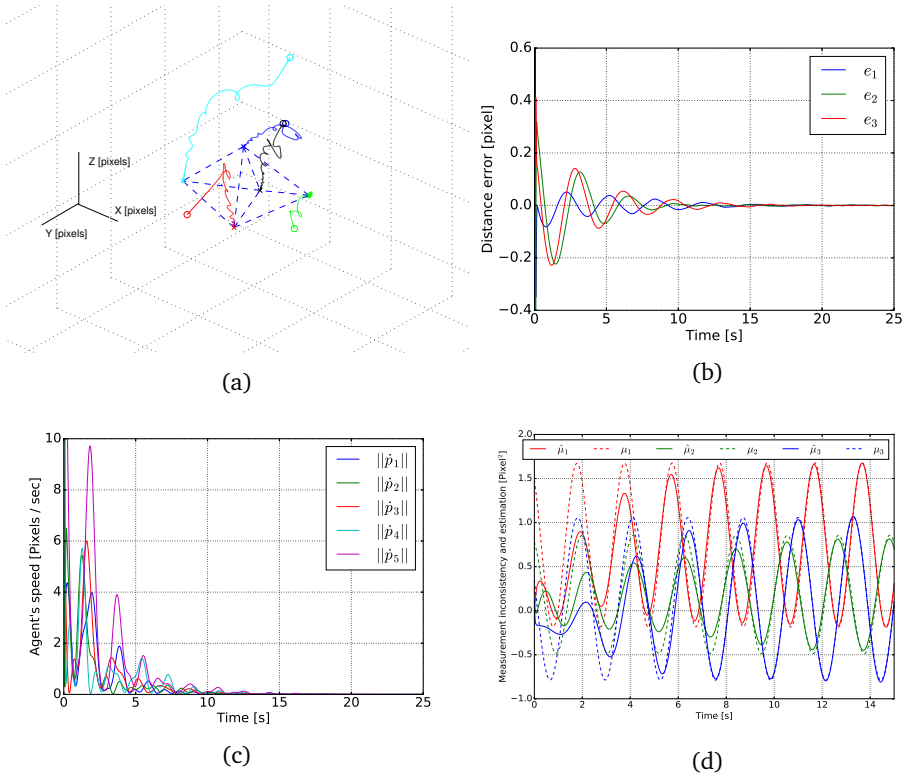

Figure 3.5: Simulation results of a 3D formation with inconsistent measurements using our proposed estimator-based gradient control where the inconsistencies are biased sinusoidal signals; (a) the plot of the trajectories where the initial positions are shown in circles and the final positions are shown in crosses; (b) the error e_k, $k = 1, 2, 3$; (c) the plot of the agents' speeds which shows that the five agents eventually stop; (d) the plot of the estimated measurements inconsistencies for the first three edges (shown in solid-line) which asymptotically converge to the actual ones (shown in dashed-line).

agent i can be written as

$$\dot{\hat{\mu}}_k = -z_k^T \left(\sum_{l=1}^{|\mathcal{E}|} b_{il}\, z_l \left(e_l + s_{1_{il}} (\mu_l - \hat{\mu}_l) \right) \right). \tag{3.33}$$

The estimating agent i is employing the compromised position by a mismatch z_k and its own velocity in the bracket at (3.33) for the dynamics of $\hat{\mu}_k$. We will show that when the formation starts close to the desired infinitesimally and minimally rigid one, the local estimator $\hat{\mu}_k$ will remain constant once the velocity of the

corresponding estimating agent is zero, i.e., we remove the undesired collective motion in the steady-state.

Let us compute the error system derived from (3.5) and (2.4) employing the distributed estimator dynamics (3.32)

$$\dot{e} = -2D_z^T\overline{B}^T\overline{B}D_z e - 2D_z^T\overline{B}^T\overline{S}_1 D_z(\mu - \hat{\mu}), \tag{3.34}$$

therefore the system composed by (3.33) and (3.34) is autonomous in view of (2.19).

Theorem 3.8. *Consider the autonomous system given by (3.33) and (3.34). Then the equilibrium points e^* and $\hat{\mu}^*$ are exponentially stable. Furthermore, $\dot{p}(t) \to \mathbf{0}$ and the steady-state deformation of the shape satisfies $||e||^2 \leqslant 2||\mu - \hat{\mu}(0)||^2 + ||e(0)||^2$. For the particular cases of triangles and tetrahedrons, the equilibrium is $e^* = \mathbf{0}$, i.e., $\hat{\mu}^* = \mu$.*

Proof. Consider the following Lyapunov function candidate

$$V = \frac{1}{4}||e||^2 + \frac{1}{2}||\xi||^2, \tag{3.35}$$

with $\xi = \mu - \hat{\mu}$, which satisfies

$$\begin{aligned}\frac{\mathrm{d}V}{\mathrm{d}t} &= \frac{1}{2}e^T\dot{e} + \xi^T\dot{\xi} \\ &= -e^T D_z^T\overline{B}^T\overline{B}D_z e - e^T D_z^T\overline{B}^T\overline{S}_1 D_z\xi \\ &- \xi^T D_z^T\overline{S}_1^T\overline{S}_1 D_z\xi - \xi^T D_z^T\overline{S}_1^T\overline{B}D_z e \\ &= -||\overline{B}D_z e + \overline{S}_1 D_z\xi||^2 \\ &= -||R(z)^T e + S_1^T(z)\xi||^2,\end{aligned} \tag{3.36}$$

therefore e and ξ are bounded. By invoking the LaSalle's invariance principle the states e and ξ converge exponentially to the largest invariance set given by

$$\mathcal{T} \triangleq \{e, z, \xi : \overline{B}D_z e + \overline{S}_1 D_z\xi = \mathbf{0}_{m|\mathcal{V}|\times 1}\}, \tag{3.37}$$

in the compact set

$$\mathcal{Q} \triangleq \{e, \xi : \frac{1}{2}||e||^2 + ||\xi||^2 \leqslant \rho\}, \tag{3.38}$$

with $0 < \rho \leqslant 2V(0)$. In order words $e(t) \to e^*$ and $\xi(t) \to \xi^*$ as t goes to infinity and from (3.5) we also have that $\dot{p}(t) \to \mathbf{0}$ as t goes to infinity, therefore we can also conclude that $z(t) \to z^*$ as t goes to infinity, where e^*, ξ^* and z^* are fixed points satisfying (3.37). In general we have that e^* and ξ^* are not zero vectors, therefore $z^* \notin \mathcal{Z}$, but it is also clear that $||e^*|| \leqslant 2\rho$. Hence, for a sufficiently small

ρ the resultant (distorted) formation will also be infinitesimally and minimally rigid.

Now we are going to show that $e^*, \xi^* = \mathbf{0}$ for triangles and tetrahedrons. Since triangles and tetrahedrons are derived from complete graphs, the distorted shape when ρ is sufficiently small will also be a triangle or a tetrahedron, i.e., we are excluding non-generic situations (e.g., collinear or coplanar alignments of the agents in $\mathbb{R}^2$ or $\mathbb{R}^3$). In the triangular case we have two possibilities after choosing the estimating agents: their associated directed graph is cyclic (each agent estimates one mismatch) or acyclic (one agent estimates two mismatches and one of the other two agents estimate the remaining mismatch).

The cyclic case for the estimating agents in the triangle corresponds to the following matrices

$$B = \begin{bmatrix} 1 & 0 & -1 \\ -1 & 1 & 0 \\ 0 & -1 & 1 \end{bmatrix}, \; S_1 = \begin{bmatrix} 1 & 0 & 0 \\ 0 & 1 & 0 \\ 0 & 0 & 1 \end{bmatrix},$$

and by substituting them into the equilibrium condition in $\mathcal{T}$ we have that

$$\left.\begin{array}{rl} z_1^* e_1^* - z_3^* e_3^* + z_1^* \xi_1^* & = \mathbf{0} \\ z_2^* e_2^* - z_1^* e_1^* + z_2^* \xi_2^* & = \mathbf{0} \\ z_3^* e_3^* - z_2^* e_2^* + z_3^* \xi_3^* & = \mathbf{0} \end{array}\right\}. \tag{3.39}$$

Since the steady-state formation is also a triangle for a sufficiently small ρ, then z_1^*, z_2^* and z_3^* are linearly independent. Therefore from (3.39) we have that $e_3^*, e_1^*, e_2^* = 0$ respectively and consequently we have that $\xi_1^*, \xi_2^*, \xi_3^* = 0$.

Without loss of generality the acyclic case for the estimating agents in the triangle corresponds to the following matrices

$$B = \begin{bmatrix} -1 & 0 & -1 \\ 1 & 1 & 0 \\ 0 & -1 & 1 \end{bmatrix}, \; S_1 = \begin{bmatrix} 0 & 0 & 0 \\ 1 & 1 & 0 \\ 0 & 0 & 1 \end{bmatrix}, \tag{3.40}$$

and by substituting them into the equilibrium condition in $\mathcal{T}$ we have that

$$\left.\begin{array}{rl} -z_1^* e_1^* - z_3^* e_3^* & = \mathbf{0} \\ z_2^* e_2^* + z_1^* e_1^* + z_2^* \xi_2^* + z_1^* \xi_1^* & = \mathbf{0} \\ z_3^* e_3^* - z_2^* e_2^* + z_3^* \xi_3^* & = \mathbf{0} \end{array}\right\}. \tag{3.41}$$

It is immediate from the first equation in (3.41) that $e_1^*, e_3^* = 0$ and then from the third equation in (3.41) we derive that $e_2^*, \xi_3^* = 0$, and hence $\xi_1^*, \xi_2^* = 0$ from the second equation in (3.41).

For the sake of brevity we omit the proof for the tetrahedrons, but analogous to

the analysis for the triangles, the key idea behind the proof is that the three relative vectors associated to an agent are linearly independent in 3D. □

3.3.1 Controlling the shape-distortion

In Theorem 3.8, we have shown the use of distributed estimators which have an undesirable effect of a stead-state shape distortion where the error norm $||e||$ is bounded by a constant $\sqrt{2\rho} > 0$. Since $||e||$ is a combination of all errors in every edge, we cannot use ρ to prescribe a zero asymptotic error for some focus edges or to concentrate the bound only on some edges. This property is relevant if we want to reach a prescribed distance for a high-degree of accuracy for some edges. By exploiting the result in Theorem 3.8 for triangles or tetrahedrons, we can construct a network topology (based on a star topology) that enables us to impose the error bound only on one edge while guaranteeing that the other errors converge to zero. We show this in the following proposition.

Proposition 3.9. *Consider the same mismatched formation control system as in Theorem 3.8 with the equilibrium set given by $\mathcal{T}$ as in (3.37). Consider the triangular formation defined by B and S_1 as in (3.40) for the incidence matrix and the estimating agents respectively. For any new agent $i, i \geqslant 4$ added to the formation, if we only link it to the agents 2 and 3, and at the same time we let the agents 2 and 3 to be the estimating agents for the mismatches in the new added links, then for a sufficiently small ρ as in (3.38)*

$$\lim_{t\to\infty} e_k(t) = 0, \, \forall k \neq 2, \tag{3.42}$$

and $|e_2(t)| \leqslant \sqrt{2\rho}$ for all t.

Proof. Clearly a star topology has been used for the new added agents, where the central node is the triangle formed by agents $1, 2$ and 3. Note that the newly added agent $i, i \geqslant 4$ is forming a triangle with agents 2 and 3. Therefore, as explained in Theorem 3.8, if ρ is sufficiently small, then the resultant distorted formation is also formed by triangles. We prove the claim by induction. First we derive the equations from $\mathcal{T}$ as in (3.37) for the proposed star topology with four agents

$$\left.\begin{aligned} -z_1^* e_1^* - z_3^* e_3^* &= \mathbf{0} \\ z_2^* e_2^* + z_1^* e_1^* - z_4^* e_4 + z_2^* \xi_2^* + z_1^* \xi_1^* + z_4^* \xi_4 &= \mathbf{0} \\ z_3^* e_3^* - z_2^* e_2^* - z_5^* e_5 + z_3^* \xi_3^* + z_5^* \xi_5 &= \mathbf{0} \\ z_4^* e_4^* + z_5^* e_5^* &= \mathbf{0} \end{aligned}\right\}. \tag{3.43}$$

As explained in the last part of the proof of Theorem (3.8), it is clear that the errors e_1^*, e_3^*, e_4^* and e_5^* must be zero and $e_2^2 \leqslant \rho$. For any newly added agent $i \geqslant 5$, we add

a new equation to (3.43) of the form

$$z_l^* e_l^* + z_{l+1}^* e_{l+1}^* = \mathbf{0}, \tag{3.44}$$

where l and $l+1$ are the labels of the two newly added edges. Thus for a sufficiently small ρ we have that z_l^* and z_{l+1}^* are linearly independent so $e_l^*, e_{l+1}^* = 0$. □

3.3.2 Experimental results

In this section we experimentally validate the results in Theorem 3.8 for a team of three robots where the prescribed shape is an equilateral triangle with side-length of 250 pixels. The sensing topology is given by the following incidence matrix

$$B = \begin{bmatrix} -1 & 0 & 1 \\ 1 & -1 & 0 \\ 0 & 1 & -1 \end{bmatrix}, \tag{3.45}$$

therefore note that the estimating agents are following an cyclic scheme. The three robots have implemented the control law (3.5) but with $l = 1$ for the quadratic potential function (2.10), hence D_z is substituted by $D_{\hat{z}}$ in (3.5) and (3.32). In addition we have added a control gain $c = 3.5 \times 10^{-1}$ to all the robots in order to prevent saturations in their motors. We have set to the robots the following three distance mismatches

$$\mu = \begin{bmatrix} 10 & 15 & -35 \end{bmatrix}^T. \tag{3.46}$$

In order to estimate and compensate them, the three local estimators follow the dynamics given by (3.33). The experimental results are discussed in Figure 3.6

3.4 Concluding remarks

In this chapter we have presented two distributed estimator-based gradient controllers for stabilizing rigid formations in $\mathbb{R}^2$ and $\mathbb{R}^3$. These estimators are run locally by a set of agents called the estimating agents. The first estimator proposed in Section 3.2, based on the internal model principle, handles periodic time-varying measurement inconsistencies with known frequencies but unknown amplitudes, phases and offsets. However, in addition to choosing the estimating agents in a specific way, a controller gain has to satisfy a lower bound. The estimator works effectively to remove the undesired effects of deformation in the steady-state shape and the eventual collective motion. In comparison, the second estimator presented in Section 3.3 is gain independent and the estimating agents can be chosen arbitrarily. It has been shown the effectiveness of the estimator for formations with triangles and tetrahedron as desired shapes. However, only the removal of the

steady-state collective motion is guarantee for a generic formation, nevertheless, it has been shown that the deformation of the steady-state shape can be focused on selected inter-distances.

All the findings in this chapter have been validated in experimental results for a team of four mobile robots in $\mathbb{R}^2$ and numerical simulations have been done for formations in $\mathbb{R}^3$.

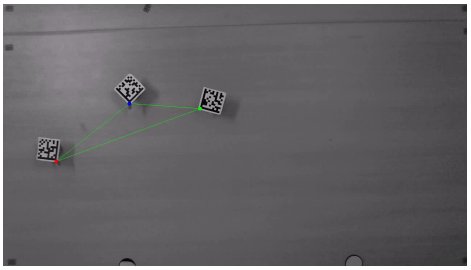

(a) Time $t = 0$ secs.

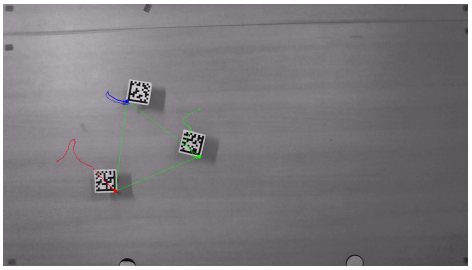

(b) Time $t = 50$ secs.

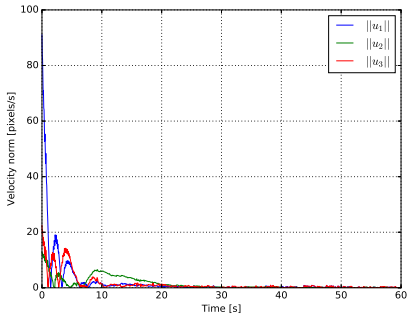

(c)

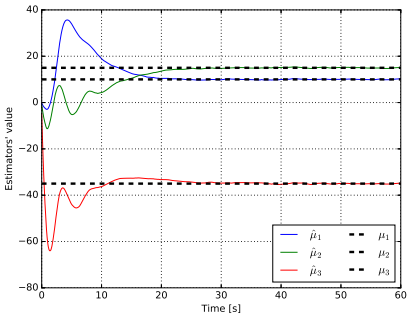

(d)

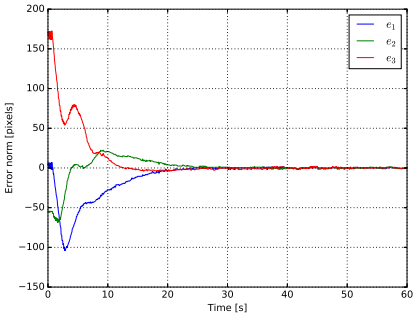

(e)

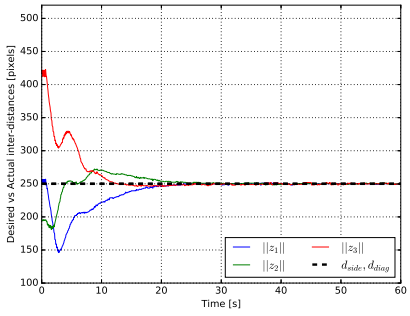

(f)

Figure 3.6: Experimental results of a team of three robots forming an equilateral triangle with sensing topology as given in (3.45). The robots $1, 2$ and 3 have been marked with red, blue and green colors respectively in the video caps. The setup suffers of the distance mismatches given in (3.46). In order to remove the undesired effects caused by the mismatches we have installed a local estimator with dynamics (3.33) in each robot. Indeed the undesired collective motion is removed as it is shown in (c). Furthermore, all the robots estimate their mismatches as it is shown in (d). Hence, the formation converges to the desired one as shown in (b), (e) and (f).

Chapter 4

Distributed rotational and translational motion control of formations

What if I apply some mismatches to this formation in purpose? Mmm but wait a minute, you said that mismatches are a bad thing aren't they? You see, the right man in the wrong place can make all the difference in the world.

Half-Life.

COORDINATED robot tasks, such as, the enclosing of a target [51], area exploration & surveillance [15, 20, 86] and the vehicle platooning for energy efficiency [71, 81], can be achieved by combining two different cooperative controls: multi-agent formation control and group motion control. The former is to achieve and maintain a specific desired shape of a multi-agent formation as it has been shown in Chapter 2, while the latter to guide the motion of the group as a whole. For simple formations, such as, line formations in the vehicle platooning problem, these two control problems can be solved simultaneously by using the passivity-based control approach as pursued in [26]. However, for formations in more complicated shapes, these two control problems are usually tackled separately, namely using the gradient-based strategies for formation control and leader-follower coordination for motion control, where for the latter the leader moves according to a desired trajectory and the followers simply track the leader [9]. But when the separately designed formation controller and motion controller are jointly in force as in the common scenario in practice, conflict often occurs: the shape of the formation is distorted when an agent compromises between the demands from formation and motion controls as to where and how it needs to move [6, 69].

While efforts have been made before to solve such conflict by installing velocity sensors in addition to position sensors on mobile agents and thus compensating the distortion with the help of the more sensed information [9], we in this chapter take a much more head-on approach. We generalize the gradient-based distributed formation control law for both control objectives, i.e., we simultaneously guarantee no shape distortion ($e = \mathbf{0}$) in the steady-state desired formation motion even without the knowledge of any additional sensed information in comparison to the

conventional control. The surprisingly simple structure of our proposed control law opens possibilities to solve other difficult problems, such as collective rotational motion or the enclosing of a moving target. It facilitates even to study the formation coordination task for agents governed by higher-order dynamics as we will see in Chapter 6.

Motivated by the findings in [74], we treat in this chapter the mismatches in prescribed inter-agent distances not as the annoying source of deteriorating formation control performances, but to the contrary, as the profitable parameters of novel gradient control that solves formation and motion controls simultaneously without sacrificing the performance of one for the other. The key idea is to introduce a pair of mismatches as *motion parameters* that "reconcile" each other for every pair of neighboring agents in order to steer the formation. Here by *reconciling* we mean that the corresponding pairs of motion parameters are designed to satisfy a set of equations to be specified later related to the formation's translational or rotational motion under which no distortions appear in the steady-state formation shape. In fact, we will show that the desired steady-state motion is a function of the desired steady-state shape $\mathcal{Z}$.

The proposed gradient-based formation-motion joint controller using the mentioned distributed motion parameters has several advantages. First, one can achieve precisely the desired steady-state formation shape and the group motion simultaneously, including rotational motion, in a distributed fashion. To the best of our knowledge, no such result has been reported in the literature. For single-integrator agent dynamics, we relate analytically the magnitude of these motion parameters to the speed of the group motion. Second, our proposed approach enables us to align the formation with respect to a global coordinate frame by adding a simple control term to an arbitrary agent when guiding the group in motion. In comparison, in the literature such an alignment is usually obtained by assigning a leader who knows the global frame and letting the other agents (followers) estimate the leader's velocity employing a distributed estimator [9]. Obviously in our approach, such estimators are not needed at all. Third, one can easily use our method to address the target tracking and enclosing problem both in $\mathbb{R}^2$ and $\mathbb{R}^3$ where one assigns the formation shape to specify how the target is enclosed and tracked by the pursuers. In comparison to the solution of such problems in [43, 54] among other works, we do not confine our formation to follow the same circular trajectory nor require *all* enclosing agents to measure their relative positions with respect to the target.

The rest of the chapter is organized as follows. The design of the desired steady state motion with the desired formation shape is described in Section 4.1; the corresponding stability analysis is presented in Section 4.2. We apply the distributed motion parameters for the design of the translation of a formation in global coordinates in Section 4.3; another application addressing the target tracking and enclosing problem is presented in Section 4.4.

4.1 Mismatches as distributed motion parameters

We start recalling equation (3.2), where in the presence of a mismatch in the prescribed distance in every edge, system (2.16) can be rewritten using (2.27) as

$$\dot{p} = -\overline{B} D_z e - \overline{S}_1 D_z \mu. \tag{4.1}$$

In Chapter 3 and other works [35, 44, 59, 74], the vector μ is addressed as a small disturbance. In this chapter we substitute the mismatches by motion parameters, and instead of having one motion-parameter per prescribed distance, we consider a pair of motion parameters per edge. More precisely, one motion parameter for each agent i and j in the edge $\mathcal{E}_k = (i, j)$. We will then design these motion parameters in the following way: the motion parameters are used to control the steady-state movement of the formation without distorting the final desired shape.

We consider a pair of parameters $\frac{\mu_k}{c} \in \mathbb{R}$ and $\frac{\tilde{\mu}_k}{c} \in \mathbb{R}$ (scaled by a gain $c \in \mathbb{R}$) for being added to the term d_k^2 for each agent in the edge $\mathcal{E}_k = (i, j)$. More precisely, agent i uses a *controlled* distance $d_k^2 + \frac{\mu_k}{c}$ and correspondingly, agent j, $d_k^2 - \frac{\tilde{\mu}_k}{c}$. For the edge $\mathcal{E}_k = (i, j)$ we include these parameters to the gradient descent controller in (2.25) and (2.26) and apply the same gain c, namely

$$\begin{aligned} u_i^k &= c z_k (||z_k||^2 - d_k^2) - \mu_k z_k \\ u_j^k &= -c z_k (||z_k||^2 - d_k^2) - \tilde{\mu}_k z_k, \end{aligned}$$

where μ_k and $\tilde{\mu}_k$ are not mismatches anymore but motion parameters. The two equations above lead to the following compact form

$$\dot{p} = -c R(z)^T e + \overline{A}(\mu, \tilde{\mu}) z, \tag{4.2}$$

where the elements a_{ik} of A are constructed in a very similar way as in the incidence matrix as

$$a_{ik} \triangleq \begin{cases} \mu_k & \text{if} \quad i = \mathcal{E}_k^{\text{tail}} \\ \tilde{\mu}_k & \text{if} \quad i = \mathcal{E}_k^{\text{head}} \\ 0 & \text{otherwise.} \end{cases} \tag{4.3}$$

Note that if $\tilde{\mu}_k = 0$ for all $k \in \{1, \ldots, |\mathcal{E}|\}$, then (4.2) is identical to (4.1) with $c = 1$. The gain c is a free design parameter for achieving exponential stability of the formation as we will see later in the stability analysis.

One important property of (4.2) is that each agent i can work with only its own local frame O_i. One can see this more in detail in the following lemma.

Lemma 4.1. *The control law applied in (4.2) can be implemented for each agent i using only its local frame O_i, i.e., each agent can use its own coordinate system to*

measure the relative position and a global coordinate system is not involved.

The proof is omitted for the sake of brevity, but is straightforward by following similar arguments as in [9, 19].

In order to induce some desired steady-state motion of the formation in the desired shape, we can manipulate μ and $\tilde{\mu}$ at the equilibrium of (4.2). Then the steady-state motion will be a function of the desired shape $z^* \in \mathcal{Z}$ and $\mu, \tilde{\mu}$:

$$\dot{p}^* = \overline{A}(\mu, \tilde{\mu}) z^*. \tag{4.4}$$

Before discussing on how to design the motion parameters μ and $\tilde{\mu}$ in order to keep $\mathcal{Z}$ invariant, let us first recall some facts from rigid body mechanics [42]. As in the case of points in a rigid body, the steady-state velocity of every agent $\dot{p}_i^*$ at the desired rigid formation shape can be decomposed into

$$\dot{p}_i^* = \dot{p}_c^* + \underbrace{{}^b\omega \times {}^b p_i^*}_{\dot{p}_{i_\omega}^*}, \tag{4.5}$$

where ${}^b\omega$ is the angular velocity of the rigid formation (similar to that for the rigid body). In particular, in view of (4.2) with A as defined in (4.3), the velocity (4.5) at the desired shape $z^* \in \mathcal{Z}$ is given by

$$\dot{p}_c^* + \dot{p}_{i_\omega}^* = \sum_{k=1}^{|\mathcal{E}|} a_{ik} z_k^*. \tag{4.6}$$

Let us decompose the motion parameters into $\mu = \mu_v + \mu_\omega$ and $\tilde{\mu} = \tilde{\mu}_v + \tilde{\mu}_\omega$, where $\mu_v, \tilde{\mu}_v \in \mathbb{R}^{|\mathcal{E}|}$ and $\mu_\omega, \tilde{\mu}_\omega \in \mathbb{R}^{|\mathcal{E}|}$ will be used to assign the desired translational and rotational velocity, respectively, of the rigid formation. Using this decomposition, we can rewrite (4.6) for all the agents into the following compact form

$$\dot{p}^* = \underbrace{\overline{A}(\mu_v, \tilde{\mu}_v) z^*}_{\mathbf{1}_{|\mathcal{V}|\times 1} \otimes \dot{p}_c^*} + \underbrace{\overline{A}(\mu_\omega, \tilde{\mu}_\omega) z^*}_{\dot{p}_\omega^*}, \tag{4.7}$$

where $\dot{p}_\omega^* \in \mathbb{R}^{m|\mathcal{V}|}$ is the stacked vector of all the rotational velocities $\dot{p}_{i_\omega}^*, i \in \{1, \ldots, |\mathcal{V}|\}$.

In the desired shape, the stacked vector ${}^b z^*$ of relative positions ${}^b z_k^*, k \in \{1, \ldots, |\mathcal{E}|\}$ in O_b becomes a constant. This is due to the fact that O_b follows the steady-state motion, and thus according to (4.7) the velocities ${}^b\dot{p}_c^*$ and ${}^b\dot{p}_{i_\omega}^*$ become also constant. In particular, if ${}^b\omega = 0$, then we will have a drift of the desired formation in O_g; otherwise for a nonzero constant vector ${}^b\omega$, the formation will follow a closed circular orbit (which is always the case in 2D formations) when ${}^b\omega$ is perpendicular to ${}^b\dot{p}_c^*$, or otherwise a helical trajectory in O_g. Figure 4.1

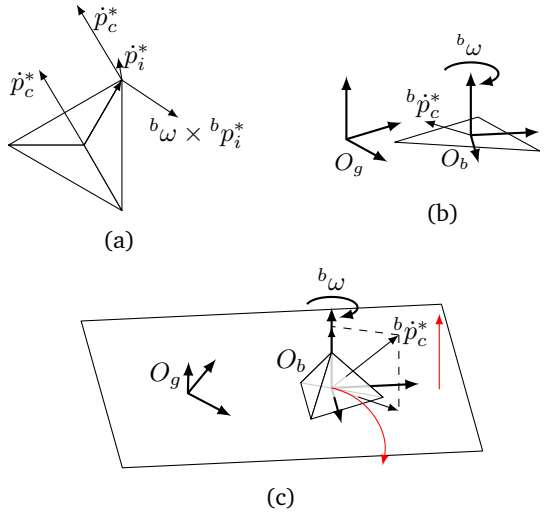

Figure 4.1: Illustration of the steady-state motion in different frames of coordinates: (a) in O_g, the steady-state velocity $\dot{p}_i^*$ can be decomposed into translational and rotational term given by (4.5); (b) in O_b the steady-state velocity vector ${}^b\dot{p}_i^*$ becomes constant. For 2D formations the steady-state trajectory in O_g becomes a circular closed orbit since ${}^b\omega$ and ${}^b\dot{p}_c^*$ are perpendicular; and (c) in general for 3D formations ${}^b\omega$ and ${}^b\dot{p}_c^*$ are not perpendicular, and therefore the resultant trajectory (shown in red) is helical in O_g.

shows an illustration of the these facts on the steady-state velocity of the desired formation expressed in either O_g and O_b.

Now we are ready to show how to design the motion parameters μ and $\tilde{\mu}$ in (4.7). Note that the steady-state motion must not distort the desired shape, i.e., the motion parameters have to be designed such that $\mathcal{Z}$ is an invariant set in (4.7). In a similar way as in (4.1), the desired steady-state velocity (4.4) in O_b can be rewritten as

$$
\begin{aligned}
{}^b\dot{p}^* &= \overline{S}_1 D_{{}^b z^*}\, \mu + \overline{S}_2 D_{{}^b z^*}\, \tilde{\mu} = \begin{bmatrix} \overline{S}_1 D_{{}^b z^*} & \overline{S}_2 D_{{}^b z^*} \end{bmatrix} \begin{bmatrix} \mu \\ \tilde{\mu} \end{bmatrix} \\
&= T({}^b z^*) \left(\begin{bmatrix} \mu_v \\ \tilde{\mu}_v \end{bmatrix} + \begin{bmatrix} \mu_\omega \\ \tilde{\mu}_\omega \end{bmatrix} \right),
\end{aligned}
$$

where $S_2 = S_1 - B$. The motion parameters will be used to design both velocities in (4.7) with respect to O_b as in Figure 4.1c since they are constant in such a frame. Note that the knowledge about O_b is only needed during the design stage for the desired steady-state velocity. During the implementation of the distributed control law, the agents only need to know about their own O_i's as shown in Lemma 4.1.

We now demonstrate how to design the velocity ${}^b\dot{p}_c^*$ employing the motion parameters. It is important to note that in an infinitesimally and minimally rigid framework, the minimum number of edges associated to a node is two in $\mathbb{R}^2$ or three in $\mathbb{R}^3$. So if ${}^bz^* \in \mathcal{Z}$ then the relative positions ${}^bz_k^*$'s associated to agent i can span the whole $\mathbb{R}^2$ for the planar formations (or $\mathbb{R}^3$ in the 3D case). This implies that the domain of the desired velocity ${}^b\dot{p}_i^*$ is the whole space and it can be assigned by an appropriate choice of μ and $\tilde{\mu}$ (c.f. (4.6)). Since the velocity ${}^b\dot{p}_c^*$ is the same for all the agents, we set the following requirement for μ_v and $\tilde{\mu}_v$

$$\overline{B}^T(\mathbf{1}_{|\mathcal{V}|\times 1} \otimes {}^b\dot{p}_c^*) = \overline{B}^T T({}^bz^*) \begin{bmatrix} \mu_v \\ \tilde{\mu}_v \end{bmatrix} = \mathbf{0}_{m|\mathcal{E}|\times 1}, \tag{4.8}$$

which implies that $[\begin{smallmatrix} \mu_v \\ \tilde{\mu}_v \end{smallmatrix}] \in \mathrm{Ker}\{\overline{B}^T T({}^bz^*)\}$. However, since in general the kernel of $T({}^bz^*)$ can be non-trivial, there may exist non-zero $[\begin{smallmatrix} \mu_v \\ \tilde{\mu}_v \end{smallmatrix}]$ such that ${}^b\dot{p}^* = \mathbf{0}_{m|\mathcal{V}|\times 1}$, which is irrelevant for our motion control. Taking this into account, the set of motion parameters μ_v and $\tilde{\mu}_v$ should satisfy

$$\begin{bmatrix} \mu_v \\ \tilde{\mu}_v \end{bmatrix} \in \mathcal{U} \triangleq P_{\mathrm{Ker}\{T({}^bz^*)\}^\perp} \left\{ \mathrm{Ker}\{\overline{B}^T T({}^bz^*)\} \right\}, \tag{4.9}$$

where $P_{\mathcal{X}}$ stands for the projection over the space $\mathcal{X}$. The lower bound for the degrees of freedom of choosing the elements of μ_v and $\tilde{\mu}_v$ for constructing ${}^b\dot{p}_c^*$ can obviously be given by the number of motion parameters of the agent that has the least number of neighbors. In other words,

$$\dim\{\mathcal{U}\} \geqslant \min_i\{|\mathcal{N}_i|\}, \tag{4.10}$$

where $\mathcal{N}_i$ is defined in Section 2.1 and $\mathcal{U}$ in (4.9). Consequently, we propose the following algorithm to compute μ_v and $\tilde{\mu}_v$ for given ${}^b\dot{p}_c^*$ and ${}^bz^*$.

Algorithm 4.2. *1. Choose an agent i with the least number of neighbors.*

2. *Assign μ_{v_k} and $\tilde{\mu}_{v_k}$ associated to agent i that solves ${}^b\dot{p}_c^* = \sum_{k=1}^{|\mathcal{E}|} a_{ik}\, {}^bz_k^*$.*

3. *Compute a basis V that spans the space defined in (4.9).*

4. *Compute a vector $v \in \mathbb{R}^{2|\mathcal{E}|}$ employing the basis V such that the previously computed μ_{v_k}'s and $\tilde{\mu}_{v_k}$'s are the k'th and $(|\mathcal{E}|+k)$'th elements of v. Then, the rest of elements of v are necessarily the motion parameters defining ${}^b\dot{p}_c^*$ for the whole formation, i.e., $v = [\begin{smallmatrix} \mu_v \\ \tilde{\mu}_v \end{smallmatrix}]$.*

From (4.3) it is clear that the implementation of the motion parameters is distributed, while the computation in Algorithm 4.2 is centralized since it requires the knowledge of O_b and $\mathcal{Z}$. On the other hand, the motion parameters only need

to be computed once since the desired speed of the motion can be modified by just rescaling μ_v and $\tilde{\mu}_v$. For a new agent j joining the formation, its motion parameters for the translational motion can be computed in a distributed way. Consider agent j joins the formation: if it enquires a neighboring agent i about ${}^i\dot{p}_c^*$ and O_i, then it becomes straightforward for agent j to compute the corresponding motion parameters for the desired ${}^j\dot{p}_c^*$ by only following the second step of Algorithm 4.2.

Now we proceed to show how to design the motion parameters for the rotational velocity ${}^b\dot{p}_\omega^*$ in (4.7), i.e., the rotational motion of the agents around the centroid. Note that this rotational motion maintain the constant norms $||z_k^*||$'s but not the relative positions z_k^*'s. Since $\frac{1}{2}\frac{\mathrm{d}||z_k||^2}{\mathrm{d}t} = z_k^T\dot{z}_k$, we can impose the following condition for maintaining constant $||z_k^*||$,

$$D_{z^*}^T\dot{z}^* = D_{z^*}^T\overline{B}^T T(z^*)\begin{bmatrix}\mu_\omega\\ \tilde{\mu}_\omega\end{bmatrix} = \mathbf{0}_{|\mathcal{E}|\times 1}. \tag{4.11}$$

As discussed after equation (4.7) the relative positions ${}^bz_k^*$ are constant because O_b is rotating with the rigid formation. However, for having such rotation of the formation, the constant velocities ${}^b\dot{p}_{\omega_i}^*$ must be designed in order to keep the norms $||{}^bz_k||$'s constant. Therefore, we impose the following restricting condition for μ_ω and $\tilde{\mu}_\omega$ in addition to (4.11)

$$D_{{}^bz^*}^T\overline{B}^T T({}^bz^*)\begin{bmatrix}\mu_\omega\\ \tilde{\mu}_\omega\end{bmatrix} = \mathbf{0}_{|\mathcal{E}|\times 1}. \tag{4.12}$$

As in the case for calculating the motion parameters for ${}^b\dot{p}_c^*$, the set of motion parameters μ_ω and $\tilde{\mu}_\omega$ has to satisfy

$$\begin{bmatrix}\mu_\omega\\ \tilde{\mu}_\omega\end{bmatrix} \in \mathcal{W} \triangleq P_{\mathcal{U}^\perp}\left\{\mathrm{Ker}\{D_{{}^bz^*}^T\overline{B}^T T({}^bz^*)\}\right\}, \tag{4.13}$$

where $\mathcal{U}$ is as in (4.9). We remark that the dimension of $\mathcal{W}$ in (4.13) is at least, one less than the dimension of $\mathcal{U}$ in (4.9). This is due to the fact ${}^b\dot{p}_{i_\omega}^*$ is perpendicular to ${}^bp_i^*$ (as shown in (4.5)) and hence, the degree-of-freedom for choosing $\left[\begin{smallmatrix}\mu_\omega\\ \tilde{\mu}_\omega\end{smallmatrix}\right]$ is at least one less than that for choosing $\left[\begin{smallmatrix}\mu_v\\ \tilde{\mu}_v\end{smallmatrix}\right]$. The calculation of the motion parameters μ_ω and $\tilde{\mu}_\omega$ for a desired ${}^b\omega$ can be done in a similar way to Algorithm 4.2

Algorithm 4.3. *1. Choose an agent i with the least number of neighbors.*

2. *Assign μ_{ω_k} and $\tilde{\mu}_{\omega_k}$ associated to agent i that solves ${}^b\omega = ({}^bp_i^*)\times\left(\sum_{k=1}^{|\mathcal{E}|} a_{ik}\,{}^bz_k^*\right)$.*
3. *Compute a basis W that spans the space defined in (4.13).*
4. *Compute a vector $\mathrm{w}\in\mathbb{R}^{2|\mathcal{E}|}$ employing the basis W such that the previously computed μ_{ω_k}'s and $\tilde{\mu}_{\omega_k}$'s are the k'th and $(|\mathcal{E}|+k)$'th elements of w. Then, the*

rest of elements of w *are necessarily the motion parameters defining* ${}^b\omega$ *for the whole formation, i.e.,* $\mathrm{w} = \left[\begin{smallmatrix}\mu_\omega \\ \tilde{\mu}_\omega\end{smallmatrix}\right]$.

As before the implementation of μ_ω and $\tilde{\mu}_\omega$ is fully distributed but their computation at the design stage is not. On the other hand, they only need to be computed once and the angular speed can be regulated by just rescaling their magnitude.

If we want to design different trajectories in O_g as in Figure 4.1, we only need to change the speed of ${}^b\dot{p}_c^*$ and ${}^b\omega$. Unfortunately, if a new agent j joins the formation, then the centroid will change, requiring to recompute μ_ω and $\tilde{\mu}_\omega$. Nevertheless, if the *instantaneous center of rotation* [42] $p_r \in \mathbb{R}^m$ is independent of the new agent, e.g., as we will see in the target enclosing problem where it will be fixed at agent 1, then agent j can still compute its motion parameters by only asking local information from a neighboring agent i, i.e., its ${}^i\dot{p}_i^*$ and ${}^i\dot{p}_c^*$ along with O_i and in addition we also require agent i to know about ${}^i(p_i - p_r)$.

Example 4.1. Let us continue with Example 2.1 on the triangular formation. In the following discussion, we will show how to find $\left[\begin{smallmatrix}\mu_v \\ \tilde{\mu}_v\end{smallmatrix}\right]$ and $\left[\begin{smallmatrix}\mu_\omega \\ \tilde{\mu}_\omega\end{smallmatrix}\right]$ that satisfy (4.8) and (4.12) and that belong to the spaces defined in (4.9) and (4.13) respectively. Since triangular formation is a special case, we can obtain these motion parameters explicitly without employing the proposed algorithms 4.2 and 4.3.

Obviously for a triangular formation, it always holds that

$$z_1 + z_2 + z_3 = \mathbf{0}. \tag{4.14}$$

The control law in (4.2) with the distributed motion parameters is

$$\left.\begin{aligned} \dot{p}_1 &= c(-z_1 e_1 + z_3 e_3) + \mu_1 z_1 + \tilde{\mu}_3 z_3 \\ \dot{p}_2 &= c(-z_2 e_2 + z_1 e_1) + \mu_2 z_2 + \tilde{\mu}_1 z_1 \\ \dot{p}_3 &= c(-z_3 e_3 + z_2 e_2) + \mu_3 z_3 + \tilde{\mu}_2 z_2 \end{aligned}\right\}.$$

In order to compute μ_v and $\tilde{\mu}_v$ for a given ${}^b\dot{p}_c^*$ with ${}^bz = {}^bz^* \in \mathcal{Z}$, we need to solve for the following three equations that are derived from (4.8)

$$\left.\begin{aligned} {}^bz_1^*(\mu_{v_1} - \tilde{\mu}_{v_1}) + {}^bz_3^*\tilde{\mu}_{v_3} - {}^bz_2^*\mu_{v_2} &= \mathbf{0} \\ {}^bz_2^*(\mu_{v_2} - \tilde{\mu}_{v_2}) + {}^bz_1^*\tilde{\mu}_{v_1} - {}^bz_3^*\mu_{v_3} &= \mathbf{0} \\ {}^bz_3^*(\mu_{v_3} - \tilde{\mu}_{v_3}) + {}^bz_2^*\tilde{\mu}_{v_2} - {}^bz_1^*\mu_{v_2} &= \mathbf{0} \end{aligned}\right\}. \tag{4.15}$$

Substituting (4.14) into (4.15) we obtain the following conditions for μ_v and $\tilde{\mu}_v$

(any four implying the remaining one)

$$\left.\begin{array}{rl} \mu_{v_1}+\mu_{v_2}+\mu_{v_3} & =\mathbf{0} \\ \tilde{\mu}_{v_1}+\tilde{\mu}_{v_2}+\tilde{\mu}_{v_3} & =\mathbf{0} \\ \mu_{v_2}+\tilde{\mu}_{v_3} & =\mathbf{0} \\ \mu_{v_3}+\tilde{\mu}_{v_1} & =\mathbf{0} \\ \mu_{v_1}+\tilde{\mu}_{v_2} & =\mathbf{0} \end{array}\right\}, \tag{4.16}$$

which has a non-trivial solution with two degrees of freedom satisfying (4.10). Obviously the set of equations in (4.16) is independent of $\mathcal{Z}$. One can check that solutions to (4.16) always satisfy (4.8). Indeed, substituting (4.16) in (4.8), we arrive at

$$\begin{bmatrix} m_1 & m_1 & m_1 \\ m_2 & m_2 & m_2 \\ -m_1-m_2 & -m_1-m_2 & -m_1-m_2 \end{bmatrix} {}^b z^* = \mathbf{0}_{6\times 1}, \tag{4.17}$$

where $m_1, m_2 \in \mathbb{R}$ are constants depending on μ_v and $\tilde{\mu}_v$, and the last equation is due to (4.14), which is independent of $\mathcal{Z}$. Note that $T({}^b z^*)$ has a trivial kernel since the three ${}^b z_k$'s are not colinear. Therefore the motion parameters $\left[\begin{smallmatrix}\mu_v \\ \tilde{\mu}_v\end{smallmatrix}\right]$ satisfying the set of equations (4.16) are in $\mathcal{U}$ as defined in (4.9) and obviously this space has dimension two.

Now we will show on how to calculate the motion parameters $\left[\begin{smallmatrix}\mu_\omega \\ \tilde{\mu}_\omega\end{smallmatrix}\right]$ which can form a basis for $\mathcal{W}$ in (4.13). First we notice that for a triangle we have

$$p_c = \frac{1}{3}\sum_{i=1}^{3} p_i,$$

and

$${}^b p_i^* = {}^b_g R(p_c^* - p_i^*) = \frac{1}{3}({}^b z^*_{[k+2]} - {}^b z_k^*), k = i \in \{1,2,3\}, \tag{4.18}$$

where p_c^* and p_i^* are the positions of the centroid and the agents when the formation is at $z^* \in \mathcal{Z}$, respectively, the matrix ${}^b_g R$ is the rotational matrix relating the attitude of O_b with respect to O_g and $[i] \triangleq 1 + \mathrm{mod}_3(i)$, with $\mathrm{mod}_n(\cdot)$ be the modulus operator with respect to n.

Since we want to have only rotational motion of the agents around the centroid of the triangle, we have to set the velocity of the centroid $\dot{p}_c^*$ as follows

$$\dot{p}_c^* = \frac{1}{3}\sum_{i=1}^{3} \dot{p}_{i_\omega}^* = \frac{1}{3}\sum_{k=1}^{3} (\mu_{\omega_k} + \tilde{\mu}_{\omega_k}) z_k^* = \mathbf{0},$$

which together with the triangular property (4.14) leads to the following set of

conditions (with two of them implying the third) for μ_ω and $\tilde{\mu}_\omega$

$$\mu_{\omega_k} + \tilde{\mu}_{\omega_k} - \mu_{\omega_{[k+2]}} - \tilde{\mu}_{\omega_{[k+2]}} = 0,\ k \in \{1,2,3\}, \tag{4.19}$$

which is independent of $\mathcal{Z}$. As mentioned after equation (4.13) that

$$\left({}^b\dot{p}^*_{i_\omega}\right)^T {}^b p^*_i = 0,\ i \in \{1,2,3\},$$

which together with (4.6) and (4.18) implies that

$$(\mu_{\omega_k}\, {}^b z^*_k + \tilde{\mu}_{\omega_{[k+2]}}\, {}^b z^*_{[k+2]})^T ({}^b z^*_{[k+2]} - {}^b z^*_k) = 0,\ k \in \{1,2,3\}. \tag{4.20}$$

Using (2.24), the two set of equations (4.19) and (4.20) define the following algebraic condition for μ_ω and $\tilde{\mu}_\omega$

$$\begin{bmatrix} f_1 & 0 & 0 & 0 & 0 & \tilde{f}_1 \\ 0 & f_2 & 0 & \tilde{f}_2 & 0 & 0 \\ 0 & 0 & f_3 & 0 & \tilde{f}_3 & 0 \\ 1 & -1 & 0 & 1 & -1 & 0 \\ 0 & 1 & -1 & 0 & 1 & -1 \\ -1 & 0 & 1 & -1 & 0 & 1 \end{bmatrix} \begin{bmatrix} \mu_\omega \\ \tilde{\mu}_\omega \end{bmatrix} = \mathbf{0}_{6\times 1}, \tag{4.21}$$

where

$$\left.\begin{array}{ll} f_k & = -\frac{3}{2}d_k^2 + \frac{1}{2}(d_{[k+1]}^2 - d_{[k+2]}^2) \\ \tilde{f}_k & = \frac{3}{2}d_{[k+2]}^2 + \frac{1}{2}(d_k^2 - d_{[k+1]}^2) \end{array}\right\},\ k \in \{1,2,3\}. \tag{4.22}$$

Since (4.21) ensures that the norms $||z^*_k||$ are constant with a rotational motion around the centroid p_c, it implies that μ_ω and $\tilde{\mu}_\omega$ satisfying (4.21) also fulfill (4.13).

Note that the last three rows of the matrix in (4.21) form the matrix $\begin{bmatrix} B^T & B^T \end{bmatrix}$ with B as in (2.23), which implies that the matrix in (4.21) has at least one eigenvalue equal to zero. The multiplicity of the zero eigenvalue must be one because the dimension of $\mathcal{W}$ is one. Indeed, as discussed after (4.13), the dimension of $\mathcal{W}$ is at least one less than the dimension of $\mathcal{U}$, which is two, but it cannot be zero since (4.21) has non-trivial solution. Therefore we have only one degree of freedom for the six motion parameters in μ_ω and $\tilde{\mu}_\omega$, which directly implies that $\left[\begin{smallmatrix} \mu_\omega \\ \tilde{\mu}_\omega \end{smallmatrix}\right]$ satisfying (4.21) forms a basis of $\mathcal{W}$.

Let $\mathrm{w} \in \mathcal{W}$ be an unitary vector. In this case the motion parameters μ_ω and $\tilde{\mu}_\omega$ clearly satisfy

$$\begin{bmatrix} \mu_\omega \\ \tilde{\mu}_\omega \end{bmatrix} = a\mathrm{w}, \quad a \in \mathbb{R}\backslash\{0\}, \tag{4.23}$$

where a is a parameter that determines the angular speed $||{}^b\omega||$. Since we know the steady-state velocity ${}^b\dot{p}^*_{i_\omega}$ by design and the radius of the orbit around the centroid

$||{}^b p_i^*||$, the steady-state angular speed can be set by the formula

$$\begin{aligned}||{}^b\omega|| &= \frac{||{}^b\dot{p}_{i_\omega}^*||}{||{}^b p_i^*||},\ i \in \{1,2,3\} \\ &= 3|a|\frac{||\mu_{\omega_k}{}^b z^*{}_k + \tilde{\mu}_{\omega_{[k+2]}}{}^b z^*{}_{[k+2]}||}{||{}^b z^*{}_{[k+2]} - {}^b z^*{}_k||},\ k \in \{1,2,3\}.\end{aligned}$$

Note that the sign of a denotes the sign of the rotation and $a = 0$ means no rotation at all.

The unit vector w in (4.23) can be computed directly for the special case of having an equilateral or an isosceles triangle as shown in the following proposition.

Proposition 4.4. *If ${}^b z^* \in \mathcal{Z}$ defines an equilateral triangle, then the eigenvector w in (4.21) corresponding to the eigenvalue 0 is given by*

$$\mathrm{w} = \frac{1}{\sqrt{6}}\,\mathbf{1}_{6\times 1}.$$

If ${}^b z^* \in \mathcal{Z}$ defines an isosceles triangle with $d_1 = d_2$, then

$$\mathrm{w} = \alpha\left[\frac{3d_3^2}{2d_1^2+d_3^2} \quad 2-\frac{3d_3^2}{2d_1^2+d_3^2} \quad 1 \quad 2-\frac{3d_3^2}{2d_1^2+d_3^2} \quad \frac{3d_3^2}{2d_1^2+d_3^2} \quad 1\right]^T, \tag{4.24}$$

with $\alpha \in \mathbb{R}^+$ being a normalizing factor.

Proof. For the equilateral case we have $d_k = d, k \in \{1,2,3\}$. Then $f_k = -\tilde{f}_k$ in (4.22) and in addition to (4.19) it follows that $\mu_{\omega_k} = \tilde{\mu}_{\omega_k}, k \in \{1,2,3\}$. Therefore $\mathrm{w} = \frac{1}{\sqrt{6}}\,\mathbf{1}_{6\times 1}$.

For the isosceles case, without loss of generality, let $d_1 = d_2$. By evaluating (4.20) for the agents 1 and 3 we have

$$\tilde{\mu}_3(||z_3^*||^2 - {z_3^*}^T z_1^*) - \mu_1(||z_1^*||^2 - {z_1^*}^T z_3^*) = 0 \tag{4.25}$$

$$-\mu_3(||z_3^*||^2 - {z_3^*}^T z_2^*) + \tilde{\mu}_2(||z_2^*||^2 - {z_2^*}^T z_3^*) - = 0, \tag{4.26}$$

where we have used the identity ${}^b z_i^T {}^b z_j = z_i^T z_j$. For an isosceles triangle it holds that $z_1^T z_3 = z_2^T z_3$ and $||z_1|| = ||z_2||$. Consequently, it follows from (4.25) and (4.26) that we can choose $\mu_{\omega_3} = \tilde{\mu}_{\omega_3}$ and $\mu_{\omega_1} = \tilde{\mu}_{\omega_2}$. Substituting this fact to (4.19) we get that $\mu_{\omega_2} = \tilde{\mu}_{\omega_1}$. Direct substitution of these relations into (4.20) gives us (4.24). □

As it was mentioned before, by default all computations of μ and $\tilde{\mu}$ are for $l = 2$ for the potential function (2.10). Nevertheless it is worth to note that for $l = 1$, instead of dealing with the relative positions ${}^b z_k^*$'s as in (4.15), we deal with the unitary vectors ${}^b \hat{z}_k^*$'s for the computation of the motion parameters. Therefore the

motion parameters for the steady-state velocity ${}^b\dot{p}^*$ with $l = 1$ are valid for any scaled version of the triangle defined by $\mathcal{Z}$. As we will see, this will have important implications in Chapter 5 for scaling infinitesimally and minimally rigid formations at the same time that we preserve the desired motion.

Remark 4.5. Note that in the case of dealing with the unitary vectors ${}^b\hat{z}_k^*$'s for the computation of μ and $\tilde{\mu}$, in general we cannot take advantage of the property (4.14) anymore.

4.2 Stability analysis

In the previous section we have shown how to design the desired steady-state behavior of the formation. Here, we provide the stability analysis of the closed-loop system. In particular we show that the control law applied in (4.2), with A designed as in Section 4.1, indeed steers the formation, at least locally, to the desired formation motion.

Similar to (2.17) and (2.18), we derive from (4.2) the following closed-loop system with the motion parameters

$$\dot{z} = -c\overline{B}^T R(z)^T e + \overline{B}^T \overline{A} z \tag{4.27}$$

$$\dot{e} = -2cR(z)R(z)^T e + 2R(z)\overline{A}z. \tag{4.28}$$

Note that as shown in Proposition 2.16, the error system (4.28) is autonomous since the elements of $R(z)\overline{A}z \in \mathbb{R}^{|\mathcal{E}|}$ are linear combinations of the inner products $z_i^T z_j = g_{ij}(e)$. Therefore we can write (4.28) as

$$\dot{e} = -2cQ(e)e + 2f(e), \tag{4.29}$$

with $Q(e)$ as in (2.20) with $l = 2$ and $f(e) = R(z)\overline{A}(\mu, \tilde{\mu})z$. Note that $f(e)$ is closely related to the desired shape $\mathcal{Z}$ since $z \in \mathcal{Z}$ implies $f(\mathbf{0}) = \mathbf{0}_{|\mathcal{E}|\times 1}$. However, in general $z \in \mathcal{D}$ does not necessarily imply $f(\mathbf{0}) = \mathbf{0}_{|\mathcal{E}|\times 1}$ since

$$R(z)\overline{A}(\mu, \tilde{\mu})z = D_z^T \overline{B}^T T(z) \begin{bmatrix} \mu \\ \tilde{\mu} \end{bmatrix}$$

is designed to be zero only at $z \in \mathcal{Z}$ but not at arbitrary $z \in \mathcal{D}$.

Theorem 4.6. *There exist constants $\rho, c^* > 0$ such that for system (4.29), $e = \mathbf{0}$ corresponding to $z \in \mathcal{Z}$ with the motion parameters $\left[\begin{smallmatrix} \mu_v \\ \tilde{\mu}_v \end{smallmatrix}\right]$ and $\left[\begin{smallmatrix} \mu_\omega \\ \tilde{\mu}_\omega \end{smallmatrix}\right]$ belonging to the spaces (4.9) and (4.13) respectively is locally exponentially stable for all $c \geqslant c^*$ in the compact set $\mathcal{Q} \triangleq \{e : ||e||^2 \leqslant \rho\}$. In particular, the formation will converge exponentially to the shape defined by $\mathcal{Z}$ and the velocity ${}^b\dot{p}_i$ will converge to ${}^b\dot{p}_i^*$ for*

$i \in \{1, \ldots, |\mathcal{V}|\}$.

Proof. We divide the proof in two parts. Firstly we analyze the inter-agent distance dynamics and show that the shape formed eventually by the agents is the desired shape. Secondly we analyze the individual agent dynamics in order to show that they converge to the steady-state motion defined by the motion parameters.

Consider the following candidate Lyapunov function

$$V = \frac{1}{4}||e||^2,$$

with its time derivative given by

$$\frac{\mathrm{d}V}{\mathrm{d}t} = \frac{1}{2}e^T\dot{e} = -c\, e^T Q(e)e + e^T f(e).$$

As shown in Proposition 2.16, there exists a constant $\rho > 0$ such that $Q(e)$ is positive definite in the compact set $\mathcal{Q} \triangleq \{e : ||e||^2 \leqslant \rho\}$ since $Q(\mathbf{0})$ is positive definite as the framework is infinitesimally minimally rigid at $z \in \mathcal{Z}$. Since $f(e)$ is real analytic with $f(\mathbf{0}) = \mathbf{0}_{|\mathcal{E}|\times 1}$ at $z \in \mathcal{Z}$ because of (4.8) and (4.12), it is also locally Lipschitz in $\mathcal{Q}$. Therefore there exists a constant $q \in \mathbb{R}^+$ such that

$$\begin{aligned}\frac{\mathrm{d}V}{\mathrm{d}t} &\leqslant -c\lambda_{\min}||e||^2 + e^T f(e)\\ &\leqslant (-c\lambda_{\min} + q)||e||^2,\end{aligned} \tag{4.30}$$

where $\lambda_{\min}$ is the minimum eigenvalue of $Q(e)$ in $\mathcal{Q}$. Thus if one chooses $c \geqslant c^* > \frac{q}{\lambda_{\min}}$, then the local exponential stability of the origin of (4.29) follows, showing that the formation converges exponentially to the desired shape defined by $\mathcal{Z}$.

For the second part of the proof, we substitute $e(t) \to \mathbf{0}$ and $z(t) \to \mathcal{Z}$ as $t \to \infty$ into (4.2), which gives us

$$\dot{p}(t) - \bar{A}(\mu, \tilde{\mu})z(t) \to \mathbf{0}, \text{ as } t \to \infty.$$

In other words, the velocity of the agents converges exponentially to the desired velocities given by ${}^b\dot{p}_c^*$ and ${}^b\dot{p}_{i_\omega}^*$ for all i. □

The findings in [76, 77], based on the exponential convergence property of the autonomous error signal in (4.29), suggest the implementation of the controller (4.2) using a distributed self-event triggered strategy, i.e., the control law u_i in (4.2) is updated by the agent i at discrete local events, where the self-triggered strategy is based on local information. This scheme can be adopted directly to our proposed motion control law. This allows us to parsimoniously use the sensors for minimizing energy and bandwidth consumption.

Example 4.2. Let us continue with the Example 4.1 and show how to compute $f(e)$ and q in (4.30) for the special case of the triangular formation. First we notice that using (2.24), we can identify $f(e)$ as a linear function of e as follows

$$f(e) = R(z)\overline{A}z = \frac{1}{2}F(\mu, \tilde{\mu})(e + d),$$

where $d = \begin{bmatrix} d_1^2 & d_2^2 & d_3^2 \end{bmatrix}^T$ and $F(\mu, \tilde{\mu}) \in \mathbb{R}^{3\times 3}$ is given by

$$F(\mu, \tilde{\mu}) = \begin{bmatrix} 2(\mu_1 - \tilde{\mu}_1) + \mu_2 - \tilde{\mu}_3 & \mu_2 + \tilde{\mu}_3 & -\mu_2 - \tilde{\mu}_3 \\ -\mu_3 - \tilde{\mu}_1 & 2(\mu_2 - \tilde{\mu}_2) + \mu_3 - \tilde{\mu}_1 & \mu_3 + \tilde{\mu}_1 \\ \mu_1 + \tilde{\mu}_2 & -\mu_1 - \tilde{\mu}_2 & 2(\mu_3 - \tilde{\mu}_3) + \mu_1 - \tilde{\mu}_2 \end{bmatrix}.$$

It can be checked that $F(\mu, \tilde{\mu})d = \mathbf{0}_{3\times 1}$, since $f(\mathbf{0}) = \mathbf{0}_{3\times 1}$. This means that

$$f(e) = \frac{1}{2}Fe. \tag{4.31}$$

If we substitute (4.31) into (4.30) we have that $q = \frac{1}{2}||F||_2$, where $||\cdot||_2$ is the induced 2-norm.

We would like to pinpoint two special cases. Firstly we notice that for $\mu_\omega = \mathbf{0}$ and $\tilde{\mu}_\omega = \mathbf{0}$ we have that $\overline{B}^T\overline{A}z$ is zero in (4.27) because of (4.17). In this case, $f(e) = \mathbf{0}$ for all e. Secondly, if $\mathcal{Z}$ defines an equilateral triangle, then F is skew symmetric in view of Proposition 4.4. This means that $e^TFe = 0$ for all e in (4.30). Therefore both special cases have $q = 0$, and hence for any $c > 0$ the origin of (4.28) is locally exponentially stable. The same special cases can be derived for 3D tetrahedrons just following the same arguments for the triangular case in Example 4.1.

Remark 4.7. Note that the condition (4.19) is independent of $z(t)$ in the triangular case, implying that for all t the centroid of the triangular formation is stationary. Therefore $p_c(t) = \frac{1}{3}\sum_i^3 p_i(0)$.

It is important to note that we are assuming that the measurements done by the agents are not biased with respect to each other, i.e., we do not consider any *undesired* mismatches that will affect the performance of the motion controller.

The results from Theorem 4.6 allow one to design the behaviour of the steady-state motion of the desired formation. However, these results are restricted to the design of the velocities ${}^b\dot{p}_i^*$ for all i, which are obviously defined in O_b. In particular, for the case of having only translational motion, i.e., $\left[\begin{smallmatrix}\mu_\omega \\ \tilde{\mu}_\omega\end{smallmatrix}\right] = \mathbf{0}_{2|\mathcal{E}|\times 1}$, the steady-state orientation of O_b with respect to O_g is unknown and depends on the initial condition $p(0)$. Similarly, for the rotational motion around the centroid, i.e., $\left[\begin{smallmatrix}\mu_v \\ \tilde{\mu}_v\end{smallmatrix}\right] = \mathbf{0}_{2|\mathcal{E}|\times 1}$, the steady-state position of the centroid p_c of the formation also depends on $p(0)$.

Throughout the following two sections, we are going to extend the results of Theorem 4.6 in order to overcome the issues mentioned above. The first extension concerns the control of the steady-state orientation of O_b with respect to O_g in the special case of having only a translational motion. The second extension deals with the control of the instantaneous center of rotation for the formation, which is closely related to the problem of tracking and enclosing a target as briefly mentioned at the beginning of this chapter.

4.3 Translational motion with controlled heading

Suppose that the motion parameters have been assigned such that the steady-state motion of the formation defines a pure translation, i.e., $\left[\begin{smallmatrix}\mu_\omega\\ \tilde{\mu}_\omega\end{smallmatrix}\right] = \mathbf{0}$. In this special case, we are interested in controlling the steady-state orientation of O_b with respect to O_g, and consequently the heading of the translational motion in O_g. This task can be accomplished if we control only one relative position among all the ${}^b z_k$'s with respect to O_g. Without loss of generality we set the relative position z_1 associated to edge $\mathcal{E}_1 = (1, 2)$ for achieving this task. Since $z^* \in \mathcal{Z}$ defines an infinitesimally minimally rigid formation, if we control the orientation of z_1 then the orientation of the rest z_k's will also be controlled. In other words, we are setting the desired orientation of the formation in O_g with the following relation

$$z_1^* = {}^g_b R \, {}^b z_1^*, \tag{4.32}$$

where z_1^* has the orientation with respect to O_g given by the desired rotational matrix ${}^g_b R \in \mathbb{R}^{m\times m}$ defining the steady-state orientation of O_b with respect to O_g.

We will use the following potential function in order to settle the orientation controller for z_1 implemented by the agents in $\mathcal{E}_1$

$$V_{1o} = \frac{1}{2}||z_1 - z_1^*||^2, \tag{4.33}$$

and define the alignment error

$$e_{1o} = z_1 - z_1^*.$$

The orientation controller derived from the gradient of (4.33) is

$$\nabla_{p_1} V_{1o} = -\nabla_{p_2} V_{1o} = e_{1o}. \tag{4.34}$$

Note that we require agents 1 and 2 to know O_g, since they will need ${}^i z_1^*$ for the computation of (4.34) in O_i. Let us introduce some definitions before writing in a compact form the dynamics of the agents including the controller (4.34). Define

the orientation error vector

$$e_o \triangleq \text{col}\{e_{1o}, \ldots, e_{ko}\} \in \mathbb{R}^{m|\mathcal{E}|},$$

where $e_{ko} = \mathbf{0}_{m\times 1}$ for all $k \neq 1$, and the following *augmented* incidence matrix

$$B_a = \begin{bmatrix} B_o & \mathbf{0}_{2\times(|\mathcal{E}|-1)} \\ \mathbf{0}_{(|\mathcal{V}|-2)\times 1} & \mathbf{0}_{(|\mathcal{V}|-2)\times(|\mathcal{E}|-1)} \end{bmatrix} \in \mathbb{R}^{|\mathcal{V}|\times|\mathcal{E}|},$$

where

$$B_o = \begin{bmatrix} 1 & -1 \end{bmatrix}^T,$$

describes the neighbor relationships for the alignment task and B_a has been adjusted to have the same dimensions of B. Now we can extend the control law in (4.2) including the controller (4.34) in agents 1 and 2 as follows

$$u = c(-R(z)^T e - \overline{B}_a e_o) + \overline{A} z. \tag{4.35}$$

As we have done earlier, we derive the following closed-loop system by substituting (4.35) into (2.4)

$$\begin{aligned} \dot{z} &= -c(\overline{B}^T R(z)^T e + \overline{B}^T \overline{B}_a e_o) + \overline{B}^T \overline{A} z \\ \dot{e} &= -2c(R(z)R(z)^T e + R(z)^T \overline{B}_a e_o) + 2D_z^T \overline{B}^T \overline{A} z \qquad (4.36) \\ \dot{e}_o &= \overline{B}_a^T \dot{p} = -c(\overline{B}_a^T R(z)^T e + \overline{B}_a^T \overline{B}_a e_o) + \overline{B}_a^T \overline{A} z. \qquad (4.37) \end{aligned}$$

Without restricting the value for the desired velocity ${}^b\dot{p}_c^*$, we introduce the following assumption on $\mathbb{G}$ and the construction of ${}^b\dot{p}_c^*$.

Assumption 4.8. For 2D (3D) formations the subset of agents $\mathcal{H} \triangleq \{1, 2, 3, (4)\}$ forms a complete subgraph $\mathbb{G}_h \subseteq \mathbb{G}$. In addition for the desired shape $z^* \in \mathcal{Z}$ the agents in $\mathcal{H}$ form a triangle (tetrahedron). The desired velocities ${}^b\dot{p}_i^* = {}^b\dot{p}_c^*$ for $i \in \mathcal{H}$ are constructed employing only the motion parameters derived from $\mathbb{G}_h$.

Under Assumption 4.8, from Example 4.1 we have that

$$\overline{B}_a^T \overline{A} z = \mathbf{0}_{m|\mathcal{E}|\times 1}. \tag{4.38}$$

The Assumption 4.8 is imposed only on the agents in $\mathcal{H}$ in order to make easier the following analysis. For the other agents we construct their motion parameters in μ_v and $\tilde{\mu}_v$ with the only condition of satisfying (4.9).

We are ready now to present and prove the following convergence result.

Theorem 4.9. *Consider a minimally and infinitesimally $\mathcal{Z}$. Suppose that A as in (4.3) is not zero, its motion parameters $\left[\begin{smallmatrix}\mu \\ \tilde{\mu}\end{smallmatrix}\right]$ define a pure translational motion and*

Assumption 4.8 is satisfied. Then, there exists constants $\rho, c^* > 0$ such that the origin of the error systems (4.36) and (4.37) are locally exponentially stable for all $c \geqslant c^*$ in the compact set $\mathcal{Q} \triangleq \{e, e_{1o} : ||\begin{smallmatrix} e \\ e_{1o} \end{smallmatrix}||^2 \leqslant \rho\}$. In particular, the formation will converge exponentially to the shape defined by $z \in \mathcal{Z}$ with $z_1 = z_1^*$, and the velocity of the centroid

$$\dot{p}_c(t) \to {}^g_b R \dot{p}_c^*, \quad t \to \infty \tag{4.39}$$

where ${}^g_b R$ is the desired rotational matrix between O_b and O_g as given in (4.32).

Proof. First we prove the convergence of the formation to the desired shape $\mathcal{Z}$. Consider the following candidate Lyapunov function

$$V = \frac{1}{4}||e||^2 + \frac{1}{2}||e_o||^2, \tag{4.40}$$

whose time derivative is

$$\begin{aligned} \frac{\mathrm{d}V}{\mathrm{d}t} &= \frac{1}{2}e^T\dot{e} + e_o^T\dot{e}_o = -c\Big(e^T R(z)R(z)^T e + e^T R(z)\overline{B}_a e_o \\ &\quad + e_o^T\overline{B}_a^T R(z)^T e + e_o^T\overline{B}_a^T\overline{B}_a e_o\Big) + e^T f(e) \\ &= -c||R(z)^T e + \overline{B}_a e_o||^2 + e^T f(e), \end{aligned} \tag{4.41}$$

where $f(e)$ is as in (4.29) and we have employed (4.38) under the Assumption 4.8. Because of the zero elements of e_o and B_a, we can further rewrite (4.41) as

$$\frac{\mathrm{d}V}{\mathrm{d}t} = -c\begin{bmatrix} e^T & e_{1o}^T \end{bmatrix} Q \begin{bmatrix} e^T & e_{1o}^T \end{bmatrix}^T + e^T f(e), \tag{4.42}$$

where

$$Q = \begin{bmatrix} R(z)R(z)^T & R_{2m}(z)\overline{B}_o \\ \overline{B}_o^T R_{2m}(z)^T & \overline{B}_o^T\overline{B}_o \end{bmatrix},$$

with the matrix $R_{2m}(z)$ being the first $2m$ columns of $R(z)$, regarding the relative positions involving the agents 1 and 2. According to Theorem 2.14, the first term of (4.42) coming from the gradient of a potential function is strictly negative in the compact set $\mathcal{Q}$ for some positive constant ρ excluding the origins of e and e_{1o}. Thus Q is positive definite in $\mathcal{Q}$. Since $f(e)$ is locally Lipschitz with $f(\mathbf{0}) = \mathbf{0}_{|\mathcal{E}|\times 1}$ at $z \in \mathcal{Z}$ there exists a constant $q \in \mathbb{R}^+$ such that

$$\frac{\mathrm{d}V}{\mathrm{d}t} \leqslant (-c\lambda_{\min} + q)\left|\left|\begin{bmatrix} e \\ e_{1o} \end{bmatrix}\right|\right|^2,$$

where $\lambda_{\min}$ is the minimum eigenvalue of Q in $\mathcal{Q}$. Therefore choosing $c \geqslant c^* > \frac{q}{\lambda_{\min}}$ implies that (4.40) is not increasing if $e(0), e_{1o}(0) \in \mathcal{Q}$. Hence the origin of the system formed by (4.36) and (4.37) is exponentially stable.

For the second part of the proof, note that $e_{1o}(t) \to \mathbf{0}$ as $t \to \infty$ implies that $z_1(t) \to z_1^*$ as $t \to \infty$, and because $z(t) \to \mathcal{Z}$ as $t \to \infty$, we have that

$$\dot{p}(t) - \left(\mathbf{1}_{|\mathcal{V}|\times 1} \otimes {}^{g}_{b}R^{b}\dot{p}_c^*\right) \to \mathbf{0}, \text{ as } t \to \infty,$$

i.e., all agents converge to the same velocity $\dot{p}_i^* = {}^{g}_{b}R^{b}\dot{p}_c$. □

Remark 4.10. It is possible to assign only one agent as a leader for the orientation of the formation. In such a case the neighbor relationships for the alignment are described by a directed graph. In fact this directed graph consists of only two nodes and therefore it is strongly connected. The stability analysis can be worked out employing as a potential function the one shown in [21] for strongly connected directed graphs in substitution of the potential $\frac{1}{2}||e_o||^2$ in (4.40).

Remark 4.11. If one does not want any steady-state movement, i.e., $A = \mathbf{0}_{|\mathcal{V}|\times|\mathcal{E}|}$, then the local exponential stability of the desired aligned formation happens for any $c > 0$.

Remark 4.12. The constant q in the proof of Theorem 4.9 is the same as that in the proof of Theorem 4.6. For triangular and tetrahedron formations, the convergence to the desired shape with the desired heading occurs for any $c > 0$ since $q = 0$.

The steady-state behavior of the formation is pretty similar to an unicycle model travelling with a constant speed. We highlight that this configuration is relevant in applications such as [64], where the authors propose a distributed algorithm for enclosing a known area by agents travelling at a constant speed, e.g., airplanes flying at a constant altitude. With our presented work, it is possible to replace each agent in [64] by a subgroup of agents travelling with a constant speed where a leader controls the heading of the subgroup. Note that the standard approach for the translational motion of a rigid formation is to assign a velocity to a leader and the other agents are equipped with local estimators in order to track the velocity of the leader [9]. In the special case of having the formation travelling at a constant speed, we have shown in Theorem 4.9 that such estimators are not necessary, reducing the complexity of the implementation of the control law. In addition in our algorithm the order of the agents in the formation is preserved with respect to the direction of motion. Finally, in Theorem 4.9 we have shown that the convergence to the desired velocity is exponential and not only asymptotic as in the leader-follower case.

4.3.1 Experimental results

In this experiment we will validate the results from Theorem 4.9. We consider four robots that have a square with 225 pixels (45.0mm) for the length of the side as

a prescribed shape $\mathcal{Z}$. The incidence matrix describing the sensing topology for maintaining the prescribed shape and the derived $A(\mu, \tilde{\mu})$ are

$$B = \begin{bmatrix} 1 & 0 & -1 & 1 & 0 \\ -1 & 1 & 0 & 0 & 0 \\ 0 & -1 & 1 & 0 & 1 \\ 0 & 0 & 0 & -1 & -1 \end{bmatrix}, \; A = \begin{bmatrix} \mu_1 & 0 & \tilde{\mu}_3 & \mu_4 & 0 \\ \tilde{\mu}_1 & \mu_2 & 0 & 0 & 0 \\ 0 & \tilde{\mu}_2 & \mu_3 & 0 & \mu_5 \\ 0 & 0 & 0 & \tilde{\mu}_4 & \tilde{\mu}_5 \end{bmatrix}.$$

We designate the robot number 1 to be the agent that controls the orientation of z_1, which is associated to the edge $\mathcal{E}_1 = (1, 2)$. As usual for the experiments we take $l = 1$ for the potential function (2.10), so the implemented control law is

$$u = c(-\overline{B} D_{\hat{z}} e - \overline{B}_a e_o) + \overline{A} z.$$

The chosen speed for the translation is 5 pixels/s (1cm/s), and we set the desired heading of the translational motion to be the same as the one defined by the direction of ${}^b z_1$. Because of simplicity and in order to show that Assumption 4.8 is only a sufficient condition, for achieving the mentioned desired steady-state velocity we set the motion parameters as

$$\mu = \begin{bmatrix} -5 & 0 & 0 & 0 & 5 \end{bmatrix}^T, \; \tilde{\mu} = \begin{bmatrix} -5 & 0 & 0 & 0 & 5 \end{bmatrix}^T. \tag{4.43}$$

At the beginning of the experiment robot 1 has for the desired orientation the vector $z_1^* = \begin{bmatrix} 225 & 0 \end{bmatrix}^T$ pixels. Therefore the desired heading of the formation is zero radians with respect to O_g. The robots start in random positions close to the origin of O_g. During the experiment, once the agent 1 reaches the imaginary vertical line crossing the position $\begin{bmatrix} 1100 & 0 \end{bmatrix}^T$ pixels, the value of z_1^* changes to $\begin{bmatrix} -225 & 0 \end{bmatrix}^T$ pixels. Therefore the formation will switch to a heading of π radians with respect to O_g. The gain c has been set to 3.5×10^{-2}. As a remark the chosen c is smaller than the conservative c^* in Theorem 4.9.

Remark 4.13. Since all the unicycle robots have the same reference point for the feedback linearization, once the system is at $e = \mathbf{0}$ and $e_o = \mathbf{0}$, i.e., all the robots have the same velocity $\dot{p}_c^*$, the headings of the robots achieve consensus, i.e., all the unicycle robots are pointing at the same direction.

We proceed to discuss the experimental results presented in Figure 4.2. The initial positions of the robots are shown in (a) and the squared configuration of the formation with zero rads of heading after 90 seconds is shown in (b). The error and speed plots corresponding to the experiment are shown in (e) and (f). The desired speed of 5 pixels/s (1 cm/s), is achieved in a short time as it is shown in (f). The orientation leader is marked with a red dot in the video captures, as well as its trajectory. The relative position ${}^b z_1$ corresponding to the edge $\mathcal{E}_1 = (1, 2)$ has been

also marked in red, whereas the rest of sensed relative positions have been marked in green. The desired orientation for z_1^* at the beginning is zero rads, so O_g and O_b have the same orientation. The steady-state velocity ${}^b\dot{p}_c^*$ has been designed to have the same direction as ${}^bz_1$. Therefore the steady-state translation of the formation is heading to the right in (b). The norm of the orientation error e_o is shown in (e) in red color. At the time $t = 186$ secs, the orientation leader changes the desired orientation of z_1^* to π rads, i.e., horizontal motion to the left as it can be noticed in (c) and (d). The video capture (c) shows the rearranging of the agents for the new desired orientation. Finally in (d) at time $t = 283$ secs it is shown that the formation achieves the new desired heading of π rads along with the desired speed of 5 pixels/s as it is shown in (f). Note that O_b is only defined once the square is formed.

4.4 Tracking and enclosing a target

The target enclosing problem addresses the scenario of having a team of *enclosing* agents with the objective of surrounding some specific independent target which is either stationary or moving with an unknown (constant) velocity. Furthermore, in orbiting missions, we not only require the agents to surround the target but to circumnavigating it. Many work has been done in this area such as [43, 68] among others. However they usually do not allow the manipulation of the desired formation consisting of the enclosing agents together with the target; all of the agents are usually restricted to follow the same circular trajectory around the target, which is at the center of the circle. It is worth noting that in other works, such as in [54], the complexity of the controller is much higher than the one proposed in this paper using the motion parameters. Furthermore, other drawbacks that are usually present in many works is that all the enclosing agents have to measure their relative positions or distances to the target, and the proposed algorithms have only been tested in 2D scenarios.

It has been shown in Section 4.1 that the instantaneous center of rotation p_r for the desired steady-state motion of the formation is fixed in O_g. Note that for $\dot{p}_c^* = \mathbf{0}_{m\times 1}$, i.e., $\left[\begin{smallmatrix}\mu_v\\ \tilde{\mu}_v\end{smallmatrix}\right] = \mathbf{0}_{2|\mathcal{E}|\times 1}$, the instantaneous center of rotation p_r is coincident with p_c. However the steady-state of p_r in Theorem 4.6 depends on the initial condition $p(0)$. In this section we are going to associate p_r to the target to be enclosed, and without loss of generality we set $p_1 = p_r$. Furthermore, we will assume that $\dot{p}_1 = \hat{v}_1 \in \mathbb{R}^m$ is constant and unknown to the enclosing agents. Let us define

$$B_d \triangleq \tilde{I}B,$$

where $\tilde{I}_{|\mathcal{V}|\times|\mathcal{V}|}$ is obtained from the identity matrix setting its first element to zero. With this operation we are setting all the elements of the first row of B_d to zero.

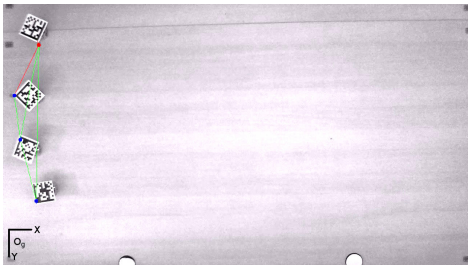

(a) Time $t = 0$ secs.

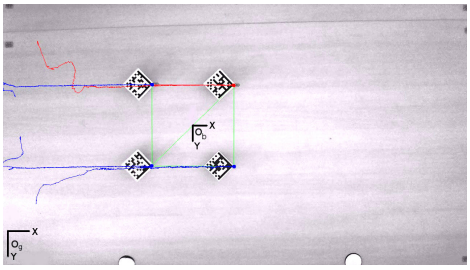

(b) Time $t = 90$ secs.

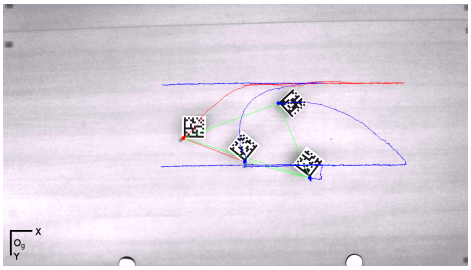

(c) Time $t = 195$ secs.

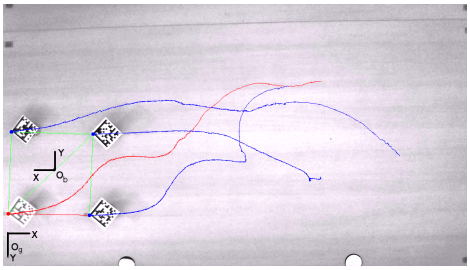

(d) Time $t = 283$ secs.

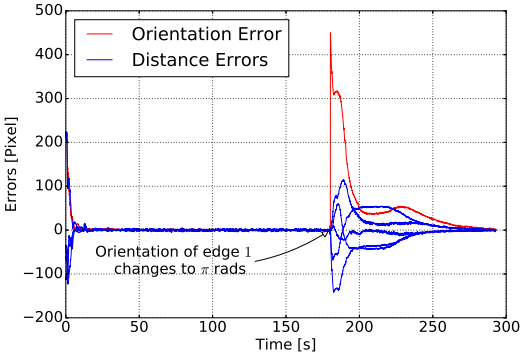

(e)

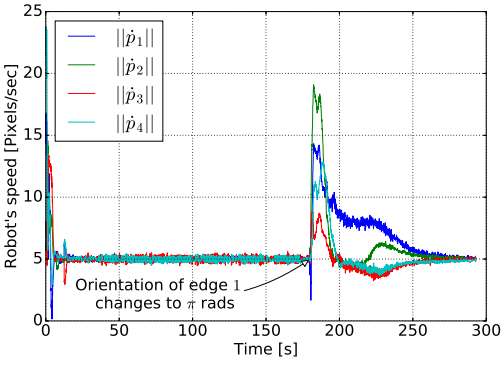

(f)

Figure 4.2: Experimental results of a 2D squared formation traveling with desired heading and speed.

The interpretation for B_d is that some of the enclosing agents are measuring their relative positions with respect to the target, and that obviously the target is not interacting with the rest of the formation.

In order to estimate the unknown $\hat{v}_1$ by the enclosing agents, we will use an estimator $\hat{v}_i$ for each enclosing agent, whose dynamics is

$$\dot{\hat{v}}_i = -\kappa \nabla_{p_i} V,\ i \in \{2, \ldots, |\mathcal{V}|\}, \tag{4.44}$$

where $\kappa \in \mathbb{R}^+$ is a constant gain and V the potential function as used in the formation control. The estimator (4.44) can be written for all the agents in the following compact form

$$\dot{\hat{v}} = -\kappa \overline{B}_d D_z e, \tag{4.45}$$

where $\hat{v} \in \mathbb{R}^{m|\mathcal{V}|}$ is the stacked column vector of $\hat{v}_i$'s. Note that $\dot{\hat{v}}_1 = \mathbf{0}_{m\times 1}$ corresponds to the target, i.e., it does not have any estimator.

Consider the following control law

$$u = -c\overline{B}_d D_z e + \overline{A}(\mu, \tilde{\mu}) z + \hat{v}, \tag{4.46}$$

where $c \in \mathbb{R}^+$ is a positive gain. Since all the elements of the first row of B_d are zero, the first term of the control law in (4.46) is not playing a role in the target's position p_1. The motion parameters of $A(\mu, \tilde{\mu})$ have been designed to have ${}^b p_1 = {}^b p_r$ as the desired steady-state instantaneous center of rotation for the desired shape $z \in \mathcal{Z}$. Recall that the desired infinitesimally and minimally rigid formation includes p_1 and this is why we can calculate the needed motion parameters. For example if by design we set ${}^b p_1 = {}^b p_r = {}^b p_c$ then $\left[\begin{smallmatrix}\mu_v \\ \tilde{\mu}_v\end{smallmatrix}\right] = \mathbf{0}_{2|\mathcal{E}|\times 1}$ and $\left[\begin{smallmatrix}\mu_\omega \\ \tilde{\mu}_\omega\end{smallmatrix}\right]$ is as shown in Section 4.1. In general, however, the instantaneous center of rotation can be inside or outside of the area or volume defined by the enclosing agents. Note that since $p_1 = p_r$, the motion parameters of the target are zero, i.e., the elements of the first row of $A(\mu, \tilde{\mu})$ are zero. Therefore the second term in (4.46) is not playing any role in the dynamics of p_1. This is an obvious requirement since the target is not collaborating with the rest of the enclosing agents.

Our approach has two obvious limitations. Firstly we require to have more than two (three) agents including the target in 2D (3D) in order to form an infinitesimally and minimally rigid framework. Secondly, because of the definition of infinitesimally and minimally rigid framework, the desired shape including the target must exclude the ones where all the agents are collinear or coplanar in 2D or 3D respectively.

Define the error velocity as

$$e_v = \hat{v} - (\mathbf{1}_{|\mathcal{V}|\times 1} \otimes \hat{v}_1).$$

Note that the first m elements of e_v are zero, therefore

$$\overline{B}^T e_v = \overline{B}_d^T e_v, \tag{4.47}$$

and in addition one can check the following identity as well

$$B^T B_d = B^T \tilde{I} B = B^T \tilde{I}^T \tilde{I} B = B_d^T B_d. \tag{4.48}$$

Before stating the main result of this section, let us write down the closed-loop dynamics by substituting (4.46) in (2.4)

$$\dot{z} = \overline{B}^T \dot{p} = -c\overline{B}_d^T \overline{B}_d D_z e + \overline{B}^T A(\mu, \tilde{\mu}) z + \overline{B}_d^T e_v \tag{4.49}$$

$$\dot{e} = 2D_z^T \dot{z} = -2cD_z^T \overline{B}_d^T \overline{B}_d D_z e + 2f(e) + 2D_z^T \overline{B}_d^T e_v \tag{4.50}$$

$$\dot{e}_v = \dot{\hat{v}} = -\kappa \overline{B}_d D_z e, \tag{4.51}$$

where we have employed the identities (4.47) and (4.48), $f(e)$ is the same as in (4.29), and for the third term of (4.49) we have used the following well known fact

$$\overline{B}^T(\mathbf{1}_{|\mathcal{V}|\times 1} \otimes \hat{v}_1) = \overline{B}_d^T(\mathbf{1}_{|\mathcal{V}|\times 1} \otimes \hat{v}_1) = \mathbf{0}_{m|\mathcal{E}|\times 1}. \tag{4.52}$$

Theorem 4.14. *Suppose that the steady-state motion of the rigid formation ${}^b z^* \in \mathcal{Z}$ defined by the motion parameters μ and $\tilde{\mu}$ has ${}^b p_1^*$ as the instantaneous center of rotation. Suppose that agent 1 is a free target with constant velocity $\hat{v}_1$ which is unknown to the rest of the enclosing agents. Then there exist constants $\rho, c^* > 0$ such that the origins of (4.50) and (4.51) are locally asymptotically stable in the compact set $\mathcal{Q} \triangleq \{e, e_v : || \begin{smallmatrix} e \\ e_v \end{smallmatrix} ||^2 \leqslant \rho\}$. In particular, the formation will converge asymptotically to the shape defined by $\mathcal{Z}$, and the motion of the enclosing agents converge to a rotation around the target with angular speed $||\omega|| = \frac{||{}^b \dot{p}_i^*||}{||{}^b p_1^* - {}^b p_i^*||}$, $i \in \{2, \ldots, |\mathcal{V}|\}$.*

Proof. Consider the following candidate Lyapunov function

$$V = \frac{\kappa}{4}||e||^2 + \frac{1}{2}||e_v||^2,$$

where κ is as in (4.44), with time derivative given by

$$\begin{aligned}
\frac{\mathrm{d}V}{\mathrm{d}t} &= \frac{\kappa}{2} e^T \dot{e} + e_v^T \dot{e}_v \\
&= -\kappa c e^T D_z^T \overline{B}_d^T \overline{B}_d D_z e + \kappa e^T f(e) + \kappa e^T D_z^T \overline{B}_d^T e_v \\
&\quad - \kappa e_v^T \overline{B}_d D_z e \\
&\leqslant \kappa(-c\lambda_{\min} + q)||e||^2,
\end{aligned} \tag{4.53}$$

where $f(e)$ is as in (4.29) and q is obtained from $f(e)$ since it is locally Lipschitz

with $f(\mathbf{0}) = \mathbf{0}_{|\mathcal{E}|\times 1}$ if $z \in \mathcal{Z}$. Note that $M(e) = D_z^T \overline{B}_d^T \overline{B}_d D_z$ is not defined by the rigidity matrix $R(z)$ because of B_d. Nevertheless it can be checked that $M(0)$ is still positive definite if for $z \in \mathcal{Z}$ the framework is infinitesimally and minimally rigid. Therefore $M(e)$ is positive definite for some $\rho \leqslant \rho_1 \in \mathbb{R}^+$ in the compact set $\mathcal{Q}$, and then $\lambda_{\min}$ in (4.53) is the minimum eigenvalue of $M(e)$ in $\mathcal{Q}$. If one chooses $c \geqslant c^* > \frac{q}{\lambda_{\min}}$, then the time derivative (4.53) is not increasing, and it is zero if and only if $e = \mathbf{0}$. For such case, we can conclude that the shape of the formation converges to $z^* \in \mathcal{Z}$, which means that the steady-state motion of the agents will not distort the desired shape. Thus following a similar argument as in Section 4.1, the largest invariant set of the closed-loop system (4.49), (4.50) and (4.51) with $e = \mathbf{0}$ and $z^* \in \mathcal{Z}$ is given by

$$\mathcal{T} \triangleq \left\{ \hat{v} \,:\, D_{z^*}^T \overline{B}^T \left(\overline{S}_1 D_{z^*} \mu + \overline{S}_2 D_{z^*} \tilde{\mu} + \hat{v} \right) = \mathbf{0} \right\}. \tag{4.54}$$

Since $\hat{v}_1$ in $\hat{v}$ is fixed, only two steady-state motions for the agents are possible when $\hat{v} \in \mathcal{T} = \mathcal{T}_u \cup \mathcal{T}_d$. In the set $\mathcal{T}_u$ all the agents travel with the same velocity $\dot{p}_i = \hat{v}_1$ and hence $||e_v||^2 = \rho_2 \in \mathbb{R}^+$. In the set $\mathcal{T}_d$ the enclosing agents rotate around p_1 with $||e_v|| = 0$. Therefore invoking the LaSalle's invariance principle, we have that the origins of e_v and e defining $z \in \mathcal{Z}$ are locally asymptotically stable in $\mathcal{Q}$ with $\rho < \min\{\rho_1, \rho_2\}$ and

$$\dot{p}(t) - \overline{A}(\mu, \tilde{\mu}) z(t) - (\mathbf{1}_{|\mathcal{V}|\times 1} \otimes \hat{v}_1) \to \mathbf{0},\ t \to \infty, \tag{4.55}$$

which defines the steady-state rotational movement of the enclosing agents around the target. The steady-state angular speed of the enclosing agent i around the target is its speed over the radius of the rotation. Since the target is moving with velocity $\hat{v}_1$ we have to compensate it in the following formula

$$||\omega|| = \frac{||\dot{p}_i^* - \hat{v}_1||}{||p_1^* - p_i^*||} = \frac{||{}^b\dot{p}_i^*||}{||{}^b p_1^* - {}^b p_i^*||},\ i \in \{2, \ldots, |\mathcal{V}|\}, \tag{4.56}$$

where we have employed (4.55). □

Remark 4.15. For the triangular formation consisting of three agents, one being the target and the other two the enclosing ones, if $\mathcal{Z}$ defines an equilateral triangle, then we have that $e^T f(e) = e^T F e = 0$ since F is skew symmetric in view of Proposition 4.4. Therefore one can choose any $c > 0$ since $q = 0$ in (4.53). Also note that q is the same constant in the proofs of Theorems 4.14 and 4.6.

Remark 4.16. The minimum number of enclosing agents sensing their relative positions with respect to the target is the same as the minimum number of edges needed for a node belonging to an infinitesimally and minimally rigid framework. Therefore for planar frameworks the number is two and for 3D frameworks the

number is three.

Remark 4.17. The estimation of the constant velocity of the target is based on the internal model principle as it has been used in [9] or in Chapter 3. This implies that the velocity of the target might be also driven by a superposition of finite sinusoidal signals with known frequency but unknown phase and amplitude. In such a case, the dynamics of the estimator (4.45) have to be modified in order to include such frequencies.

Remark 4.18. The enclosing agents employ their own local coordinate system in view of Lemma 4.1. Therefore each enclosing agent i estimates the velocity of the target $\hat{v}_1$ in O_i.

Since $\hat{v}_1$ is unknown, the conservative region of attraction $\mathcal{Q}$ is difficult to stablish or estimate. Nevertheless we can avoid the undesired equilibrium set $\mathcal{T}_u \subset \mathcal{T}$ as in (4.54) when $\rho_2 \leqslant \rho \leqslant \rho_1$. Firstly note that the constants ρ_1 and ρ_2 are mainly determined by $p(0)$ and $\hat{v}(0)$ respectively. Secondly we know that $\mathcal{T}_u$ determines a pure translation for all the agents. Suppose that the enclosing agents can measure the angular velocity ${}^i\omega$, e.g., with a gyroscope. If $\hat{v}(t)$ converges to $\mathcal{T}_u$, then ${}^i\omega$ will converge to zero as fast as $z(t)$ approaches $\mathcal{Z}$. Furthermore, u_i for all i will converge to $\hat{v}_1$. Therefore, we can program the agents such that when ${}^i\omega$ is *almost zero* at $t = t^*$, their estimators are reset to $\hat{v}_i(t^*) = u_i(t^*)$. Since $z(t^*)$ is *very close* to $\mathcal{Z}$, then certainly the errors $e(t^*)$, $e_v(t^*) \in \mathcal{Q}$ with $\rho < \rho_2$.

In the case that we do not require the enclosing agents to rotate around the target, we can combine the results of the Theorems 4.9 and 4.14. The result of such combination is: the enclosing agents estimate the unknown velocity of the target; the enclosing agents form a rigid formation together with the target, whose orientation with respect to the target can be determined by a leader. Furthermore in such a special case we have that $A = \mathbf{0}_{|\mathcal{V}|\times|\mathcal{E}|}$, and therefore $q = 0$ in Theorems 4.9 and 4.14.

We finish by emphasizing again that the results presented here do not need measuring any relative velocity, and not all of the enclosing agents need to measure their relative positions with respect to the target agent.

4.4.1 Experimental results

We consider the scenario of having three pursuers and one independent target, set as agent 1, with constant velocity $\hat{v}_1 = \begin{bmatrix} -3 & 0.35 \end{bmatrix}^T$ pixels/s. The velocity $\hat{v}_1$ is unknown for the three pursuers. We ask the pursuers to form the shape in Figure 4.3 together with the target. The incidence matrix B corresponding to the sensing

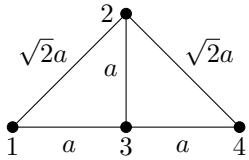

Figure 4.3: Desired shape for the three pursuers together with the target. The target corresponds to the node number 1 and a is a scale factor.

topology for the shape in Figure 4.3 and the derived matrix $A(\mu, \tilde{\mu})$ are

$$B = \begin{bmatrix} 1 & 0 & -1 & 0 & 0 \\ -1 & 1 & 0 & -1 & 0 \\ 0 & -1 & 1 & 0 & -1 \\ 0 & 0 & 0 & 1 & 1 \end{bmatrix}, \; A = \begin{bmatrix} \tilde{\mu}_1 & 0 & \tilde{\mu}_3 & 0 & 0 \\ \mu_1 & \mu_2 & 0 & \tilde{\mu}_4 & 0 \\ 0 & \tilde{\mu}_2 & \mu_3 & 0 & \tilde{\mu}_5 \\ 0 & 0 & 0 & \mu_4 & \mu_5 \end{bmatrix}.$$

We ask the pursuers to maintain the following set of inter-agent distances

$$d = \begin{bmatrix} \sqrt{2}a & a & a & \sqrt{2}a & a \end{bmatrix}^T, \tag{4.57}$$

where $a = 130$ pixels. We choose $l = 1$ for the potential (2.10) and implement the controls (4.45) and (4.46) to the robots. Note that again since $l = 1$, D_z has to be replaced by $D_{\tilde{z}}$. The motion parameters for orbiting around the target p_1 are

$$\mu = \begin{bmatrix} 0 & 0 & 0 & -2a\gamma\sqrt{2} & 2a\gamma \end{bmatrix}^T, \; \tilde{\mu} = \begin{bmatrix} 0 & a\gamma & 0 & -a\gamma\sqrt{2} & 0 \end{bmatrix}^T, \tag{4.58}$$

where $\gamma \in \mathbb{R}$. Note that μ_1 and $\tilde{\mu}_3$ are zero since they correspond to the target. The agents 2 and 3 are only using $\tilde{\mu}_4$ and $\tilde{\mu}_2$ respectively since z_4^* and z_2^* are perpendicular to z_1^*. We set the desired stationary angular speed to 0.038 rads/s, therefore from (4.56) the value of γ is

$$||\omega^*|| = \frac{||{}^b\dot{p}_3^*||}{||{}^bp_1^* - {}^bp_3^*||} = \frac{a\gamma}{a} = \gamma = 0.038\text{rads/s}.$$

We have set the control gains κ and c to 1×10^{-2} and 1×10^{-1} respectively in (4.45) and (4.46). The gain κ has been chosen small in order to prevent saturation in the robots. The chosen c is smaller than c^* in $\mathcal{Q}$, showing the conservative result of c^* in Theorem 4.14. The initial values $\hat{v}_i(0)$ for $i \in \{2, 3, 4\}$ of the estimators have been set to zero.

We proceed to discuss the experimental results in Figure 4.4. The pursuers start at the left of the scene whereas the target starts at the right in (a). The pursuers are tagged with blue dots and the target with a red dot as well as their trajectories.

The sensed relative positions are marked with colors, the pink ones concern the target and the green ones concern only the pursuers. Note that there is a pursuer that does not track the target at all. The pursuers have two tasks. The first one is to form the prescribed shape with the target as the one shown in Figure 4.3 with the side lengths defined in (4.57). The second one is to orbit around the target with an angular speed $||\omega^*|| = 0.0308$ rads/s. The designed motion parameters employed for satisfying such requirements are in (4.58). In addition the target travels with a constant velocity $\hat{v}_1 = [-3 \quad 0.35]^T$ pixels/sec, which is unknown to the pursuers. We have set the control gains c and κ to 1×10^{-1} and 1×10^{-2}. The gain κ has been set low in order to prevent the E-pucks to do not reach the saturation level in their velocities. We show the estimation of the two components of $\hat{v}_1$ by the pursuers in (e) and (f). The asymptotic convergence of the estimated v is slow due to the low values of κ and c. The convergence of the distance errors to zero in (g) with the estimation of $\hat{v}_1$, lead for the convergence of the angular speed of the pursuers around the target to $||\omega^*||$ as it is shown in (h). The angular speed around the target is computed as $||\omega_i|| = \frac{||(P^{\perp}_{({}^b p_1 - {}^b p_i)})\dot{p}_i||}{||{}^b p_1 - {}^b p_i||}$. It is shown from (b) to (d) how the pursuers enclose the target and circumnavigate it with the prescribed shape shown in Figure 4.3.

4.5 Concluding remarks

In this chapter we have presented a distributed motion controller for rigid formations, which is compatible with the popular gradient-based controllers. The proposed controller allows us to design the steady-state formation motion in the desired shape with respect to a frame attached to the rigid formation. The steady-state velocity vector can be decomposed into two independent terms: one for the constant translation of the centroid of the formation and the other for a constant rotational formation motion around its centroid. Such design has been achieved by adding distributed motion parameters to the prescribed distances between the agents. Two main applications based on the motion controller have been presented: the first is controlling the heading of a pure translational formation motion and the second is addressing the problem of enclosing and tracking a target.

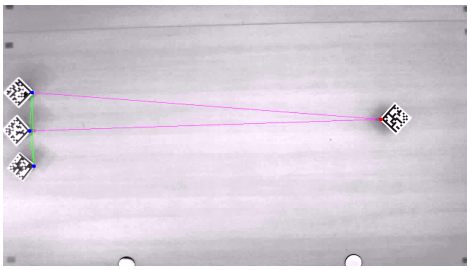

(a) Time $t = 0$ secs.

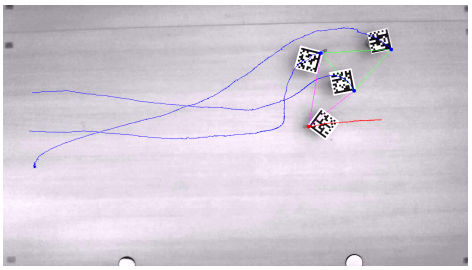

(b) Time $t = 68$ secs.

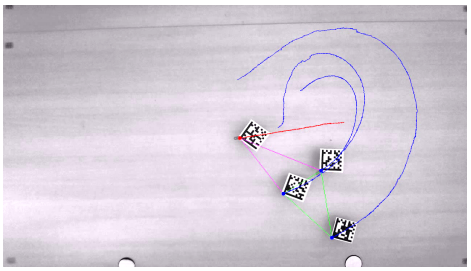

(c) Time $t = 135$ secs.

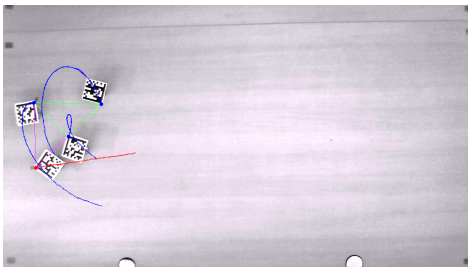

(d) Time $t = 335$ secs.

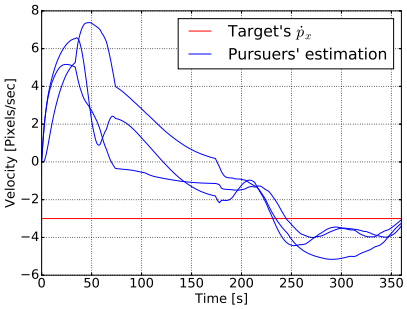

(e)

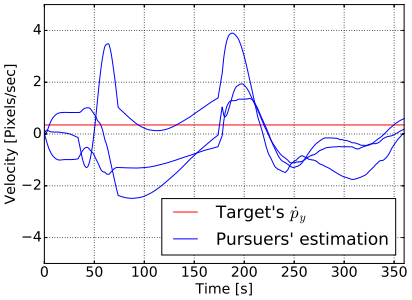

(f)

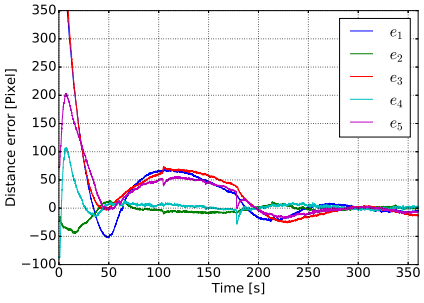

(g)

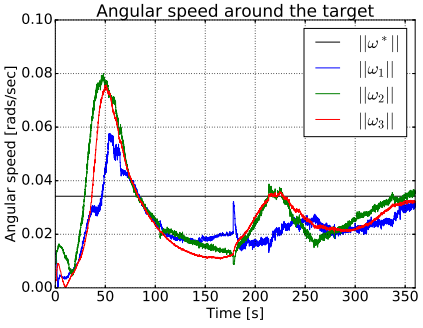

(h)

Figure 4.4: Experimental results of a team of three pursuers tracking and enclosing an independent target.

Chapter 5
Scaling-control of formations

Look behind you, a three-headed scaled monkey!
The secret of Monkey Island.

SCALING the shape of a formation of team of robots is a natural way of interacting with the surrounding environment, e.g., it might be desirable to rescale the formation in situations of obstacle avoidance or for changing the area covered by the team. Work addressing this topic has been done, however some drawbacks in the approaches presented in [6, 70] are that they require global information, e.g., knowing about the centroid of the formation or about the desired velocity by all the robots and that they have to compromise the performance among the different tasks, i.e., they cannot achieve precisely the desired shape, the desired steering and the desired scaling rate simultaneously. This is inherently due to the fact of having a strategy based on assigning priorities to the different tasks. In fact, a common practice for changing the scale of the shape is to command a new setting point for the desired shape, i.e., a step input. This is a non desirable practice in actual systems since the exponential convergence nature of the distance-based gradient controller presented in Chapter 2 makes easier to reach saturation levels in the system's actuators if we are far from the equilibrium. Moreover, besides of the exponential convergence, there is not any other result characterizing the transient behaviour between two scaled shapes by just employing a step input.

In this chapter we will continue extending the findings from the previous chapter by proposing a distributed algorithm for controlling the following three tasks simultaneously:

i) Formation scale-free shape keeping, i.e., the formation's shape will converge to a shape in a set of a desired infinitesimally and minimally congruent rigid $\mathcal{Z}_{\mathcal{S}}$;

ii) Steering the scale-free formation as a whole with a combination of a constant translation velocity and a constant angular velocity applied at its centroid;

iii) *Precise scaling* of the formation, i.e., controlling precisely the rate of growing

or shrinking of a shape formation in $\mathcal{Z}_{\mathcal{S}}$. The proposed control law even allows the changing between two different shapes.

In particular by precise scaling we mean to make the formation to converge to an infinitesimally and minimally congruent rigid shape in $\mathcal{Z}_{\mathcal{S}}$ for a given desired time varying scaling signal $s(t)$. The results of this chapter employ the findings in [88] about the already introduced bearing rigidity theory. In fact these findings have been recently employed in order to control the translational motion of a rigid formation with a precise scaling rate in [89] with a similar approach to the position-based control in [9], where all the agents share a common frame of coordinates and they want to achieve a set of relative unit vectors represented in such a common reference. In [89] the translational motion is achieved by assigning the desired velocity to at least two leaders, where the rest of the followers estimate such a velocity. In order to control the rate of growing of the scale the leaders' velocity is not free of choice and it is constrained by knowing the desired velocity of the centroid together with its position, i.e., more global information is required.

We will show in this chapter that our proposed solution is different and it stands on the distance-based control strategy. The approach presented in this chapter has several advantages such as not requiring a common frame of coordinates for the agents, it is estimator free and it does not require complex global information like the position of the centroid and its desired velocity. Furthermore, the distance-based approach also allows rotational motion, a feature lost in the position-based control since the stationary orientation is globally fixed by design.

By unifying the following two results on motion control by the distributed motion parameters and on bearing rigidity theory, one can control simultaneously both the motion of the prescribed rigid shape and its scaling in a precise way, i.e., not distorting a scale-free shape for a desired rate of growing/shrinking. Moreover, following the same strategy we can show how to control the changing of the shape among different rigid formations.

In addition to the formation-motion-scaling controller, we present two algorithms as natural extensions of the work in [88] where the scale of a rigid formation is chosen by controlling only the length of one edge and the shape is controlled by keeping the relative unit vectors constant. This proposed strategy is considerable simpler approach than those in the recent works of [22, 53, 62], where for the same task they require the use of estimators, i.e., leader-follower approach, or the computation of specific gains.

The rest of the chapter is organized as follows. In Section 5.1 we present two algorithms where the scale of the infinitesimally and minimally rigid shape is determined by controlling only one edge. Section 5.2 explains the design of the motion controller with precise scaling/morphing of the formation by introducing distributed parameters in a distance-based controller. Also in this section we

demonstrate the exponential convergence of our proposed algorithm. As usual we present experimental results at the end of each section.

5.1 Scaling-control by controlling one edge

In this subsection we are going to employ the position-based strategy in order to control a team of agents for forming an infinitesimally and minimally rigid shape where the scale will be determined by controlling only the inter-distance associated to one edge. The difference with respect to other works such as in [22, 53, 62] is that we do not require the use of estimators nor the knowledge on stabilizing control gains a priori. Furthermore, our approach uses only local frame of coordinates, i.e., no common frame of coordinates is assumed. In this case, we can relax the sensing requirements for the robots, for instance most of them can work with only directional sensors, i.e., they measure $\hat{z}_k$, except for the *scaling leaders*.

For a desired deployment of agents given by an infinitesimally and minimally rigid $\mathcal{Z}_R$, one can always construct it as a combination of the scale-free shape $\hat{\mathcal{Z}}_R$ and the scale can be set by $\mathcal{Z}_s$. In fact many of the information in $\mathcal{Z}_s$ is redundant because of bearing rigidity and we only need to know the scale factor s for only one edge. Thus for the gradient based control in (2.9) we propose the following potential function, which has clearly a minimum at $\mathcal{Z}_R$ with $||z_k|| = sd_k$ for all $k \in \{1, \dots, |\mathcal{E}|\}$

$$V(z) = \frac{1}{2}\sum_{k=1}^{|\mathcal{E}|} ||\hat{z}_k - \hat{z}_k^*||^2 + \frac{1}{2}(||z_1|| - sd_1)^2, \tag{5.1}$$

where the first term uses the $\hat{z}_k^*$'s from the desired scale-free shape $\hat{\mathcal{Z}}_R$ and the second term is only using sd_1 from $\mathcal{Z}_s$ (assuming without loss of generality that $\mathcal{E}_1 = (1, 2)$) with $s \in \mathbb{R}^+$ being a scale factor.

Let $B \in \mathbb{R}^{|\mathcal{V}|\times|\mathcal{E}|}$ be the incidence matrix used for defining $\hat{\mathcal{Z}}_R$ and let the matrix ${}^sB \in \mathbb{R}^{|\mathcal{V}|\times|\mathcal{E}|}$ to have the same first column as B and set the rest of elements to zero. With these definitions at hand we can write the control input in (2.4) derived

from the gradient of (5.1) as

$$\begin{aligned} u_i &= -\sum_{k=1}^{|\mathcal{E}|}\Bigg(b_{ik}\left(I_m-\hat{z}_k\hat{z}_k^T\right)\frac{1}{||z_k||}(\hat{z}_k-\hat{z}_k^*) \\ &\quad + {}^sb_{ik}\hat{z}_k\Big(||z_k||-sd_k\Big)\Bigg) \\ &= \sum_{k=1}^{|\mathcal{E}|}\Bigg(-b_{ik}P^{\perp}_{\hat{z}_k}\frac{1}{||z_k||}\hat{z}_k^* - {}^sb_{ik}\hat{z}_k\Big(||z_k||-sd_k\Big)\Bigg), \end{aligned} \tag{5.2}$$

where since $P_x^{\perp}$ is the orthogonal projection operator over the vector x, we have that $P_x^{\perp}x=\mathbf{0}$, and b_{ik} and ${}^sb_{ik}$ are the elements of B and ${}^sB$ respectively. We can further write in a compact form the dynamics of all the agents as

$$\dot{p} = -\overline{B}D_{P^{\perp}_{\hat{z}}}\overline{D}_{\tilde{z}}e_f - {}^s\overline{B}D_zD_{\tilde{z}}e_s, \tag{5.3}$$

where $e_f\in\mathbb{R}^{m|\mathcal{E}|}$ is the stacked vector of *formation errors* $e_{f_k}=\hat{z}_k-\hat{z}_k^*$, $e_s\in\mathbb{R}^{|\mathcal{E}|}$ is the stacked vector of the *scale errors* $e_{s_k}=||z_k||-sd_k$ and we recall from Chapter 2 that $P^{\perp}_{\hat{z}}\in\mathbb{R}^{m|\mathcal{E}|\times m}$ is the stacked matrix of operators $P^{\perp}_{\hat{z}_k}$ and $\tilde{z}\in\mathbb{R}^{|\mathcal{E}|}$ is the stacked vector of $\frac{1}{||z_k||}$.

Using these notations, the closed-loop autonomous system is given by

$$\dot{z} = -\overline{B}^T\overline{B}D_{P^{\perp}_{\hat{z}}}\overline{D}_{\tilde{z}}e_f - \overline{B}^T{}^s\overline{B}D_zD_{\tilde{z}}e_s \tag{5.4}$$

$$\begin{aligned} \dot{e}_f &= -\overline{D}_{\tilde{z}}D_{P^{\perp}_{\hat{z}}}\overline{B}^T\overline{B}D_{P^{\perp}_{\hat{z}}}\overline{D}_{\tilde{z}}e_f \\ &\quad - \overline{D}_{\tilde{z}}D_{P^{\perp}_{\hat{z}}}\overline{B}^T{}^s\overline{B}D_zD_{\tilde{z}}e_s \end{aligned} \tag{5.5}$$

$$\dot{e}_{s_1} = \hat{z}_1(u_1-u_2). \tag{5.6}$$

Note that because of the zero elements of ${}^sB$, the scaled errors e_k for $k\in\{2,\dots,|\mathcal{E}|\}$ do not play any role in the above closed loop system. Now we are ready to present the following result.

Theorem 5.1. *There exists a positive constant ρ such that the origin of the error system (5.5)-(5.6) is asymptotically stable in the compact set $\mathcal{Q}\triangleq\{\frac{1}{2}||e_{s_1}||^2+\frac{1}{2}||e_f||^2\leqslant\rho\}$, i.e., the desired shape $\mathcal{Z}_R$ is locally asymptotically stable with only robots 1 and 2 controlling the scale s of the shape. Furthermore, the position of all the robots converge to p^* determined by the initial conditions $p(0)$.*

Proof. The fact that the agents 1 and 2 are choosing the scale of the formation follows from the definition of $\mathcal{Z}_R$ as the combination of $\mathcal{Z}_s$ and $\hat{\mathcal{Z}}_R$ where we are only taking the edge $\mathcal{E}_1=(1,2)$ from $\mathcal{Z}_s$ for defining the scale of the desired shape.

For proving the stability of the desired formation, consider the following Lya-

punov candidate function

$$V(e_f, e_{s_1}) = \frac{1}{2}||e_f||^2 + \frac{1}{2}||e_{s_1}||^2, \tag{5.7}$$

whose time derivative is given by

$$\begin{aligned}\frac{\mathrm{d}V}{\mathrm{dt}} &= e_f^T \dot{e}_f + e_{s_1}^T \dot{e}_{s_1} \\ &= -\begin{bmatrix} e_f^T & e_s^T \end{bmatrix} \begin{bmatrix} \overline{D}_{\tilde{z}} & \mathbf{0} \\ \mathbf{0} & D_{\tilde{z}} \end{bmatrix} H(z) \begin{bmatrix} \overline{D}_{\tilde{z}} & \mathbf{0} \\ \mathbf{0} & D_{\tilde{z}} \end{bmatrix} \begin{bmatrix} e_f \\ e_s \end{bmatrix} \\ &= -||\overline{B} D_{P_{\tilde{z}}^\perp} \overline{D}_{\tilde{z}} e_f + {}^s\overline{B} D_z D_{\tilde{z}} e_s||^2 \\ &= -||\nabla_p V(z)||^2 \end{aligned} \tag{5.8}$$

where

$$H(z) = \begin{bmatrix} D_{P_{\tilde{z}}^\perp} \overline{B}^T \overline{B} D_{P_{\tilde{z}}^\perp} & D_{P_{\tilde{z}}^\perp} \overline{B}^T {}^s\overline{B} D_z \\ D_z^T {}^s\overline{B}^T \overline{B} D_{P_{\tilde{z}}^\perp} & D_z^T {}^s\overline{B}^T {}^s\overline{B} D_z \end{bmatrix}. \tag{5.9}$$

Consider the compact set $\mathcal{Q} \triangleq \{\frac{1}{2}||e_{s_1}||^2 + \frac{1}{2}||e_f||^2 \leqslant \rho\}$ with $\rho \in \mathbb{R}^+$ sufficiently small. It follows from Theorem 2.14 and LaSalle's invariance principle that (5.8) implies the asymptotic stability of the origin of e_f and e_{s_1} in $\mathcal{Q}$ for sufficiently small ρ. Therefore $p(t)$ converges asymptotically to a point p^* such that $\overline{B}^T p^* = z^* \in \mathcal{Z}_R$. Since the centroid of the formation is fixed and the orientation of the formation with respect to O_g converges to the one determined by R we can conclude that p^* must be unique. □

In general $H(z)$ is not positive-definite, but Theorem 2.14 guarantees the stability of the desired shape if the initial conditions start close to it. We know that not always all the e_{f_k}'s are free of choice for obvious geometrical reasons. For example, in distance-based control for an infinitesimally rigid formation one can always write (locally) all the inter-distances based only on the inter-distances of an underlying infinitesimally and minimally rigid formation as it was shown in [59]. In position-based control the same reasoning applies to the inter-positions if there exist loops in $\mathcal{G}$. These geometrical findings are intimately related to the fact that the null space of $H(z)$ is avoided in a neighborhood of the desired shape in view of Theorem 2.14.

Remark 5.2. Based on the works in [59] and [88], where in the former, the authors study the local exponential convergence of distance-based infinitesimally rigid formations while in the latter the authors study the same property for the bearing-based formation control, we conjecture that the convergence rate in Theorem 5.1 is also exponential. This is due to the similarity in the control law, i.e., gradient-based law, and the Lyapunov function admits a similar time-derivative as in (5.8). The

difficulty in our case is to analyze $H(z)$ in (5.9) which is only positive semi-definite in the neighborhood of $\mathcal{Z}_R$.

We would like to highlight, as it is pointed out in [88], that the control law in Theorem 5.1 requires both the directional and range sensing information because of the computation of $D_{\tilde{z}}$. This range sensing requirement can be dropped for all the agents excepting for the agents 1 and 2, e.g., by using the control law

$$u = -\overline{B} D_{P_{\tilde{z}}^{\perp}} e_f - {}^{s}\overline{B} D_z e_s. \tag{5.10}$$

The stability of the closed loop system at the desired shape can be analyzed using the same Lyapunov function as in (5.7). In this case, its time derivative has a slightly different form and is given by

$$\frac{\mathrm{d}V}{\mathrm{d}t} = -\begin{bmatrix} e_f^T & e_s^T \end{bmatrix} \begin{bmatrix} \overline{D}_{\tilde{z}} & \mathbf{0} \\ \mathbf{0} & D_{\tilde{z}} \end{bmatrix} H(z) \begin{bmatrix} e_f \\ e_s \end{bmatrix}. \tag{5.11}$$

In the particular cases where all the z_k in $\mathcal{Z}_R$ have almost the same norm, e.g., the shape is composed of almost equilateral triangles or tetrahedra, the Lyapunov function in the neighborhood of the prescribed shape is decreasing and the trajectory converges to the largest invariance set in $\left\{(e_f, e_s) : \left[\begin{smallmatrix} e_f^T & e_s^T \end{smallmatrix}\right] \left[\begin{smallmatrix} \overline{D}_{\tilde{z}} & \mathbf{0} \\ \mathbf{0} & D_{\tilde{z}} \end{smallmatrix}\right] H(z) \left[\begin{smallmatrix} e_f \\ e_s \end{smallmatrix}\right] = 0\right\}$ which is given by the desired shape.

For covering more general shapes we refer to the analysis presented in [88], where the authors show the non-positiveness of a similar expression as the one given in (5.11). As it has been discussed in Section 4.3, in addition to not requiring range sensors for the agents, we can also relax the requirement of having two agents controlling the scale since only one agent can do such a task. Indeed if we choose only the agent 1 for controlling the magnitude of z_1, then in order to show the stability of the system, instead of using the term $\frac{1}{2}||e_{s_1}||^2$ in the Lyapunov function (5.7), we can employ an energy function for direct strongly connected graphs as it has been suggested in [21]. Note that in such a situation the graph defining the sensing topology for controlling the scale of the formation is not undirected anymore, therefore we lose the property about the centroid as stated in Lemma 2.17.

5.1.1 Distributed scaling-control without a common frame of coordinates

In the previous section, the robots have lost the nice property of working only with their local frame of coordinates due to the use of $\hat{\mathcal{Z}}_R$. This is due to the fact that in the definition of $\hat{\mathcal{Z}}_R$ we employ the bearing function $\hat{z}$ as in Definition 2.10, where all the $\hat{z}_k$ refer to the same frame of coordinates.

In Chapter 2 we have already introduced that the shapes in a infinitesimally and minimally congruent rigid family share the same scalar products $\hat{z}_l^T \hat{z}_n$ where l and n are the two edges of $\mathbb{G}$ sharing the same node. Using this fact, it is still possible to have a distributed control law, at least in $\mathbb{R}^2$, where a team of agents form an *orientation-free shape* $\mathcal{Z}_s$ with s determined by only controlling one edge. We first show that a control law for achieving $\mathcal{Z}_\mathcal{S}$ in 2D can be implemented in a distributed fashion. This is a particular result derived from [67], where the authors study the distributed feasibility of general gradient descent controllers.

Proposition 5.3. *Consider a team of n agents in $\mathbb{R}^2$ where the sensing topology of the infinitesimally and minimally rigid shape has been constructed employing only the Henneberg insertions. Then for forming a prescribed shape $\mathcal{Z}_\mathcal{S}$, the gradient-descent control derived from the potential function*

$$V(\hat{z}) = \sum_{l=1}^{|\mathcal{V}|-2} V_l, \tag{5.12}$$

where V_l is the potential function that corresponds to the formation of the l'th triangle, namely

$$\begin{aligned} V_l &= {}^lV_1 + {}^lV_2 + {}^lV_3 \\ &= \frac{1}{2}(\hat{z}_i^T \hat{z}_j - \hat{z}_i^{*^T} \hat{z}_j^*)^2 + \frac{1}{2}(\hat{z}_j^T \hat{z}_k - \hat{z}_j^{*^T} \hat{z}_k^*)^2 + \frac{1}{2}(\hat{z}_k^T \hat{z}_i - \hat{z}_k^{*^T} \hat{z}_i^*)^2, \end{aligned} \tag{5.13}$$

with i, j, k be the three edges of the l'th triangle, can be implemented in a distributed fashion if the three agents forming the l'th triangle know about the desired $\hat{z}_i^{*^T} \hat{z}_j^*, \hat{z}_j^{*^T} \hat{z}_k^*$ and $\hat{z}_k^{*^T} \hat{z}_i^*$.[1]

Proof. From Lemma 2.12 we have that an infinitesimally and minimally rigid shape in $\mathcal{Z}_\mathcal{S}$ is also infinitesimally bearing rigid in $\mathbb{R}^2$. Therefore the collection of desired scalar products $\hat{z}_m^{*^T} \hat{z}_n^*$ where the edges m and n share a common node in the graph $\mathbb{G}$ define a family of infinitesimally and minimally congruent rigid formations. Without loss of generality, let us assume that the agents $1, 2$ and 3 form the triangle 1 with $\mathcal{E}_1 = (1, 2), \mathcal{E}_2 = (2, 3)$ and $\mathcal{E}_3 = (3, 1)$ in $\mathcal{Z}_\mathcal{S}$, then compute the following

[1] It is clear that a generic triangle can be determined by only two of these desired scalar products, but for the sake of completeness we consider the three of them.

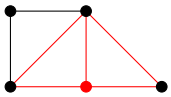

Figure 5.1: In Proposition 5.3 the needed information (relative positions) by the agent marked in red is also marked with the same color. Note that the needed vectors belong to the triangles where the agent is a node from. No communication is needed at all since we can exploit the identity $z_i + z_j + z_k = \mathbf{0}$ as defined in Proposition 5.3.

gradient of V_1 for agent 1

$$\frac{\partial^1 V_1}{\partial p_1} = \left(\frac{\hat{z}_2}{||z_1||} - \hat{z}_1 \hat{z}_1^T \hat{z}_2 \right) e_1 \tag{5.14}$$

$$\frac{\partial^1 V_2}{\partial p_1} = \left(\frac{\hat{z}_3}{||z_2||} + \hat{z}_2 \hat{z}_2^T \hat{z}_3 \right) e_2 \tag{5.15}$$

$$\frac{\partial^1 V_3}{\partial p_1} = \left(\frac{z_3 - z_1}{||z_3||||z_1||} - \frac{\hat{z}_1 ||z_3|| - \hat{z}_3 ||z_1||}{||z_3||^2 ||z_1||^2} \right) e_3, \tag{5.16}$$

where $e_1 = \hat{z}_1^T \hat{z}_2 - \hat{z}_1^{*^T} \hat{z}_2^*, e_2 = \hat{z}_2^T \hat{z}_3 - \hat{z}_2^{*^T} \hat{z}_3^*$ and $e_3 = \hat{z}_3^T \hat{z}_1 - \hat{z}_3^{*^T} \hat{z}_1^*$. From the sensing topology we know that agent 1 is able to measure z_1 and z_3 and the other inter-position can be easily obtained from $z_2 = -z_1 - z_3$. Therefore the gradient of V_1 can be implemented in a distributed way by agent 1 if it knows e_1, e_2 and e_3. We can easily derive the same result for agents 2 and 3. Since we construct the sensing topology by only Henneberg insertions, then by induction it is also clear that the agents involved in the l'th triangle will only need the information related to it. □

We provide an example of the needed information by an arbitrary agent in a 2D formation constructed by Hennerberg insertions in Figure 5.1.

The local stability of $\mathcal{Z}_\mathcal{S}$ by employing the gradient-descent control presented in Proposition 5.3 is guaranteed by Theorem 2.14. Note that the potential function in Proposition 5.3 can be extended to having agents 1 and 2 controlling s in $\mathcal{Z}_\mathcal{S}$ and furthermore, as in Theorem 4.9 they can also control the orientation of $\mathcal{Z}_\mathcal{S}$ with respect to O_g. Note that the major advantage of using the gradient-based control based on the potential function as in Proposition 5.3 over the one in Theorem 5.1 is that the agents can work in their own coordinate system since the desired dot products are scalars and not vectorial quantities. On the other hand, the agents require additional information and the gradients in (5.14)-(5.16) are more cumbersome with respect to the control law in Theorem 5.1.

5.1.2 Experimental results

In this experiment we want to validate the proposed controller in Theorem 5.1. We consider four robots with the following sensing topology

$$B = \begin{bmatrix} 1 & 0 & -1 & 1 & 0 \\ -1 & 1 & 0 & 0 & 0 \\ 0 & -1 & 1 & 0 & 1 \\ 0 & 0 & 0 & -1 & -1 \end{bmatrix}, \tag{5.17}$$

which have a scale-free regular square as a prescribed shape $\hat{\mathcal{Z}}_R$. More precisely the shape is given by the following set of unit vectors

$$\begin{aligned} \hat{z}_1^* &= \begin{bmatrix} 1 & 0 \end{bmatrix}^T, & \hat{z}_2^* &= \begin{bmatrix} 0 & 1 \end{bmatrix}^T, \\ \hat{z}_4^* &= \begin{bmatrix} 0 & 1 \end{bmatrix}^T, & \hat{z}_5^* &= \begin{bmatrix} 1 & 0 \end{bmatrix}^T, \\ \hat{z}_3^* &= \begin{bmatrix} -\cos\frac{\pi}{4} & -\sin\frac{\pi}{4} \end{bmatrix}^T. \end{aligned}$$

Note that the square will be oriented along the X axis of O_g. We implement the control law (5.3) with B as in (5.17) and ${}^sB$ as

$${}^sB = \begin{bmatrix} 1 & 0 & 0 & 0 & 0 \\ 0 & 0 & 0 & 0 & 0 \\ 0 & 0 & 0 & 0 & 0 \\ 0 & 0 & 0 & 0 & 0 \end{bmatrix}.$$

In this case, robot 1 will be the *scaling leader* defining the scale of $\hat{\mathcal{Z}}_R$ by just adjusting the desired inter-distance in the edge $\mathcal{E}_1$. For avoiding a possible saturation in the actuators of the robots, we apply the gain $c_f = 1 \times 10^4$ to the first term of (5.3) responsible for the control of the scale-free square, and the gain $c_s = 5 \times 10^{-2}$ to the second term of (5.3) responsible for the control of the inter-distance of the edge $\mathcal{E}_1$. Robot 1 will choose among two different scales $\mathcal{Z}_{s_1}$ and $\mathcal{Z}_{s_2}$ of the scale-free regular square $\hat{\mathcal{Z}}_R$ with $s_1 = 1$ and $s_2 = 2$. We choose for the scale $s_1 = 1$ the inter-distance for $d_1 = 225$ pixels. In particular the scaling leader will follow the sequence of stages

$$\begin{aligned} &1) \quad t = 0, \quad s = s_1 \\ &2) \quad t = 90, \quad s = s_2 \\ &3) \quad t = 180, \quad s = s_1. \end{aligned}$$

In order to test and speed up the convergence rate once the formation is close to the desired shape, we boost the control gains by making them twice larger once

$e_s < 30$ pixels in the stage $1)$ and $e_s < 70$ in the stage $3)$. We do not modify the original gains during the stage $2)$.

We proceed to discuss the experimental results from Figure 5.2. The robot marked in red is the scaling leader, deciding the size of the square by controlling the inter-distance marked in red. The rest of edges are marked in green color. In order to speed up the convergence to the desired shape, once the robots are close to their target the control gain is doubled. The video capture (a) shows the initial conditions for the robots, and the video captures (b), (c) and (d) show the robots at their prescribed shape before the leader changes to a new scaled one. The plot in (e) shows how all the errors converge to zero where the inter-distance error has been rescaled by a factor of 600 pixels. The plot in (f) shows how the speed of the robots eventually stop once the desired scaled shape is formed

5.2 Distributed changing-motion-control of rigid formations

Suppose that a team of agents wants to double the scale of the current desired shape that they are forming. If the agents are following a distance-based control law, a team leader could broadcast a signal containing $s = 2$ and therefore the agents will achieve the new scaled shape in $\mathcal{Z}_{\mathcal{S}}$, or if they are following the control law (5.3) then the *scaling leaders* will adjust the length of z_1 to the new scale. However this basic strategy contains two major drawbacks. The first one is related to the fact that it cannot be guaranteed that the shape of the formation belongs to $\mathcal{Z}_{\mathcal{S}}$ during the transient. The second one is due to the fact that we are dealing with exponential convergence, i.e., we are demanding high control inputs if we are far away from our target. This is not a suitable scenario since actual agents might have saturations in their actuators.

Throughout this section we will show that the strategy of assigning distributed motion parameters for steering the formation presented in Chapter 4 can also be employed for precisely scaling over time a desired infinitesimally and minimally rigid formation, i.e., the formation will converge to a desired $\mathcal{Z}_s$ for a given $s(t)$, while at the same time the formation is traveling with a desired ${}^b v^*_{p_c}$ and ${}^b\omega$. This approach is easier and powerful in several aspects compared to the previous work presented in [89]. Firstly, we do not need estimators for traveling at a constant speed. Secondly, the desired formation can be rotated with respect to O_g by only one robot. Thirdly the robots can work using only local coordinates since we are using the distance-based control strategy.

Let us recall that similar to the control law (4.2) but by setting $l = 1$ in the

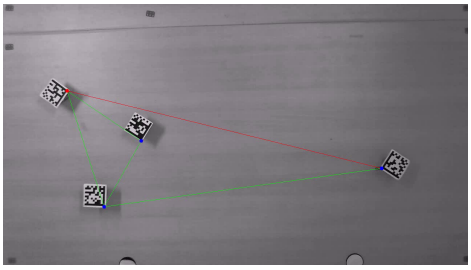

(a) Time $t = 0$ secs.

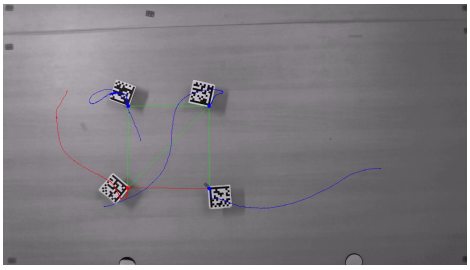

(b) Time $t = 86$ secs.

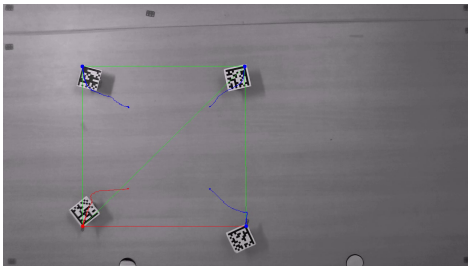

(c) Time $t = 179$ secs.

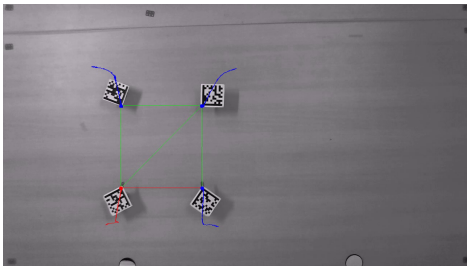

(d) Time $t = 298$ secs.

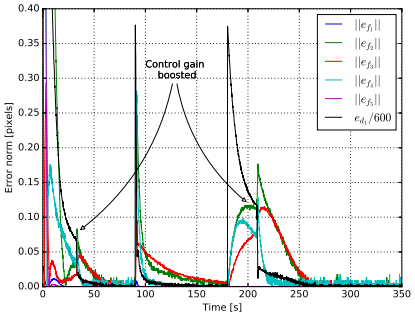

(e) Evolution of the errors e_f and e_s.

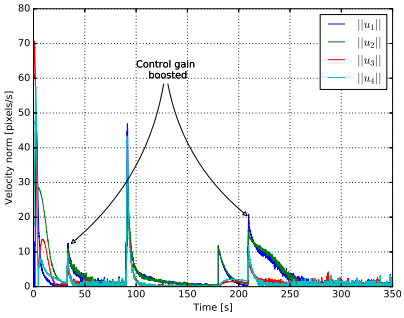

(f) Speed of the robots.

Figure 5.2: A team of robots forming a regular square where the scale is defined by the robots linked by the red edge.

potential function (2.10), we have that

$$u = -c\overline{B}D_{\hat{z}}e + \overline{A}(\mu, \tilde{\mu})\hat{z}. \tag{5.18}$$

Suppose that the formation is at the prescribed shape, i.e., $e = \mathbf{0}$. In this case if $\overline{A}(\mu, \tilde{\mu})\hat{z}$ defines translations, rotations and a scaling of an infinitesimally and minimally congruent rigid shape in $\mathcal{Z}_{\mathcal{S}}$, then the shape of the formation will be invariant under such an additional control term. Note that from (5.18) when $e = \mathbf{0}$

the control law for robot i becomes

$$^{b}u_i = \sum_{k=1}^{|\mathcal{E}|} a_{ik}\, {}^{b}\hat{z}_k^*, \tag{5.19}$$

where ${}^{b}\hat{z}^* \in \mathcal{Z}_{\mathcal{S}}$. Recall that the elements a_{ik} of A are related to μ and $\tilde{\mu}$ as in (4.3).

Similar to the spaces $\mathcal{U}$ and $\mathcal{W}$ for μ and $\tilde{\mu}$ for computing ${}^{b}\dot{p}_c^*$ and ${}^{b}\omega$ in Section 4.1, we derive

$$\begin{bmatrix}\mu_v \\ \tilde{\mu}_v\end{bmatrix} \in \hat{\mathcal{U}} \triangleq P_{\mathrm{Ker}\{T({}^{b}\hat{z}^*)\}^{\perp}} \left\{ \mathrm{Ker}\{\overline{B}^T T({}^{b}\hat{z}^*)\} \right\} \tag{5.20}$$

$$\begin{bmatrix}\mu_\omega \\ \tilde{\mu}_\omega\end{bmatrix} \in \hat{\mathcal{W}} \triangleq P_{\hat{\mathcal{U}}^{\perp}} \left\{ \mathrm{Ker}\{D_{^{b}\hat{z}^*}^T \overline{B}^T T({}^{b}\hat{z}^*)\} \right\}, \tag{5.21}$$

that are the spaces to be used by μ and $\tilde{\mu}$ in (5.19) for a desired given motion and we remind that $P_{\mathcal{X}}$ stands for the projection over the space $\mathcal{X}$.

We introduce now the new changing parameters μ_s and $\tilde{\mu}_s$ to be added to the already introduced $\mu_v, \tilde{\mu}_v, \mu_\omega$ and $\tilde{\mu}_\omega$, which will be responsible for the scaling of the formation. In order to compute $\mu_s, \tilde{\mu}_s$ we need to look at the bearing rigidity matrix $D_{P_{\hat{z}}^{\perp}}^T \overline{B}^T$, whose transpose was employed previously in the control law (5.3). It has been shown in [88] that the meaning of the kernel of the bearing rigidity matrix stands for translations and scalings of the desired shape. Therefore in a similar way as before the following condition

$$\begin{bmatrix}\mu_s \\ \tilde{\mu}_s\end{bmatrix} \in \mathcal{S} \triangleq P_{\hat{\mathcal{U}}^{\perp}} \left\{ \mathrm{Ker}\{D_{P_{^{b}\hat{z}^*}^{\perp}}^T \overline{B}^T T({}^{b}\hat{z}^*)\} \right\}, \tag{5.22}$$

will give us the space of changing parameters responsible for the scaling of the formation. An example of the three spaces $\hat{\mathcal{U}}, \hat{\mathcal{W}}$ and $\mathcal{S}$ for infinitesimally and minimally congruent regular squares is given in Figure 5.3.

5.2.1 Design of the controller for precise morphing and motion of the formation

Here by precise scaling we mean the control of the robots such that the inter-distances follow a time varying $d(t)$ but with the shape in $\mathcal{Z}_{\mathcal{S}}$. More precisely, we set $e_k(t) = ||z_k(t)|| - d_k(t)$ for $k \in \{1, \ldots, |\mathcal{E}|\}$ with $\mathcal{Z} \in \mathcal{Z}_{\mathcal{S}}$ in a family of infinitesimally and minimally congruent rigid shapes. For simplicity we set the

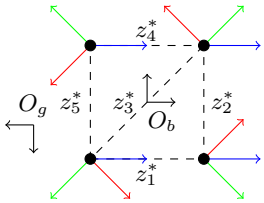

Figure 5.3: The velocity of the robots at the desired shape is the linear combination of the unit vectors from their associated relative positions (black dashed lines) given by (5.19). In order to keep the shape in the family of infinitesimally and minimally congruent regular squares, the velocity of the robots can be split in three terms. The common velocity ${}^b\dot{p}_c^*$ of the centroid is marked in blue and it is given by the motion parameters μ_v and $\tilde{\mu}_v$. The rotational velocity about the centroid defining ${}^b\omega$ is marked in red and it is given by the motion parameters μ_ω and $\tilde{\mu}_\omega$. The velocity responsible for scaling the formation has been marked in green and it is given by the morphing parameters μ_s and $\tilde{\mu}_s$. Note that these velocities are constant with respect to O_b since by definition the unit vectors ${}^b\hat{z}_k^*$ for all $k \in \{1, \dots, |\mathcal{E}|\}$ are constant in $\mathcal{Z}_\mathcal{S}$, therefore the design of the morphing-motion parameters has to be done employing ${}^b\hat{z}$ instead of $\hat{z}$.

following relation in the edge $\mathcal{E}_k$

$$d_k(t) = s(t)d_k^* + d_k^*, \tag{5.23}$$

where $s(t) \in \mathbb{R}$ is a time-variant scaling signal which is assumed to be at least C^1 and d_k^* is defined for a particular $\mathcal{Z}$. We remark here that the form used in (5.23) is for convenience purposes of design. One can of course choose $d_k(t) = s(t)d_k^*$. Without loss of generality, we assume that $s(0) = 0$. Obviously, for well-posedness, we also impose that $s(t)$ is defined properly such that $d_k(t) > 0$ for all t and $k \in \{1, \dots, |\mathcal{E}|\}$.

It is clear that the desired linear speed $||{}^b v_{p_c}^*||$ and the desired angular speed $||{}^b\omega^*||$ are related to the norm of $\mu_v, \tilde{\mu}_v$ and $\mu_\omega, \tilde{\mu}_\omega$ respectively. It can also be easily checked that the speed $\frac{\mathrm{d}}{\mathrm{dt}} d_k(t)$ is also related to the norms of μ_s and $\tilde{\mu}_s$.

We derive the dynamics of z and e from (5.18) considering that we have time varying desired inter-distances

$$\dot{z} = -c\overline{B}^T\overline{B}D_{\hat{z}}e + \overline{B}^T\overline{A}(\mu, \tilde{\mu})\hat{z} \tag{5.24}$$

$$\dot{e} = -cD_{\hat{z}}^T\overline{B}^T\overline{B}D_{\hat{z}}e + D_{\hat{z}}^T\overline{B}^T\overline{A}(\mu, \tilde{\mu})\hat{z} - \dot{d}, \tag{5.25}$$

where we have rewritten e as the stacked vector of $e_k(t) = ||z_k(t)|| - d_k(t)$ for $k \in \{1, \dots, |\mathcal{E}|\}$, and d is the stacked vector of $d_k(t)$ also for $k \in \{1, \dots, |\mathcal{E}|\}$.

In order to compensate $\dot{d}$ in (5.25) we impose the following condition for

keeping invariant e for $e = \mathbf{0}$, i.e., the formation shape is always in $\mathcal{Z}_s$

$$\dot{d} = \frac{\mathrm{d}s}{\mathrm{d}t} d^* = D_{b\hat{z}^*}^T \overline{B}^T \begin{bmatrix} \overline{S}_1 D_{b\hat{z}^*} & \overline{S}_2 D_{b\hat{z}^*} \end{bmatrix} \begin{bmatrix} \mu \\ \tilde{\mu} \end{bmatrix}, \tag{5.26}$$

so that the subtraction of the last two terms in (5.25) is zero when $e = \mathbf{0}$. Note that the solution to (5.26) for μ and $\tilde{\mu}$ includes the spaces $\hat{\mathcal{U}}$ and $\hat{\mathcal{W}}$. Therefore the changing parameters that we are looking for scaling the desired shape with a desired scaling rate are $\left[\begin{smallmatrix} \mu_s \\ \tilde{\mu}_s \end{smallmatrix}\right] \in \mathcal{S}$ such that (5.26) holds.

We will present two different general scaling cases, the first one concerning a constant growing/shrinking of the formation and the second one with a periodic change in the scale of the shape.

For the constant growing case, i.e., $s(t) = st$, where $s \in \mathbb{R}^+$ is a common constant shared by all the agents, we have that $\dot{d} = \frac{\mathrm{d}s}{\mathrm{d}t} d^* = s d^*$ in (5.26) and therefore the solution of (5.26) gives constant μ_s and $\tilde{\mu}_s$. However, as it has been shown in Chapter 4, we have that the solution for μ_s and $\tilde{\mu}_s$ is not unique since the robot i might have more than two (three) $\hat{z}_k$ available in 2D (3D) for constructing a two (three) dimensional velocity vector in (5.19).

Remark 5.4. We can always guarantee a straightforward solution to (5.26) imposing the additional condition $\tilde{\mu} = \mathbf{0}$ since it was shown in Propositions 3.5 and 3.7 that the squared matrix $D_{b\hat{z}^*}^T \overline{B}^T \overline{S}_1 D_{b\hat{z}^*}$ can be made invertible for whatever infinitesimally and minimally rigid formation if we choose the incidence matrix B in a particular way. However, this last result does not guarantee that the computed morphing parameters are only in $\mathcal{S}$, for example, it can be checked that in a triangular formation they will also involve a rotation.

Considering the periodic scaling case we have that $s(t) = s\sin(\omega t)$, which satisfies $\dot{d} = \frac{\mathrm{d}s}{\mathrm{d}t} d^* = s\omega\cos(\omega t) d^*$. Therefore the changing parameters μ_s and $\tilde{\mu}_s$ for the periodic case are the same ones previously calculated for the constant growing case but multiplied by the periodic signal $\omega\cos(\omega t)$, which is obviously independent of the actual shape.

5.2.2 Stability analysis

Before presenting the main result of this section, we need to show first that the error system in (5.25) only depends on e. Note that the system is not completely autonomous since e depends on the non-constant signal $d(t)$. Indeed, the second term at the right hand side of (5.25) depends on the dot products of the form $\hat{z}_i^T \hat{z}_j$ for $i, j \in \{1, \ldots, |\mathcal{E}|\}$ and as in (2.19), we have that

$$\hat{z}_i^T \hat{z}_j = \hat{g}_{ij}(e), \quad i, j \in \{1, \ldots, |\mathcal{E}|\}, \tag{5.27}$$

where $\hat{g}_{ij}$ is a local smooth function around the shape $z \in \mathcal{Z}_s$. Note that when $z \in \mathcal{Z}_s$, the subtraction of the second and third terms in the right hand side of (5.25) vanish because of (5.26), therefore we can write the following local function

$$f(e) = D_{\hat{z}}^T \overline{B}^T \overline{A}(\mu, \tilde{\mu})\hat{z} - \dot{d}, \tag{5.28}$$

where in this case

$$z \in \mathcal{Z}_s \implies f(\mathbf{0}) = \mathbf{0}, \tag{5.29}$$

and recall from (2.20) that the matrix in the first term of the right hand side of (5.25) can be rewritten as

$$Q(e) = D_{\hat{z}}^T \overline{B}^T \overline{B} D_{\hat{z}}, \tag{5.30}$$

where $Q(\mathbf{0})$ is positive definite if $\mathcal{Z}_{\mathcal{S}}$ defines a family of infinitesimally and minimally congruent rigid shapes.

Theorem 5.5. *Consider the distributed parameters* $[\begin{smallmatrix}\mu_v \\ \tilde{\mu}_v\end{smallmatrix}]$, $[\begin{smallmatrix}\mu_\omega \\ \tilde{\mu}_\omega\end{smallmatrix}]$ *and* $[\begin{smallmatrix}\mu_s \\ \tilde{\mu}_s\end{smallmatrix}]$ *belonging to the spaces (**??**), (**??**) and (5.22) respectively. Then, there exist constants* $\rho, c^* > 0$ *such that the origin of the system (5.25), corresponding to* $z \in \mathcal{Z}_s$ *with time-varying* $s(t)$ *as in (5.23), is locally exponentially stable for all* $c \geqslant c^*$ *in the compact set* $\mathcal{Q} \triangleq \{e : ||e||^2 \leqslant \rho\}$. *In particular, the formation will converge exponentially fast to the time-varying shape defined by* $\mathcal{Z}_s$ *with the speed* $\frac{\mathrm{d}s(t)}{\mathrm{d}t}$ *satisfying (5.26) and the agents' velocities*

$$^b\dot{p}_i(t) \to {}^b\dot{p}_i^*,\ t \to \infty,\ i \in \{1, \ldots, |\mathcal{V}|\}, \tag{5.31}$$

where the $^b\dot{p}_i^*$*'s are given by the desired* $^b\dot{p}_c^*$, $^b\omega$ *and* $\frac{\mathrm{d}s(t)}{\mathrm{d}t}$, *that are determined by* $[\begin{smallmatrix}\mu_v \\ \tilde{\mu}_v\end{smallmatrix}]$, $[\begin{smallmatrix}\mu_\omega \\ \tilde{\mu}_\omega\end{smallmatrix}]$ *and* $[\begin{smallmatrix}\mu_s \\ \tilde{\mu}_s\end{smallmatrix}]$.

Proof. Consider the following candidate Lyapunov function

$$V = \frac{1}{2}||e||^2, \tag{5.32}$$

whose time derivative satisfies

$$\frac{\mathrm{d}V}{\mathrm{d}t} = e^T\dot{e} = -ce^T Q(e)e + e^T f(e), \tag{5.33}$$

with $f(e)$ and $Q(e)$ as in (5.29) and (5.30) respectively. Since in a neighborhood of $\mathcal{Z}_s$ the formation is still infinitesimally and minimally rigid, $Q(e)$ is positive definite in the compact set $\mathcal{Q}$ for a sufficiently small ρ. Furthermore, $f(e)$ is locally Lipschitz in the compact set $\mathcal{Q}$ and $f(\mathbf{0}) = \mathbf{0}$ with $z \in \mathcal{Z}_s$, therefore there exists a constant $q \in \mathbb{R}^+$ such that

$$\frac{\mathrm{d}V}{\mathrm{d}t} \leqslant (-c\lambda_{\min} + q)||e||^2, \tag{5.34}$$

where $\lambda_{\min}$ is the minimum eigenvalue of $Q(e)$ in $\mathcal{Q}$. Thus if one chooses $c \geqslant c^* > \frac{q}{\lambda_{\min}}$, then the exponential stability of the origin of (5.25) follows by invoking the Theorem 4.10 from [47] for non-autonomous systems. Therefore we have that the formation shape converges exponentially to $\mathcal{Z}_s$.

Now we substitute $e(t) \to \mathbf{0}$ and $\hat{z}(t) \to \mathcal{Z}_s$ as t goes to infinity into (5.18), which gives us

$$\dot{p}(t) - \bar{A}(\mu, \tilde{\mu})\hat{z}(t) \to \mathbf{0}, \quad t \to \infty. \tag{5.35}$$

In other words, the velocity of the formation converges exponentially fast to the desired velocity given as a superposition of ${}^b v^*_{p_c}$ and ${}^b\omega^*$ with the scaling speed $\frac{\mathrm{d}s(t)}{\mathrm{d}t}$ satisfying (5.26). □

The main advantage of the result of Theorem 5.5 is that we can still steer the formation while at the same time changing the scale of the shape. In practice this result can be applied in the following sense, by just assigning a leader that triggers and broadcast a signal for starting/stopping the common scaling signal $s(t)$. In fact, if all the agents have preprogrammed two different scales to choose from, only the starting/switching signal would be necessary since the signal $s(t)$ would stop once the new desired inter-distance is achieved. As it has been shown in Chapter 4, the Theorem 5.5 is compatible with translating the formation with a desired heading in O_g and with the problem of tracking and enclosing a target.

We would like to highlight that for some particular cases we can employ the results of Theorem 5.5 for controlling the changing of the formation shape but without restricting it to be at $\mathcal{Z}_{\mathcal{S}}$, using only the constants μ and $\tilde{\mu}$. For example, suppose that the desired motion of the shape is a pure translation, i.e., $\mu_\omega = \tilde{\mu}_\omega = \mathbf{0}$. Consider the collection of all the rectangular shapes (with an inner diagonal). The corners of whatever rectangle always form a right angle, i.e., all the infinitesimally and minimally rigid rectangles share one underlying bearing equivalent shape. If for the design of μ and $\tilde{\mu}$ we only consider the ${}^b\hat{z}^*_k$ forming the corners, we can use the result of Theorem 5.5 for changing the desired shape among different rectangles. Note that in such a case, instead of a common $s(t)$ we will use a $s_k(t)$ for determining the scaling speed of the inter-distance associated to the edge k in order to fit with the desired changing. We still have to satisfy (5.26) and in order to keep the centroid of the formation stand-still by using μ_s and $\tilde{\mu}_s$, we should modify slightly the condition (5.22) since it only holds for a particular family $\mathcal{Z}_{\mathcal{S}}$. We will see this particular example in one of the experiments in the following section. Finally if we consider changing between generic infinitesimally and minimally rigid shapes (sharing the same incidence matrix B), then in general μ and $\tilde{\mu}$ will not be constant and will depend on the different $s_k(t)$ for all $\{1, \ldots, k\}$.

5.2.3 Periodic scaling and spinning of a rigid formation

In this experiment we validate the performance of Theorem 5.5. We have four robots forming a scale-free regular square. The objective of this experiment is to design the morphing-motion parameters μ and $\tilde{\mu}$ in the control law (5.18) such that the square spins around its centroid and at the same time we vary periodically the scale of the square. We define the sensing topology of the agents by

$$B = \begin{bmatrix} 1 & 0 & -1 & 0 & -1 \\ -1 & 1 & 0 & 0 & 0 \\ 0 & -1 & 1 & -1 & 0 \\ 0 & 0 & 0 & 1 & 1 \end{bmatrix}, \tag{5.36}$$

and we define the regular square that we will periodically scale as

$$d^* = \begin{bmatrix} 300 & 300 & 300\sqrt{2} & 300 & 300 \end{bmatrix}^T \text{pixels}. \tag{5.37}$$

In order to induce the spinning motion we design the following μ_ω and $\tilde{\mu}_\omega$ satisfying (5.21)

$$\mu_\omega = \begin{bmatrix} -w & -w & 0 & w & -w \end{bmatrix}^T, \tilde{\mu}_\omega = \begin{bmatrix} -w & -w & 0 & w & -w \end{bmatrix}^T, \tag{5.38}$$

with $w = 8$. We want to vary periodically the size of the square following the desired time-varying distances

$$d_i(t) = d_i^* + 2hd_i^* \sin(\omega_s t),\ i = \{1, \ldots, 5\} \tag{5.39}$$

where we can deduce that $s(t) = 2h\sin(\omega_s t)$. In our experiment, we set $h = 0.1$ and $\omega_s = 0.2$ rads/sec. The signal $s(t)$ will be encoded to each robot and we assume that all them are synchronized. The desired μ_s and $\tilde{\mu}_s$ satisfying (5.22) and (5.26) are

$$\begin{cases} \mu_s(t) & = h\omega_s \cos(\omega_s t) \begin{bmatrix} 1 & 1 & 0 & 1 & 1 \end{bmatrix}^T \\ \tilde{\mu}_s(t) & = h\omega_s \cos(\omega_s t) \begin{bmatrix} -1 & -1 & 0 & -1 & -1 \end{bmatrix}^T. \end{cases} \tag{5.40}$$

Finally we choose $c = 3.5 \times 10^{-3}$ for (5.18), which is much smaller, after numerically checking some arbitrary values in the compact set $\mathcal{Q}$, than the conservative gain in Theorem 5.5. The experimental results are shown in Figure 5.4.

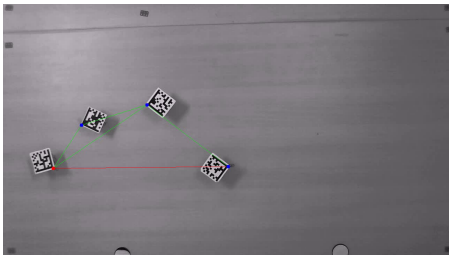

(a) Time $t = 0$ secs.

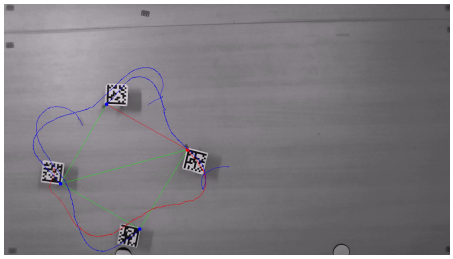

(b) Time $t = 50$ secs.

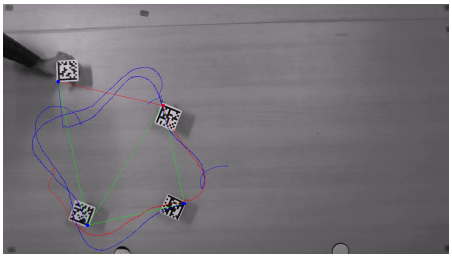

(c) Time $t = 62$ secs.

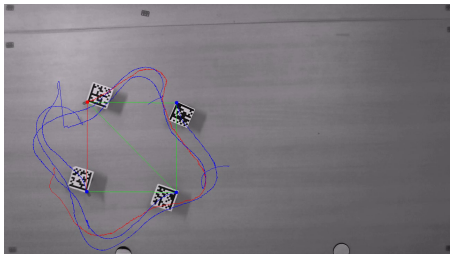

(d) Time $t = 90$ secs.

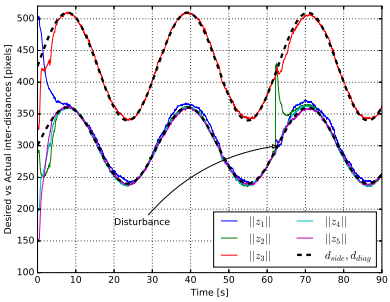

(e) Evolution of the actual inter-distances $||z_i(t)||$.

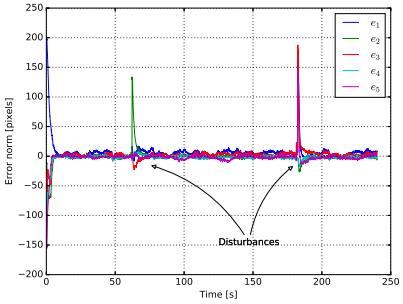

(f) Evolution of the signal errors $e_i(t)$ regarding the inter-distances.

Figure 5.4: Experimental results of a team of four robots forming a regular square whose scale follows a sinusoidal signal defined by (5.39). The robots follow the control law (5.18) with the morphing-motion parameters $\mu_\omega, \tilde{\mu}_\omega, \mu_s$ and $\tilde{\mu}_s$ defined in (5.38) and (5.40). We mark for visual purposes the robot 1 and z_1 in red. The video capture (a) shows the robots at their initial conditions and after few seconds they are following their prescribed $d_i(t)$ inter-distances. We show in (c) a disturbance in one of the robots in order to show the stability of the system. In the plot (e) the inter-distances $||z_i(t)||$ from initial random conditions converge to the desired sinusoidal signals. We can check in (f) the behaviour of the error signals, which are stable after applying disturbances.

5.2.4 Avoiding obstacles by a precise change of the shape while keeping the formation heading

In this experiment we consider a team of four travelling robots that has to avoid an obstacle on their way by controlling the morphing of the prescribed shape. The four robots have the same sensing topology defined in (5.36) and their prescribed formation is a regular square given by

$$d^* = \begin{bmatrix} 175 & 175 & 175\sqrt{2} & 175 & 175 \end{bmatrix}^T \text{ pixels.} \tag{5.41}$$

We implement the control law (5.18) such that the four robots are commanded to follow a constant velocity parallel to ${}^b z_1$ once they are at the prescribed shape. The motion parameters μ_v and $\tilde{\mu}_v$ in order to follow such desired ${}^b v^*_{p_c}$ satisfying (5.20) are given by

$$\mu_v = \begin{bmatrix} v & 0 & 0 & v & 0 \end{bmatrix}^T, \tilde{\mu}_v = \begin{bmatrix} v & 0 & 0 & v & 0 \end{bmatrix}^T. \tag{5.42}$$

with $v = 12$, i.e., the formation will follow a fixed speed of 12 pixels/s. In order to control the heading of the formation in O_g, in a similar way as in Theorem 4.9, we assign the robot 1 to control the orientation of $\hat{z}_1$ in O_g with the following extra added term in its control signal

$$u_{1_{\text{orientation}}} = -(\hat{z}_1 - \hat{z}^*_1). \tag{5.43}$$

We want to align the formation along the X axis of O_g, so we set $\hat{z}^*_1 = \begin{bmatrix} 1 & 0 \end{bmatrix}^T$. Once the robot 1 detects in front of the formation an obstacle, it broadcasts a switching signal to the other robots for changing the desired shape from a regular square to a rectangle given by

$$d^* = \begin{bmatrix} 175 & 471 & \sqrt{175^2 + 471^2} & 471 & 175 \end{bmatrix}^T \text{ pixels.} \tag{5.44}$$

A step input from the square (5.41) to the rectangle (5.44) to all the robots is not a desirable situation. For the following reasons the equilibrium of the control law (5.18) is exponentially stable, a step input from the square to the rectangle will cause the robots to reach their saturation values. Even with a small gain in the controller for avoiding the saturation, we do not control the transient between the two shapes, therefore we cannot keep the desired travelling velocity ${}^b \dot{p}^*_c$. In order to avoid such undesired scenario, we encode in the corresponding robots the

following scaling signals

$$\begin{aligned} s_2(t) = s_5(t) &= \frac{2h}{175}t \\ s_3(t) &= \frac{\mathrm{d}}{\mathrm{d}t}\frac{\sqrt{2(175^2)+350ht+h^2t^2}}{175\sqrt{2}} \\ s_1(t) = s_4(t) &= 0, \end{aligned}$$

with $h = 12$. These signals will be triggered once the leader detects the obstacle and they will be stopped by the robots themselves once they achieve the desired final rectangle. Note that we are only changing the inter-distances of the vertical sides and the diagonal of the shape. We assume that the signals $s_i(t)$ are all triggered at the same time as in the previous experiment. Since the change maintains constant the right angles at the corners between the two desired shapes, in order to use constants μ_v and $\tilde{\mu}_v$ we constrain them to use the corresponding invariant unit vectors in $\hat{z}$ during the change, i.e., $\hat{z}_1$ and $\hat{z}_4$. For the same reason the μ_s and $\tilde{\mu}_s$ will not use the vector $\hat{z}_3$ since the time derivative of $s_3(t)$ is not constant, i.e., we are going to employ only the unit vectors $\hat{z}_2(t)$ and $\hat{z}_5(t)$ defining the vertical sides. The changing parameters satisfying (5.26) for the morphing between the two desired shapes are

$$\mu_s = \begin{bmatrix} 0 & h & 0 & 0 & h \end{bmatrix}^T, \tilde{\mu}_s = \begin{bmatrix} 0 & -h & 0 & 0 & -h \end{bmatrix}^T. \tag{5.45}$$

Obviously, the parameters μ_s and $\tilde{\mu}_s$ are only applied for all the signals $s_i(t)$ and it is easy to check that they will maintain the centroid of the formation invariant during the change of the shape, so they will not disturb in any way the controlled translation given by μ_v and $\tilde{\mu}_v$. Once the obstacle is left behind, the leader will trigger again another signal in order to change the shape from the rectangle to the original regular square. In this case the scaling signals will obviously be

$$\begin{aligned} s_2(t) = s_5(t) &= -\frac{2h}{175}t \\ s_3(t) &= -\frac{\mathrm{d}}{\mathrm{d}t}\frac{\sqrt{2(175^2)+350ht+h^2t^2}}{175\sqrt{2}} \\ s_1(t) = s_4(t) &= 0, \end{aligned}$$

and the robots will stop them once the desired distances reach (5.41). Finally, the chosen gain for (5.18) is $c = 1 \times 10^{-1}$, which is again smaller than the conservative one given in Theorem 5.5. The experimental results are shown in Figure 5.5.

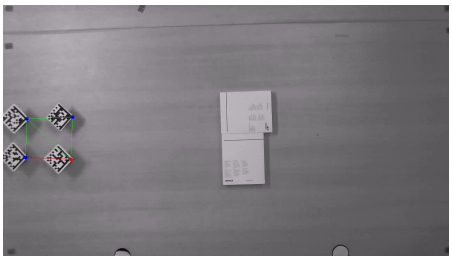

(a) Time $t = 0$ secs.

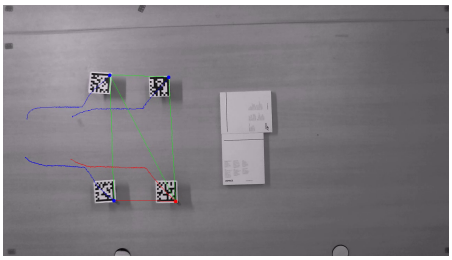

(b) Time $t = 23$ secs.

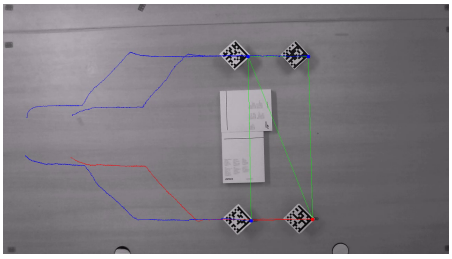

(c) Time $t = 55$ secs.

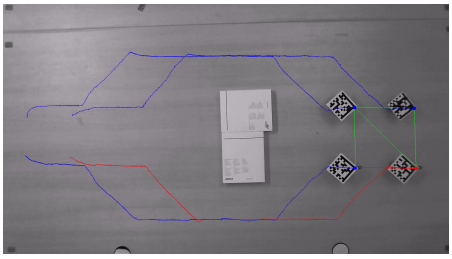

(d) Time $t = 80$ secs.

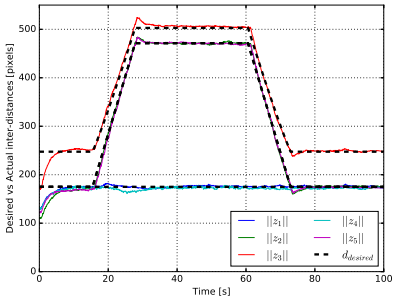

(e) Evolution of the actual inter-distances $||z_i(t)||$.

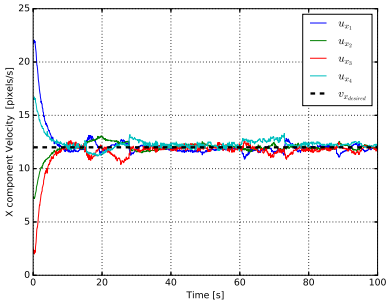

(f) Evolution of horizontal velocities $\dot{p}_x(t)$.

Figure 5.5: Experimental results of a team of four robots forming a regular square, travelling with a constant speed in the X axis direction of O_g and facing an obstacle on their way. The robot 1, marked in red, is controlling the orientation of z_1, also marked in red, using (5.43). In order to avoid the obstacle, the robots will morph their shape from a regular square defined in (5.41) to a rectangle defined in (5.44). The morphing is done in a precise way such that we control the morphing rate of shape at the same time that we control the desired horizontal velocity employing the morphing-motion parameters $\mu_v, \tilde{\mu}_v, \mu_s$ and $\tilde{\mu}_s$ in (5.42) and (5.45) in the applied control law (5.18). Once the obstacle is left behind, the robots come back to the original squared shape. In the plots (e) and (f) we can check how at the beginning the robots achieve the desired regular square with the desired travelling speed within ten seconds. Once the scaling signals are triggered, the desired distances are ramp signals. The inter-distances follow precisely these signals (morphing of the shape) with a small transitory time due to the velocity tracking controller in the robot, since it receives a step signal in the desired velocity once the scaling signals are triggered.

5.3 Concluding remarks

In this chapter we have dealt with the problem of scaling infinitesimally and minimally rigid formations. We have presented and analyzed algorithms for both, controlling the scale of a shape by means of controlling only one edge in the formation and a distributed strategy for controlling the scaling rate of a shape in a infinitesimally and minimally congruent rigid family. We have also shown that the former is completely compatible with the formation-motion control introduced in Chapter 4.

Chapter 6

Formation motion-control of second-order agents

That's the second biggest dynamics I've ever seen!

The secret of Monkey Island.

We extend the aforementioned results in Chapters 2, 3, 4 and 5 from the first-order agent case to the second-order one. As mentioned before, the second-order dynamics are more convenient since many robotic systems are described by Euler-Lagrange equations which correspond to second-order agents. In this case, the resulting formation control law can directly be used as the *desired acceleration* in a guidance system feeding the tracking controller of a mechanical system as the one proposed for quadrotors in [56] or for marine vessels in [31]. The robustness stability analysis of the closed-loop system for second-order agents, as discussed in this chapter, cannot follow the same steps as those used in [44, 59]. In particular, the error system that is considered in these papers for stability analysis is an autonomous system, which is not the case for the second-order agent as shown later in Section 6.2. Hence, we need to establish further additional steps in deriving the robustness results. In Section 6.3 we show how the distributed estimator design in Chapter 3 can be also employed in order to eliminate the undesired behaviors due to the existence of these mismatches. Finally in Section 6.4 we show how the distributed motion parameters introduced in Chapter 4 can be also employed to steer a formation of second-order agents. The experiments regarding second-order agents will be further discussed in Chapter 7, where we will employ the findings for formations of second-order agents to a team of quadcopters.

6.1 Gradient control in formations of second-order agents

We first show the exponential convergence of the formation to the desired shape and zero speed. This finding will give us a useful starting point for analyzing later the behaviour of the formation of second-order agents in the presence of distance

mismatches.

We start by recalling from Chapter 2 that the agents will be modelled by a second-order system given by

$$\begin{cases} \dot{p} = v \\ \dot{v} = u \end{cases}, \tag{6.1}$$

and as it has been done for first-order agents, in order to control the shape of the formation for each edge $\mathcal{E}_k = (i, j)$ in the infinitesimally and infinitesimally and minimally rigid framework we assign the following potential function V_k

$$V_k(||z_k||) = \frac{1}{4}(||z_k||^2 - d_k^2)^2,$$

with the gradient along p_i or p_j given by

$$\nabla_{p_i} V_k = -\nabla_{p_j} V_k = z_k(||z_k||^2 - d_k^2).$$

In order to control the agents' velocities, for each agent i in the infinitesimally and infinitesimally and minimally rigid framework we assign the following potential function S_i

$$S_i(v_i) = \frac{1}{2}||v_i||^2,$$

with the gradient along v_i be given by

$$\nabla_{v_i} S_i = v_i.$$

One can check that for the potential function

$$\phi(p, v) = \sum_{i=1}^{|\mathcal{V}|} S_i + \sum_{k=1}^{|\mathcal{E}|} V_k, \tag{6.2}$$

the closed-loop system (6.1) with the control input

$$u = -\nabla_v \phi - \nabla_p \phi, \tag{6.3}$$

becomes the following dissipative Hamiltonian system [82]

$$\begin{cases} \dot{p} = \nabla_v \phi \\ \dot{v} = -\nabla_v \phi - \nabla_p \phi. \end{cases} \tag{6.4}$$

Considering (6.2) as the storage energy function of the Hamiltonian system (6.4), one can show the local asymptotic convergence of the formation to the shape given by $\mathcal{D}$ and all the agents' velocities to zero [9, 60].

Let the following one-parameter family of dynamical systems $\mathcal{H}_\lambda$ be given by

$$\begin{bmatrix}\dot{p}\\ \dot{v}\end{bmatrix} = -\begin{bmatrix}\lambda I_{m|\mathcal{V}|} & -(1-\lambda)I_{m|\mathcal{V}|}\\ (1-\lambda)I_{m|\mathcal{V}|} & I_{m|\mathcal{V}|}\end{bmatrix}\begin{bmatrix}\nabla_p\phi\\ \nabla_v\phi\end{bmatrix}, \tag{6.5}$$

where $\lambda \in [0,1]$, which defines all convex combinations of the Hamiltonian system (6.4) and a gradient system. The family $\mathcal{H}_\lambda$ has two important properties summarized in the following lemma.

Lemma 6.1. *[60]*

- *For all $\lambda \in [0,1]$, the equilibrium set of $\mathcal{H}_\lambda$ is given by the set of the critical points of the potential function ϕ, i.e., $E_{p,v} = \left\{\begin{bmatrix}p^T & v^T\end{bmatrix}^T : \nabla\phi = 0\right\}$.*

- *For any equilibrium $\begin{bmatrix}p^T & v^T\end{bmatrix}^T \in E_{p,v}$ and for all $\lambda \in [0,1]$, the numbers of the stable, neutral, and unstable eigenvalues of the Jacobian of $\mathcal{H}_\lambda$ are the same and independent of λ.*

This result has been exploited in [72] in order to show the local exponential convergence of $z(t)$ and $v(t)$ to $\mathcal{D}$ and $\mathbf{0}_{|\mathcal{V}|\times 1}$ respectively. In the following brief exposition we revisit such exponential stability via a combination of Lyapunov argument and Lemma 6.1, which will play an important role once the formation is under the presence of distance mismatches.

As we have done in Chapter 2, we define the distance error corresponding to the edge $\mathcal{E}_k$ by

$$e_k = ||z_k||^2 - d_k^2,$$

whose time derivative is given by $\dot{e}_k = 2z_k^T\dot{z}_k$. Consider the following autonomous system derived from (6.5) with $\lambda = 0.5$

$$\dot{p} = -\frac{1}{2}\overline{B}D_z e + \frac{1}{2}v$$
$$\dot{z} = -\frac{1}{2}\overline{B}^T\overline{B}D_z e + \frac{1}{2}\overline{B}^T v \tag{6.6}$$
$$\dot{e} = -D_z^T\overline{B}^T\overline{B}D_z e + D_z^T\overline{B}^T v \tag{6.7}$$
$$\dot{v} = -\frac{1}{2}\overline{B}D_z e - v. \tag{6.8}$$

Define the speed of the agent i by

$$s_i = ||v_i||,$$

whose time derivative is given by $\dot{s}_i = \frac{v_i^T\dot{v}_i}{s_i}$. Their compact form involving all the

agents can be written as

$$\dot{s} = D_{\tilde{s}} D_v^T \dot{v} = -\frac{1}{2} D_{\tilde{s}} D_v^T \overline{B} D_z e - D_{\tilde{s}} D_v^T v, \tag{6.9}$$

where $s \in \mathbb{R}^{|\mathcal{V}|}$ and $\tilde{s} \in \mathbb{R}^{|\mathcal{V}|}$ are the stacked vectors of s_i's and $\frac{1}{s_i}$'s for all $i \in \{1, \ldots, |\mathcal{V}|\}$ respectively. Now we are ready to show the local exponential convergence to the origin of the speed of the agents and the error distances in the edges.

Lemma 6.2. *The origins $e = \mathbf{0}$ and $s = \mathbf{0}$ of the error and speed systems derived from (6.4) are locally exponentially stable if the given desired shape $\mathcal{D}$ is infinitesimally and minimally rigid.*

Proof. Consider e_λ and s_λ as the stacked vectors of the error signals e_k and speeds s_k derived from (6.5) for any $\lambda \in [0, 1]$, which includes the system (6.4) for $\lambda = 1$. From the definition of e_k, we know that all the e_λ share the same stability properties by invoking Lemma 6.1, so do s_λ as well.

Consider the following candidate Lyapunov function

$$V = \frac{1}{2}||e||^2 + ||s||^2, \tag{6.10}$$

for the autonomous system (6.6)-(6.9) derived from (6.5) with $\lambda = 0.5$. Then the time derivative of (6.10) is given by

$$\begin{aligned}
\frac{\mathrm{d}V}{\mathrm{d}t} &= e^T \dot{e} + 2 s^T \dot{s} \\
&= -e^T D_z^T \overline{B}^T \overline{B} D_z e + e^T D_z^T \overline{B}^T v - \underbrace{s^T D_{\tilde{s}} D_v^T}_{v^T} \overline{B} D_z e \\
&\quad - 2 \underbrace{s^T D_{\tilde{s}}}_{\mathbf{1}_{1\times|\mathcal{V}|}} D_v^T v \\
&\leqslant -\sigma_{\min} ||e||^2 - 2||s||^2,
\end{aligned} \tag{6.11}$$

where $\sigma_{\min}$ is the minimum eigenvalue of $D_z^T \overline{B}^T \overline{B} D_z = R(z) R(z)^T$ in the compact set $\mathcal{Q} \triangleq \{e : ||e||^2 \leqslant \rho\}$ for some $\rho > 0$. Note that for an infinitesimally and minimally rigid framework $R(z)$ is full rank excepting for non-generic situations. Therefore if the initial conditions for the error signal and the speed satisfy $||e(0)||^2 + ||s(0)||^2 \leqslant \rho$, then $\sigma_{\min} > 0$ for a sufficiently small ρ since $\mathcal{D}$ is infinitesimally and minimally rigid. Hence we have shown the local exponential convergence of $e(t)$ and $s(t)$ to the origin. □

Remark 6.3. It is worth noting that the region of attraction determined by ρ in the proof of Lemma 6.2 for $\lambda = 0.5$ might be different from the one for $\lambda = 1$, since

Lemma 6.1 only refers to the Jacobian of (6.5), i.e., the linearization of the system about the equilibrium.

It can be concluded from the exponential convergence to zero of the speeds of the agents $s(t)$ that the formation will eventually stop. This implies that $p(t)$ will converge exponentially to a finite point in $\mathbb{R}^m$ as $z(t)$ converges exponentially to $\mathcal{D}$.

6.2 Robustness issues caused by mismatches

We have already seen that when two neighboring agents disagree on the desired squared distance d_k^2 in between, namely

$$d_k^{2\,\text{tail}} = d_k^{2\,\text{head}} - \mu_k, \tag{6.12}$$

where $\mu_k \in \mathbb{R}$ is modelled as a constant mismatch, it can be checked that, in a similar way as in (3.2), this disagreement leads to rewriting the control signal (6.3) as

$$u = -v - \overline{B} D_z e - \overline{S}_1 D_z \mu. \tag{6.13}$$

Note that (3.2) can also be written as

$$u = -v - \overline{B} D_z e - \overline{A}_1(\mu) z, \tag{6.14}$$

where the elements of A_1 are

$$a_{ik} \triangleq \begin{cases} \mu_k & \text{if} \quad i = \mathcal{E}_k^{\text{tail}} \\ 0 & \text{otherwise.} \end{cases} \tag{6.15}$$

Inspired by [59], we will show how μ can be seen as a parametric disturbance in an autonomous system whose origin is exponentially stable. Consider the error signal e and the speed of the agents s derived from system (6.1) with the control input (6.3)

$$\dot{e} = 2 D_z^T \overline{B}^T v \tag{6.16}$$

$$\dot{s} = -s - D_{\tilde{s}} D_v^T \overline{B} D_z e, \tag{6.17}$$

and define

$$\alpha_{ki} = z_k^T v_i, \quad k \in \{1, \ldots, |\mathcal{E}|\}, i \in \{1, \ldots, |\mathcal{V}|\} \tag{6.18}$$

$$\beta_{ij} = v_i^T v_j, \quad i, j \in \{1, \ldots, |\mathcal{V}|\}, i \neq j. \tag{6.19}$$

We stack all the α_{ki}'s and β_{ij}'s in the column vectors $\alpha \in \mathbb{R}^{|\mathcal{E}||\mathcal{V}|}$ and $\beta \in \mathbb{R}^{\frac{|\mathcal{V}|(|\mathcal{V}|+1)}{2}}$

respectively and define $\gamma \triangleq \begin{bmatrix} e^T & s^T & \alpha^T & \beta^T \end{bmatrix}^T$. We know that for any infinitesimally and minimally rigid framework, there exists a neighborhood $\mathcal{U}_z$ about this framework such that for all $z_k, z_l \in \mathcal{U}_z$ with $k, l \in \{1, \ldots, |\mathcal{E}|\}$, we can write $z_k^T z_l$ by a smooth function $g_{kl}(e)$[59]. Then using (6.16)-(6.19) we get

$$\dot{\gamma} = f(\gamma), \tag{6.20}$$

which is an autonomous system whose origin is locally exponentially stable using the results from Lemmas 6.1 and 6.2. Obviously, in such a case, the following Jacobian evaluated at $\gamma = 0$

$$J = \left.\frac{\partial f(\gamma)}{\partial \gamma}\right|_{\gamma=\mathbf{0}},$$

has all its eigenvalues in the left half complex plane. From the system (6.1) with control law (6.13) we can *extend* (6.20) but with a parametric disturbance μ because of the third term in (3.2), namely

$$\dot{\gamma} = f(\gamma, \mu), \tag{6.21}$$

where $f(\gamma, \mathbf{0}_{|\mathcal{E}|\times 1})$ is the same as in (6.20) derived from the gradient controller. Therefore, for a sufficiently small $||\mu||$, the Jacobian $\left.\frac{\partial f(\gamma,\mu)}{\partial \gamma}\right|_{\gamma=\mathbf{0}}$ is still a stable matrix since the eigenvalues of a matrix are continuous functions of its entries. Although system (6.21) is still stable under the presence of a small disturbance μ, the equilibrium point is not the origin in general anymore but $\gamma(t) \to \hat{\gamma}(\mu)$ as t goes to infinity, where $\hat{\gamma}(\mu) \triangleq \gamma_\mu$ is a smooth function of μ with zero value if $\mu = \mathbf{0}_{|\mathcal{E}|\times 1}$ [47]. This implies that in general each component of e, s, α and β converges to a non-zero constant with the following two immediate consequences: the formation shape will be distorted, i.e., $e \neq \mathbf{0}$; and the agents will not remain stationary, i.e., $s \neq \mathbf{0}$. The meaning of having non-zero components in general in α and β is that the velocities of the agents have a fixed relation with the steady-state shape. If the disturbance $||\mu||$ is sufficiently small, then $||\hat{\gamma}(\mu)|| < \rho$ for some small $\rho \in \mathbb{R}^+$ implying that the norm of the steady-state error signal $||\hat{e}(\mu)|| < \rho$, and if further ρ is sufficiently small, then the stationary distorted shape is also infinitesimally and minimally rigid. In addition since the speeds of the agents converge to a constant (in general non-zero constant), only translations and/or rotations of the stationary distorted shape can happen.

Theorem 6.4. *Consider system (6.1) with control input (6.13) where the desired shape for the formation is infinitesimally and minimally rigid and μ is considered as a small parametric perturbation. Then, the formation will converge to a distorted infinitesimally and minimally rigid shape, i.e., $e \neq \mathbf{0}$, and the agents will converge to a steady-state collective motion that can be captured by constants angular and*

translational velocities ${}^b\omega$ and ${}^b\dot{p}_c^*$, respectively, for the distorted infinitesimally and minimally rigid formation.

Proof. Since system (6.21), derived from (6.1) and (6.13), is self-contained and its origin is locally exponentially stable with $\mu = \mathbf{0}_{|\mathcal{E}|\times 1}$, then a small parametric perturbation μ in its Jacobian will not change the exponential stability property of (6.21) but its equilibrium point. Therefore $e(t) \to e_\mu$ as t goes to infinity, where $e_\mu \in \mathbb{R}^{|\mathcal{E}|}$ is non-zero. In addition if the norm of μ is sufficiently small, then the stationary distorted shape will still be infinitesimally and minimally rigid. We also have that the elements of $s(t) \to s_\mu$ as t goes to infinity with $s_\mu \in \mathbb{R}^{|\mathcal{V}|}$ having all its elements non-negative and in general non-zero, implying that the agents will not stop in the steady-state. Since the steady-state shape of the formation locally converges to an infinitesimally and minimally rigid one, from the error dynamics (6.16) we have that

$$D_{z(t)}^T \overline{B}^T v(t) = R\left(z(t)\right) v(t) \to \mathbf{0}_{m|\mathcal{V}|\times 1}, \quad t \to \infty,$$

therefore $v(t) \to v_\mu(t)$ as t goes to infinity, where the non-constant $v_\mu(t) \in \mathbb{R}^{|\mathcal{V}|}$ belongs to the null space of $R\left(z_\mu(t)\right)$, $z_\mu(t) \in \mathcal{Z}_\mu$ and the set $\mathcal{Z}_\mu$ is defined as in (2.3) but corresponding to the inter-distances of the distorted infinitesimally and minimally rigid shape with $e = e_\mu$. Note that obviously, the evolution of $z(t)$ is a consequence of the evolution of agents' velocities in $v(t)$. The null space of $R\left(z_\mu\right)$ corresponds to the infinitesimal motions δp_i for all i while keeping the inter-distances in the distorted formation constant, namely

$$R(z_\mu)\delta p = R(z_\mu) v_\mu \, \delta t = \mathbf{0}_{m|\mathcal{V}|\times 1},$$

or in order words

$$v_i(t) \to v_{\mu_i}(t), \quad t \to \infty, \tag{6.22}$$

where the velocities $v_{\mu_i}(t)$'s for all the agents are the result of rotating and translating the steady-state distorted shape defined by $\mathcal{Z}_\mu$. This steady-state collective motion of the distorted formation can be represented by the rotational and translational velocities ${}^b\omega(t) \in \mathbb{R}^m$ and ${}^b\dot{p}_c^*(t) \in \mathbb{R}^m$ (possibly not constant) at the centroid of the distorted rigid shape. Furthermore, by definition we have that $||v_{\mu_i}(t)|| = s_{\mu_i}$. Since the speed s_{μ_i} for agent i is constant but not its velocity $v_{\mu_i}(t)$, the acceleration $a_{\mu_i}(t) = \frac{\mathrm{d}v_{\mu_i}(t)}{\mathrm{d}t}$ is perpendicular to $v_{\mu_i}(t)$. The expression of $a_{\mu_i}(t)$ can be derived from (6.13) and is given by

$$a_{\mu_i}(t) = -v_{\mu_i}(t) - \sum_{k=1}^{|\mathcal{E}|} b_{ik} z_{\mu_k}(t) e_{\mu_k} - \sum_{k=1}^{|\mathcal{E}|} a_{ik} z_{\mu_k}(t), \tag{6.23}$$

where b_{ik} are the elements of the incidence matrix, and a_{ik} are the elements of the matrix A_1 as defined in (6.15). From (6.23) it is clear that the norm $||a_{\mu_i}(t)|| = \Gamma_i(\gamma_\mu)$ is constant. In addition since $a_{\mu_i}(t)$ is a continuous function, i.e., the acceleration vector cannot switch its direction, and it is perpendicular to $v_{\mu_i}(t)$, the only possibility for the distorted formation is to follow a motion described by constant velocities ${}^b\omega$ and ${}^b\dot{p}_c^*$ at its centroid. □

Remark 6.5. In particular, in 2D the distorted formation will follow a closed orbit if $\Gamma_i(\gamma_\mu) \neq 0$ for all i, or a constant drift if $\Gamma_i(\gamma_\mu) = 0$ for all i. This is due to the fact that in 2D, ${}^b\omega$ and ${}^b\dot{p}_c^*$ are always perpendicular or equivalently $a_{\mu_i}(t)$ and $v_{\mu_i}(t)$ lie in the same plane. The resultant motion in 3D is the composition of a drift plus a closed orbit, since ${}^b\omega$ and ${}^b\dot{p}_c^*$ are constant and they do not need to be perpendicular to each other as it can be noted in Figure 4.1.

Remark 6.6. Although the disturbance μ acts on the acceleration of second-order the agents, it turns out that the resultant collective motion has the same behavior as for having the disturbance μ acting in the velocity for first-order agents as it has been shown in Chapter 2.

6.3 Estimators-based gradient control

In this section we are going to apply the same strategy of employing local estimators as in Chapter 3 in order to get rid of the undesired effects introduced by the mismatches.

Let us consider the following distributed control law with estimator

$$\begin{cases} \dot{\hat{\mu}} &= \hat{u} \\ u &= -v - \overline{B} D_z e - \overline{S}_1 D_z(\mu - \hat{\mu}) \end{cases},$$

where $\hat{\mu} \in \mathbb{R}^{|\mathcal{E}|}$ is the estimator state and $\hat{u}$ is the estimator input to be designed. Substituting the above control law to (6.1) gives us the following autonomous system

$$\dot{p} = v \tag{6.24}$$
$$\dot{v} = -v - \overline{B} D_z e - \overline{S}_1 D_z(\mu - \hat{\mu}) \tag{6.25}$$
$$\dot{z} = \overline{B}^T \dot{p} = \overline{B}^T v \tag{6.26}$$
$$\dot{e} = 2D_z^T \dot{z} = 2D_z^T \overline{B}^T v \tag{6.27}$$
$$\dot{\hat{\mu}} = \hat{u}. \tag{6.28}$$

Note that the estimating agents are again encoded in S_1, in other words, for the edge $\mathcal{E}_k$ the estimating agent is $\mathcal{E}_k^{\text{tail}}$.

Theorem 6.7. *For the autonomous system (6.24)-(6.28) that forms a rigid formation, consider a given desired formation shape and the following distributed control action for the estimator* $\hat{\mu}$

$$\hat{u} = -D_z^T \overline{S}_1^T v, \tag{6.29}$$

where the estimating agents are chosen arbitrarily. Then the equilibrium points $(p^*, v^*, z^*, e^*, \hat{\mu}^*)$ *of (6.24)-(6.28) are asymptotically stable. Furthermore,* $v^* = \mathbf{0}$ *and the steady-state deformation of the shape satisfies* $||e^*||^2 \leqslant 2||\mu - \hat{\mu}(0)||^2 + 2||v(0)||^2 + ||e(0)||^2$. *For the particular cases of triangles and tetrahedrons, the equilibrium* $e^* = \mathbf{0}$*, i.e.,* $\hat{\mu}^* = \mu$.

Proof. First we start proving that (6.29) is a distributed control law. This is clear since the dynamics of $\hat{\mu}_k$ (the k'th element of $\hat{\mu}$) are given by

$$\dot{\hat{\mu}}_k = z_k^T v_{\mathcal{E}_k^{\text{tail}}}, \tag{6.30}$$

which implies that the estimating agent $\mathcal{E}_k^{\text{tail}}$ for the edge $\mathcal{E}_k$ is only using the dot product of the associated relative position z_k and its own velocity. Note that using the notation in (6.18), the above estimator input is given by $\alpha_{k\mathcal{E}_k^{\text{tail}}}$. Consider the following Lyapunov function candidate

$$V = \frac{1}{2}||\xi||^2 + \frac{1}{2}||v||^2 + \frac{1}{4}||e||^2,$$

with $\xi = \mu - \hat{\mu}$, which satisfies

$$\begin{aligned}\frac{\mathrm{d}V}{\mathrm{d}t} &= \xi^T \dot{\xi} + v^T \dot{v} + \frac{1}{2} e^T \dot{e} \\ &= \xi^T D_z^T \overline{S}_1^T v - ||v||^2 - v^T \overline{B} D_z e - v^T \overline{S}_1 D_z \xi \\ &\quad + e^T D_z^T \overline{B}^T v \\ &= -||v||^2. \end{aligned} \tag{6.31}$$

From this equality we can conclude that ξ, v and e are bounded. Moreover, from the definition of e, z is also bounded. Thus all the states of the autonomous system (6.25)-(6.28) are bounded, so we can conclude the convergence of $v(t)$ to zero in view of (6.31). Furthermore, since the right-hand side of (6.25) is uniformly continuous, $\dot{v}(t)$ converges also to zero by Barbalat's lemma. By invoking the LaSalle's invariance principle, from (6.25) the states e, ξ and z converge asymptotically to

the largest invariance set given by

$$\mathcal{T} \triangleq \{e, z, \xi : \overline{S}_1 D_z \xi + \overline{B} D_z e = \mathbf{0}_{m|\mathcal{V}|\times 1}\}, \tag{6.32}$$

in the compact set

$$\mathcal{Q} \triangleq \{\xi, v, e : ||\xi||^2 + ||v||^2 + \frac{1}{2}||e||^2 \leqslant \rho\}, \tag{6.33}$$

with $0 < \rho \leqslant 2V(0)$. Since $v = \mathbf{0}$ for all points in this invariant set, it follows from (6.26)-(6.28) that z, e and $\hat{\mu}$ are constant in this invariant set. In other words, $z(t) \to z^*, e(t) \to e^*$ and $\xi(t) \to \xi^*$ as t goes to infinity, where z^*, e^* and $\hat{\mu}^*$ are fixed points satisfying (6.32). Note that by comparing (6.24) and (6.26) we can also conclude that $p(t) \to p^*$ as t goes to infinity. In general we have that e^* and ξ^* are not zero vectors, therefore $z^* \notin \mathcal{Z}$. It is also clear that $||e^*||^2 \leqslant 2\rho$, therefore for a sufficiently small ρ, the resultant (distorted) formation will also be infinitesimally and minimally rigid.

Showing that $e^*, \xi^* = \mathbf{0}_{m|\mathcal{E}|\times 1}$ for triangles and tetrahedrons follows immediately from the second part of the proof of Theorem 3.8 since the analysis about the same equilibrium $\mathcal{T}$. □

Remark 6.8. Following the results presented in Section 3.3.1 it is also possible to define a topology for the estimating agents such that we can focus the distortion of the shape to selected edges in Theorem 3.8.

If we adopt the same approach as in Section 3.2, we can guarantee that the mismatches can be fully compensated such that the final shape is the desired shape. We recall the following update law for each estimator as used in Section 3.2 in order to remove effectively both, the distortion and the steady-state collective motion:

$$\hat{u}_k = \kappa(e_k + \mu_k - \hat{\mu}_k), k \in \{1, \ldots, |\mathcal{E}|\}, \tag{6.34}$$

where $\kappa \in \mathbb{R}^+$ is an estimator gain that needs to be determined. For the first-order agents, it has been shown in [35] that there is a lower bound for choosing κ.

Consider now the following change of coordinates $h_k = e_k + \mu_k - \hat{\mu}_k$ and let $h \in \mathbb{R}^{|\mathcal{E}|}$ be the stacked vector of h_k's for all $k \in \{1, \ldots, |\mathcal{E}|\}$. By defining $S_2 \triangleq B - S_1$ it can be checked that the following autonomous system derived from

(6.25)-(6.28)

$$\dot{v} = -v - \overline{S}_2 D_z e - \overline{S}_1 D_z h \tag{6.35}$$

$$\dot{e} = 2D_z \overline{B}^T v \tag{6.36}$$

$$\dot{h} = 2D_z \overline{B}^T v - \kappa h \tag{6.37}$$

$$\dot{z} = \overline{B}^T v, \tag{6.38}$$

has an equilibrium at e^*, v^* and h^* equal to zero with $z^* \in \mathcal{Z}$. The linearization of the autonomous system (6.35)-(6.38) about such an equilibrium point leads to

$$\begin{bmatrix} \dot{v} \\ \dot{e} \\ \dot{h} \\ \dot{z} \end{bmatrix} = \begin{bmatrix} -\overline{I}_{|\mathcal{V}|} & -\overline{S}_2 D_{z^*} & -\overline{S}_1 D_{z^*} & \mathbf{0} \\ 2D_{z^*}\overline{B}^T & \mathbf{0} & \mathbf{0} & \mathbf{0} \\ 2D_{z^*}\overline{B}^T & \mathbf{0} & -\kappa I_{|\mathcal{E}|} & \mathbf{0} \\ \overline{B}^T & \mathbf{0} & \mathbf{0} & \mathbf{0} \end{bmatrix} \begin{bmatrix} v \\ e \\ h \\ z \end{bmatrix}. \tag{6.39}$$

From the Jacobian in (6.39) we know that the stability of the system only depends on v, e and h and not on z. We consider the following assumption that will play the same role as the one considered in the statement of Theorem 3.1 for first-order dynamics.

Assumption 6.9. The matrix $\begin{bmatrix} -\overline{I}_{|\mathcal{V}|} & -\overline{S}_2 D_{z^*} \\ 2D_{z^*}\overline{B}^T & \mathbf{0} \end{bmatrix}$ is Hurwitz.

Theorem 6.10. *If Assumption 6.9 holds then there exists a positive constant κ^* such that the equilibrium of $h = \mathbf{0}, v = \mathbf{0}$ and $e = \mathbf{0}$ (with $z^* \in \mathcal{Z}$) of the autonomous system (6.25)-(6.28) with the estimator input $\hat{u}_k$ be given by (6.34) is locally exponentially stable for all $\kappa > \kappa^* > 0$.*

Proof. Taking the Jacobian for v, e and h in (6.39) along with Assumption 6.9 as starting point, the main argument of the proof is identical to the one provided in Theorem 3.1 and it is omitted here for the sake of brevity. □

Remark 6.11. Since $v(t)$ converges exponentially to zero, it follows immediately that $p(t)$ converges exponentially to a fixed point p^*.

The Assumption 6.9 is also related to the stability of (second-order) formation control systems whose graph $\mathbb{G}$ defining the sensing topology is directed. In fact, it is straightforward to check that the matrix in the Assumption 6.9 is the Jacobian matrix for v and e in a distance-based formation control system (without mismatches) with only directed edges in $\mathbb{G}$. This relation shows how to choose the estimating agents in order to fulfill Assumption 6.9.

6.4 Distributed formation-motion control

In this section we are going to extend the findings in Chapter 4 about motion control of rigid formations from the single-integrator agent to the double integrator case. In particular we consider how to design the desired constant velocities ${}^b\omega^*$ and ${}^bv_c^*$ as in Figure 4.1 for an infinitesimally and minimally rigid formation, i.e., for $e = \mathbf{0}$. Following a similar strategy as in Section 4.1, we solve the motion control of rigid formation problem for double-integrators agents by employing mismatches as design parameters. More precisely, we assign again two motion parameters μ_k and $\tilde{\mu}_k$ to agents i and j in the edge $\mathcal{E}_k = (i, j)$ resulting in the following control law

$$u = -c_1 v - c_2 \overline{B} D_z e + \overline{A}(\mu, \tilde{\mu}) z, \tag{6.40}$$

where $c_1, c_2 \in \mathbb{R}^+$ are gains, $\mu \in \mathbb{R}^{|\mathcal{E}|}$ and $\tilde{\mu} \in \mathbb{R}^{|\mathcal{E}|}$ are the stacked vectors for all μ_k and $\tilde{\mu}_k$ and A is defined by

$$a_{ik} \triangleq \begin{cases} \mu_k & \text{if} \quad i = \mathcal{E}_k^{\text{tail}} \\ \tilde{\mu}_k & \text{if} \quad i = \mathcal{E}_k^{\text{head}} \\ 0 & \text{otherwise.} \end{cases} \tag{6.41}$$

The design of ${}^b\omega^*$ and ${}^bv_c^*$ is done via choosing appropriately the motion parameters μ and $\tilde{\mu}$, in the sense that we allow a desired steady-state collective motion but remove any distortion of the steady-state shape. The design of the motion parameters in A must take into account not only the desired acceleration but also the damping component in (6.40), which is different from the single-integrator case considered in Section 4.1.

Let the velocity error

$$e_v = v - \overline{A}_v(\mu, \tilde{\mu}) z, \tag{6.42}$$

where $A_v(\mu, \tilde{\mu})$ is designed employing the motion parameters described in Section 4.1 directly related to the desired steady-state collective velocity. When the velocity error e_v is zero and we are at the desired shape $z^*(t) \in \mathcal{Z}$ with the desired velocities in $v^*(t)$, then from (6.42) we have that

$$v^*(t) = \overline{A}_v z^*(t) \tag{6.43}$$

$$\begin{aligned} \dot{v}^*(t) &= \overline{A}_v \dot{z}^*(t) = \overline{A}_v \overline{B}^T v^*(t) = \overline{A}_v \overline{B}^T \overline{A}_v z^*(t) \\ &= \overline{A}_a z^*(t). \end{aligned} \tag{6.44}$$

Note that the desired parameters in $A_a(\mu, \tilde{\mu})$ correspond to the desired acceleration of the agents at the desired shape $\mathcal{Z}$. With this knowledge at hand we can design

the needed motion parameters for A in the control law in (6.40) as

$$A(\mu, \tilde{\mu}) = c_1 A_v(\mu, \tilde{\mu}) + A_a(\mu, \tilde{\mu}), \tag{6.45}$$

since for $e_v = \mathbf{0}_{m|\mathcal{V}|\times 1}$ and $e = \mathbf{0}_{|\mathcal{E}|\times 1}$ the control law (6.40) becomes

$$u = \overline{A}_a(\mu, \tilde{\mu}) z^*(t). \tag{6.46}$$

Note that $A(\mu, \tilde{\mu})$ can be computed directly from the motion parameters for the desired velocity as in the first-order case. We show in the next theorem that the desired collective-motion for the desired formation is stable for at least sufficiently small speeds.

Theorem 6.12. *There exist constants $\rho, \rho_\mu, \epsilon, c_1, c_2 > 0$ for system (6.1) with control law (6.40) and $A(\mu, \tilde{\mu})$ as in (6.45) and with a given desired infinitesimally and minimally rigid shape, such that if $[\begin{smallmatrix}\mu\\ \tilde{\mu}\end{smallmatrix}] \in \mathcal{M} \triangleq \{\mu, \tilde{\mu} : ||[\begin{smallmatrix}\mu\\ \tilde{\mu}\end{smallmatrix}]|| \leqslant \rho_\mu\}$, then the origin of the error dynamical system $e_v = \mathbf{0}$ and $e = \mathbf{0}$, with $e = \mathbf{0}$ corresponding to $z^*(t) \in \mathcal{Z}$, are exponentially stable in the compact set $\mathcal{Q} \triangleq \{e, e_v : \frac{\epsilon c_1 + c_2}{4}||e||^2 + \frac{1}{2}||e_v||^2 \leqslant \rho\}$. In particular, the steady-state shape is the same as the desired one and the steady-state collective motion of the formation corresponds to $v^*(t) = \overline{A}_v z^*(t)$.*

Proof. First we rewrite the control law (6.40) employing (6.42) and (6.45) as

$$u = -c_1 e_v - c_2 \overline{B} D z e + \overline{A}_a z. \tag{6.47}$$

Consider the following Lyapunov function

$$V = \frac{\epsilon c_1 + c_2}{4}||e||^2 + \frac{1}{2}||e_v||^2 + \epsilon e_v^T \overline{B} D_z e, \tag{6.48}$$

where V is positive definite in a neighborhood about $e = \mathbf{0}$ and $e_v = \mathbf{0}$ for a some sufficiently small $\epsilon \in \mathbb{R}^+$ in the compact set $\mathcal{Q}$ with $e = \mathbf{0}$ corresponding to $z \in \mathcal{Z}$.

The time derivative of (6.48) is given by

$$\begin{aligned}
\frac{\mathrm{d}V}{\mathrm{d}t} &= \frac{1}{2}(\epsilon c_1 + c_2)e^T\dot{e} + e_v^T\dot{e}_v + \epsilon e_v^T\overline{B}D_z\dot{e} + \epsilon e^T D_z^T\overline{B}^T\dot{e}_v \\
&+ \epsilon e_v^T\overline{B}D_{(\overline{B}^T v)}e \\
&= (\epsilon c_1 + c_2)e^T D_z^T\overline{B}^T(e_v + \overline{A}_v z) - c_1||e_v||^2 - c_2 e_v^T\overline{B}D_z e \\
&+ e_v^T\overline{A}_v\overline{B}^T\overline{A}_v z - e_v^T\overline{A}_v\overline{B}^T\overline{A}_v z - e_v^T\overline{A}_v\overline{B}^T e_v \\
&+ 2\epsilon e_v^T\overline{B}D_z D_z^T\overline{B}^T v - c_1\epsilon e^T D_z^T\overline{B}^T e_v - c_2\epsilon e^T D_z^T\overline{B}^T\overline{B}D_z e \\
&+ \epsilon e^T D_z^T\overline{B}^T\overline{A}_v\overline{B}^T\overline{A}_v z - \epsilon e^T D_z^T\overline{B}^T\overline{A}_v\overline{B}^T\overline{A}_v z \\
&- \epsilon e^T D_z^T\overline{B}^T\overline{A}_v\overline{B}^T e_v + \epsilon e_v^T\overline{B}D_{(\overline{B}^T v)}e \\
&= (\epsilon c_1 + c_2)e^T\underbrace{D_z^T\overline{B}^T\overline{A}_v z}_{f_1(e,\mu,\tilde{\mu})} - c_1||e_v||^2 - e_v^T\underbrace{\overline{A}_v\overline{B}^T}_{f_2(\mu,\tilde{\mu})}e_v \\
&+ 2\epsilon e_v^T\underbrace{\overline{B}D_z D_z^T\overline{B}^T}_{f_3(z)}e_v + 2\epsilon e_v^T\underbrace{\overline{B}D_z D_z^T\overline{B}^T\overline{A}_v z}_{f_4(\mu,\tilde{\mu},z,e)} \\
&- c_2\epsilon e^T\underbrace{D_z^T\overline{B}^T\overline{B}D_z}_{f_5(e)}e - \epsilon e^T\underbrace{D_z^T\overline{B}^T\overline{A}_v\overline{B}^T}_{f_6(\mu,\tilde{\mu},z)}e_v \\
&+ \epsilon e_v^T\underbrace{\overline{B}D_{(\overline{B}^T v)}}_{f_7(v)}e. \qquad (6.49)
\end{aligned}$$

Since $f_i, i \in \{1,\dots,7\}$ are locally Lipschitz functions in the compact sets $\mathcal{Q}$ and $\mathcal{M}$ and using Young's inequality to every cross-term in (6.49), we can bound $\dot{V}$ as follows

$$\begin{aligned}
\frac{\mathrm{d}V}{\mathrm{d}t} &\leqslant \bigg(c_2\Big(M_1(\mu,\tilde{\mu}) - \epsilon\lambda_5\Big) + \epsilon c_1 M_1(\mu,\tilde{\mu}) + \frac{3}{2}\bigg)||e||^2 \\
&+ \bigg(- c_1 + M_2(\mu,\tilde{\mu}) \\
&+ \epsilon^2\Big(\frac{2\lambda_3}{\epsilon} + M_4(\mu,\tilde{\mu},z) + M_6(\mu,\tilde{\mu},z) + M_7\Big)\bigg)||e_v||^2, \qquad (6.50)
\end{aligned}$$

where M_1 and M_4 are related to the Lipschitz constant of f_1 and f_4 in the compact set $\mathcal{Q}$ given μ and $\tilde{\mu}$, M_2 is the induced 2-norm of f_2 given μ and $\tilde{\mu}$, M_6 is the squared induced 2-norm of f_4 in the compact set $\mathcal{Q}$ given μ and $\tilde{\mu}$, and finally M_7 is the maximum squared induced 2-norm for f_7, λ_3 is the maximum eigenvalue of f_3 and λ_5 is the minimum eigenvalue of f_5 in the compact set $\mathcal{Q}$. First we note that for a sufficiently small ρ, then $\lambda_5 > 0$ by the same argument of having a desired infinitesimally and minimally rigid formation as in Lemma 6.2. The time derivative

(6.50) can be made negative as a result of the following steps:

- Choose a sufficiently small ρ_μ in $\mathcal{M}$ such that $M_1(\mu, \tilde{\mu}) - \epsilon\lambda_5 < 0$, i.e., downscale if necessary μ and $\tilde{\mu}$ by the same factor.
- Compute M_2 for the given $\mu, \tilde{\mu}$.
- Compute M_4 and M_6 for the given $\mu, \tilde{\mu}$ in the compact set $\mathcal{Q}$.
- Choose c_1 such that the second bracket in (6.50) is negative.
- Given c_1 choose $c_2 > c_2^*$ (employed for the calculation of ϵ) such that the first bracket in (6.50) is negative.

This guarantees the local exponential convergence of $e(t)$ and $e_v(t)$ to their origins, hence $z(t) \to z^*(t) \in \mathcal{Z}$, $v(t) \to \overline{A}_v z^*(t)$ and the stacked acceleration of the agents $a(t) \to \overline{A}_a z^*(t)$ as t goes to infinity. □

Remark 6.13. The limitation given by ρ_μ is exclusively related to the desired speed of the agents (as it has been shown in Chapter 4) and it does not restrict in any other way the desired collective motion for the formation. Therefore, once the motion parameters are given, for asserting the exponential stability of the system, one only has to downscale them if necessary.

Remark 6.14. For $\mu, \tilde{\mu} = \mathbf{0}_{|\mathcal{E}|}$ we have that $M_1, M_2, M_3, M_4, M_6 = 0$. Then employing (6.48) and applying differently the Young's inequalities in (6.49) one can prove that for $c_1, c_2 = 1$ the dissipative Hamiltonian system (6.4) is exponentially stable for a sufficiently small ϵ.

Remark 6.15. For desired constant drifts in triangular and tetrahedron formations, it can be checked from Chapter 4 that $M_1 = 0$. Therefore there is not restriction in the speed for such particular cases. In particular, one can use the Lyapunov function (6.48) with $\epsilon = 0$. It turns out that the formation with the proposed motion-shape controller is asymptotically stable for any $c_2 > 0$ for $c_1 > ||\overline{A}_v(\mu, \tilde{\mu})\overline{B}^T||^2$.

Remark 6.16. For a desired rotation about the centroid of an equilateral triangle, it can be checked from Chapter 4 that in addition to $M_1 = 0$ we have that $e_v^T f_2(\mu, \tilde{\mu}) e_v = 0$ since f_2 is skew symmetric. Therefore by using (6.48) with $\epsilon = 0$ one can prove the asymptotic stability of the origin of e_v and e for any $c_1, c_2 > 0$.

The result in Theorem 6.12 allows one to design the desired velocity for the given formation with respect to O_b as in Figure 4.1. This result extends the applications proposed in Chapter 4, e.g., for steering a infinitesimally and minimally rigid formation with a constant heading in O_g and for the tracking and enclosing of a target for second-order agents.

6.5 Concluding remarks

In this chapter we have analyzed the consequences of having a distance-based controller for rigid formations in the presence of mismatches for second-order agents, namely, a stationary distorted shape and an undesired collective motion of the formation. It turns out that, both first-order and second-order agents share precisely the same behaviour for the undesired collective motion. We have extended the estimator based solution proposed in Chapter 3 to remove the effects of the mismatches to second-order agents. We further extended the results from Chapters 4 and 5 using distributed motion parameters in order to control both the motion and the shape of the rigid formation at the same time to the second-order agents case.

Chapter 7

Formation control of a team of quadcopters

Measure with micrometer, mark with chalk, cut with axe and do not stop kicking it until it fits.

Indiana Jones: Wait!
Klaus Kerner: What now, Jones?
Indiana Jones: What about Plato's tenfold error?
Klaus Kerner: What about it?
Indiana Jones: Most of Plato's numbers were way off target.
Klaus Kerner: Hm ...
Indiana Jones: Just a thought.
Klaus Kerner: He may be right. We should divide by ten! Try one bead.

The fate of Atlantis.

UNMANNED vehicles, in particular the aerial ones also known as *drones*, are vehicles without a human pilot aboard. The first recorded use of a flying vehicle with some autonomous control occurred during the World War I in 1916, where the concept of a gyro-stabilized radio-control plane was successfully demonstrated as a *flying-bomb*. The state of the art of the drones has drastically changed since then, especially during the last decade due to the accessibility to the general public to the systems that compose a drone. Nowadays *open-source* projects such as Paparazzi [61] or Ardupilot [7] makes accessible to a person without any piloting skills to have a single autonomous drone for multiple purposes such as aerial photography, precision agriculture or area surveillance among others. However, these applications are usually limited to a one single drone and not to teams of drones, either there are not simple *real-time* solutions or they are not easy scalable and fully distributed. In this chapter we are going to develop easy implementable controllers to a quadcopter for applying the derived results in Chapter 6 in order to have a fully distributed team of quadcopters. The theoretical results of this chapter are validated in the faithful flight simulator X-Plane[1] [63].

[1] The weather in Groningen does not help too much for having a radio-control flying club around.

Figure 7.1: Flying quadcopter BeBop from Parrot company.

7.1 The quadcopter

A quadcopter is a multirotor helicopter that is lifted and propelled by four rotors. Quadcopters are classified as rotorcraft, as opposed to fixed-wing aircraft, because their lift is generated by a set of rotors. We consider that the quadcopter has a two pairs of identical fixed pitched propellers: two clockwise and two counter-clockwise. By changing the speed of each rotor it is possible to specifically generate a desired total thrust and therefore motion in 3D, and to create a desired total torque or turning force along the Z_Q axis. We will consider a typical quadcopter of one kilogram of mass and a diameter of about one meter as the one in Figure 7.1.

The first step for controlling a vehicle is always to model it. Since we are interested in controlling a formation of quadcopters with respect to the Earth we need first to define the corresponding frames of coordinates and their relations. Secondly we will set a *good enough* model for the considered quadcopter, by a good model we mean that for a vehicle with the mentioned characteristics many of the aerodynamics can be safely omitted for the demanded manoeuvrings[2]. Thirdly we will develop a set of controllers for flying autonomously a quadcopter such that they are compatbile with the findings of this thesis in order to have a flying coordinated team.

7.1.1 Frames of coordinates

We have shown throughout this thesis that if the quadcopters have equipped sensors such that they give the relative position of the vehicle with respect to their neighbors, then there is no need of more information in order to form a formation and designing a motion with respect to the shape O_b. However, this technology is still not accessible, reliable or affordable for the general public but it can be substituted by allowing communication among neighboring quadcopters if the vehicles have access to a Global Position System (GPS). Furthermore, in order to

[2]Off the record: While the classical concept of an airplane is a wing with an attached motor, the radio control plane is a motor with *an optional* attached wing.

design motions of the formation with respect to the Earth, at least one leader will need to know about a global reference.

We set the origin of the Earth-centered Earth-fixed frame O_E at the center of the planet, the Z_E axis is aligned with the rotational axis of the planet and the X_E axis is pointing to the zero-longitude meridian. Therefore O_E is rotating together with the planet. We define the Navigation frame O_N to the axes defining a tangent plane on the Earth's surface at the geodetic longitude l and latitude ϕ_g coordinates with respect to O_E. The axis X_N and Y_N points to the geographic North and East respectively. We define the Quad frame O_Q with the axis Z_Q pointing down. The attitude or alignment of the O_Q with respect to O_N is given by the following sequence of rotations:

1. Right-handed rotation about the Z_N, positive *yaw* angle ψ.

2. Right-handed rotation about the Y_N, positive *pitch* angle θ.

3. Right-handed rotation about the X_N, positive *roll* angle ϕ.

Therefore we can consider the following rotational matrix relating both navigation and quadcopter frames

$$
{}^{Q}_{N}R = \begin{bmatrix} c\theta c\psi & c\theta s\psi & -s\theta \\ -c\phi s\phi + s\phi s\theta c\psi & c\phi c\psi + s\phi s\theta s\psi & s\phi c\theta \\ s\phi s\psi + c\phi s\theta c\psi & -s\phi c\phi + c\phi s\theta s\psi & c\phi c\theta \end{bmatrix}, \tag{7.1}
$$

where we have denoted by s and c the sine and the cosine functions respectively.

In this chapter we will consider a fixed O_N close to the team quadcopters. In fact since the Earth's radius is about 6371 km, then for our purposes we can consider that the Earth is flat about a kilometer around of O_N. We consider that each quadcopter is able to measure via a localization device, its altitude h with respect to the Earth's surface and the geodetic longitude l and latitude ϕ_g. The transformation coordinates between the geodetic system and O_E is straightforward and given by

$$
{}^{E}p = \begin{bmatrix} (N+h)\cos\phi_g \cos l \\ (N+h)\cos\phi_g \sin l \\ \big(N(1-e^2)+h\big)\sin\phi_g \end{bmatrix}, \tag{7.2}
$$

where we have used the following constants defined by the World Geodetic System

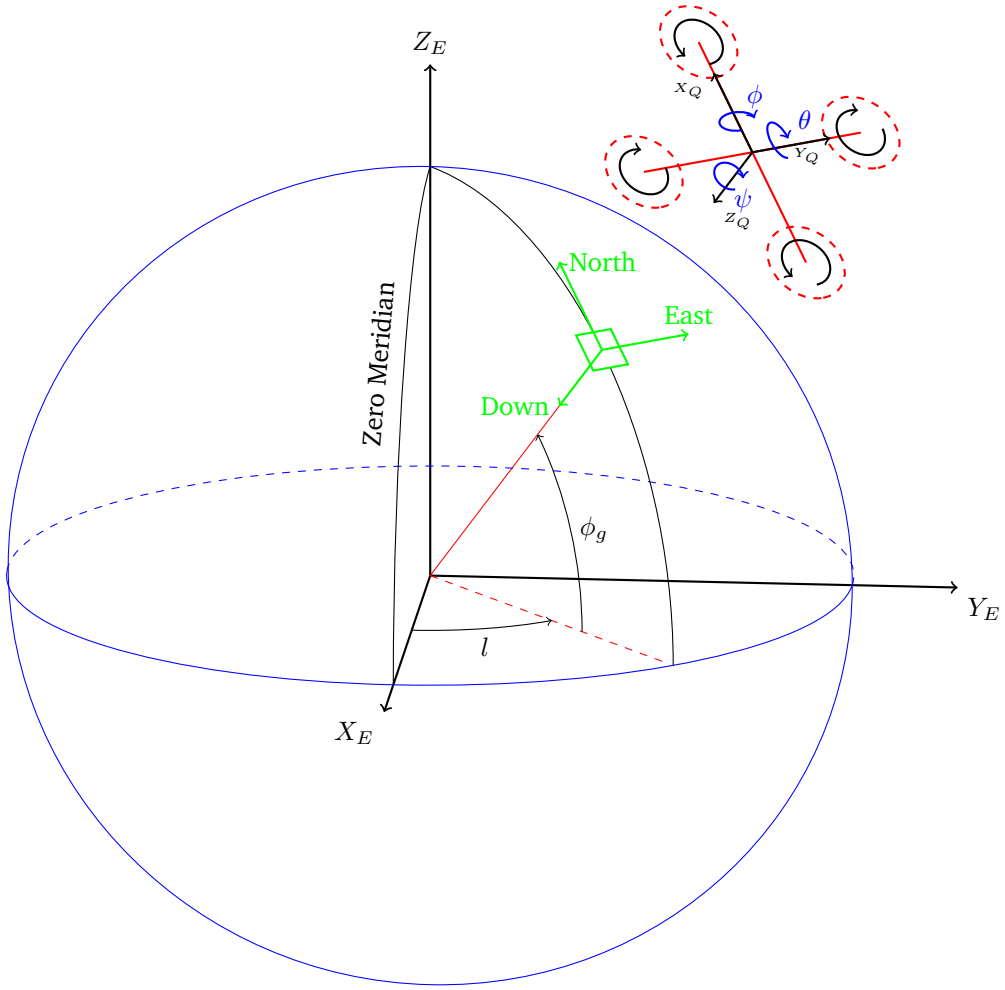

Figure 7.2: The frame of coordinates ECEF whose origin is at the center of the Earth and it rotates together with the planet. The Navigation coordinates, defined by the axes forming a plane tangent to the Earth's surface at the geodetic longitude l and latitude ϕ_g, are in green color and its X and Y axes point to the geographic North and East respectively. For simplicity the Earth has been represented as a perfect sphere in this drawing. The alignment of the Body frame with respect to the Navigation frame is given by the three attitude angles (in blue) ϕ, θ and ψ. The quadcopter almost behave as a kinematic point in 3D, in order to induce a rotation about the Z axis of the body, the propellers spin in different directions.

(WSG)-84 model [3]

$$\begin{aligned} a &\triangleq 6,378,137.0m \\ b &\triangleq 6,356,752m \\ e &= \frac{\sqrt{a^2+b^2}}{a} \\ N &= \frac{a}{\sqrt{1-e^2\sin^2\phi_g}}, \end{aligned}$$

therefore the Cartesian coordinates of the quad with respect to O_N can be computed as

$$^{N}p_{\text{Quad}} = {}^{E}_{N}R(^{E}p_{\text{Quad}} - {}^{E}p_{\text{NAV}}), \tag{7.3}$$

where the rotational matrix ${}^{E}_{N}R$ aligns the O_N frame to the O_E frame and is given by

$${}^{E}_{N}R = \begin{bmatrix} -\sin\phi_g^*\cos l^* & -\sin\phi_g^*\sin l^* & \cos\phi_g^* \\ -\sin l^* & \cos l^* & 0 \\ -\cos\phi_g^*\cos l^* & -\cos\phi_g^*\sin l^* & -\sin\phi_g^* \end{bmatrix},$$

where l^* and ϕ_g^* are the geodetic longitude and latitude respectively of the fixed O_N.

Note that in order to form a formation, the quadcopters by Lemma 4.1 do not need the matrix ${}^{E}_{N}R$ or the position ${}^{E}p_{\text{NAV}}$. The only necessary information that neighbors need to share is ${}^{E}p_{\text{Quad}}$ in order to compute the corresponding relative position. On the other hand, if we want to apply the result from Theorem 4.9, then at least one quadcopter will need the information about O_N as O_g.

7.1.2 Physical model

In this section we proceed to obtain a physical model of the quadcopter. In particular we will set a space-state model where the control inputs are the reference signals for the angular speed of the four propellers and the states are the position ${}^{N}p_{\text{Quad}}$, the velocity ${}^{N}\dot{p}_{\text{Quad}}$, the attitude angles ψ, θ and ϕ and their corresponding velocities.

Let us start with the following kinematic relation

$$\begin{bmatrix} \dot{\phi} \\ \dot{\theta} \\ \dot{\psi} \end{bmatrix} = \begin{bmatrix} 1 & t\theta s\phi & t\theta c\phi \\ 0 & c\phi & -s\phi \\ 0 & s\phi/c\theta & c\phi/c\theta \end{bmatrix} \begin{bmatrix} P \\ Q \\ R \end{bmatrix}, \tag{7.4}$$

where t is the tangent function and P, Q and R are the standard symbols for the three angular velocities measured at the quadcopter frame O_Q. In practice P, Q

and R are measured by a gyroscope on board. We will further make the following assumption

Assumption 7.1. The plane formed by the axes X_Q and Y_Q is almost parallel to the one formed by the axes X_N and Y_N.

In other words, we assume that ϕ and θ are sufficiently small angles such that

$$\begin{bmatrix} \dot{\phi} \\ \dot{\theta} \\ \dot{\psi} \end{bmatrix} \approx \begin{bmatrix} P \\ Q \\ R \end{bmatrix}. \tag{7.5}$$

We continue with writing the angular dynamics at the frame O_Q. It is well known that such dynamics correspond to the rigid body dynamics or Euler's equations

$$J\dot{\omega} = M - (\omega \times (J\omega)), \tag{7.6}$$

where J is the inertia tensor of the quadcopter, $\omega = \begin{bmatrix} P & Q & R \end{bmatrix}^T$ and $M = \begin{bmatrix} l & m & n \end{bmatrix}^T$ is the applied momentum by the propellers. Based on the symmetry of the quadcopter we can consider the following inertia tensor

$$J_Q \approx \begin{bmatrix} J_{xx} & 0 & 0 \\ 0 & J_{yy} & 0 \\ 0 & 0 & J_{zz} \end{bmatrix}, \tag{7.7}$$

where $J_{zz} \gg J_{xx} = J_{yy}$, and under Assumption 7.1 we can further write

$$\begin{cases} J_{xx}\ddot{\phi} & \approx (J_{yy} - J_{zz})\dot{\theta}\dot{\psi} + l \\ J_{yy}\ddot{\theta} & \approx (J_{zz} - J_{xx})\dot{\phi}\dot{\psi} + m \\ J_{zz}\ddot{\psi} & \approx n. \end{cases} \tag{7.8}$$

Let us now write the translational dynamics of the quadcopter at the body frame O_Q

$$\begin{cases} {}^Q\ddot{p}_x & = {}^Q\dot{p}_y R - {}^Q\dot{p}_z Q - g\sin\theta + \frac{{}^Q X_A + {}^Q X_T}{m} \\ {}^Q\ddot{p}_y & = {}^Q\dot{p}_z P - {}^Q\dot{p}_x R + g\sin\phi\cos\theta + \frac{{}^Q Y_A + {}^Q Y_T}{m} \\ {}^Q\ddot{p}_z & = {}^Q\dot{p}_x Q - {}^Q\dot{p}_y P + g\cos\phi\cos\theta + \frac{{}^Q Z_A + {}^Q Z_T}{m}, \end{cases} \tag{7.9}$$

where m is the mass of the quadcopter, g is the acceleration due to gravity, X_A, Y_A, Z_A are the aerodynamic forces present in the quadcopter and X_T, Y_T, Z_T are the forces due to the propellers. In addition to Assumption 7.1 we also consider the following

Assumption 7.2. There is almost not wind around O_N and the translational velocity ${}^{Q}\dot{p}$ is sufficiently small such that the aerodynamic forces are negligible.

Under Assumption 7.2 we have that X_A, Y_A, Z_A are zero. Since the only thrust is given by the propellers oriented along Z_Q we can then write that ${}^{Q}X_T$ and ${}^{Q}Y_T$ are zero and ${}^{Q}Z_T = -T$, i.e., the total thrust. In combination with Assumption 7.1 from (7.1) and (7.9) we have that

$$\begin{cases} {}^{N}\ddot{p}_z & \approx g - T/m \\ \phi & \approx \frac{m}{T}\left({}^{N}\ddot{p}_x \sin\psi - {}^{N}\ddot{p}_y \cos\psi\right) \\ \theta & \approx \frac{m}{T}\left({}^{N}\ddot{p}_x \cos\psi + {}^{N}\ddot{p}_y \sin\psi\right). \end{cases} \tag{7.10}$$

The approximations in (7.10) show that the vertical and horizontal motions of the quadcopter can be decoupled. Therefore, once the quadcopter is stabilized at a desired altitude ${}^{N}p_z^*$ with a thrust T^* overcoming the gravity g, in order to travel with respect to O_N with desired accelerations ${}^{N}\ddot{p}_x^*$ and ${}^{N}\ddot{p}_y^*$ we need to set the roll and pitch to ϕ^* and θ^* respectively derived from (7.10), whose dynamics are given by (7.8). In the next subsection we will show how to relate the force and moment inputs T, l, m and n in (7.10) and (7.8) with the angular speed of the propellers, which is the actual control inputs of our vehicle.

Remark 7.3. Once we have a team of quadcopters with the mission of accomplishing a 2D formation at a prescribed altitude, the desired accelerations ${}^{N}\ddot{p}_x^*$ and ${}^{N}\ddot{p}_y^*$ in (7.10) will be given by the results in Chapter 6, for example the control signal in (6.40).

7.1.3 Motors and propellers models

The propellers of the quadcopter are attached to a spinning motor in order to induce a thrust force. In aerodynamics the force originated from the propeller i can be modeled by

$$F_i = \frac{1}{2}\rho\, C\, V_i^2, \tag{7.11}$$

where ρ is the air density, V_i is the speed of the propeller into the airflow and C is an aerodynamic coefficient depending on many factors such as the Reynolds number, *angle of attack* or pitch of the propeller, size, etc. For more details in this matter we refer the reader to the excellent book [5]. Once a particular propeller has been chosen for the quadcopter, in the steady-state conditions we can consider all these factors constant (up to calibration) in (7.11), leading to

$$F_i = k_F\, \omega_i^2, \tag{7.12}$$

where ω_i is the angular speed of the propeller i. While the induce moments l and m are due mostly due to the force difference in the X_Q and Y_Q axes respectively, the induced moment n around the Z_Q axis is due to *yawing moment* originated by the spinning of the four propellers, similar to (7.11) we can consider that

$$n_i = k_M \, \omega_i^2, \tag{7.13}$$

where k_M is the corresponding yawing moment coefficient that is constant (up to calibration) when the quadcopter is at a steady-state condition.

We will consider *brushless* motors for spinning the propellers. These motors within their nominal state have a transitory time much faster than the dynamics given in (7.8) and (7.10) for our considered quadcopter. Therefore, we will assume that the setting point ω_i^* for the motor i will be the actual ω_i of the propeller, and the total thrust T and moments l, m and n at the frame O_Q can be calculated as

$$\begin{bmatrix} T \\ l \\ m \\ n \end{bmatrix} = \begin{bmatrix} -k_F & -k_F & -k_F & -k_F \\ 0 & -dk_F & 0 & dk_F \\ dk_F & 0 & -dk_F & 0 \\ -k_M & k_M & -k_M & k_M \end{bmatrix} \begin{bmatrix} \omega_1^2 \\ \omega_2^2 \\ \omega_3^2 \\ \omega_4^2 \end{bmatrix}, \tag{7.14}$$

where d is the distance from O_Q to a propeller and for the moment n we have consider the clockwise and counterclockwise rotations of the four propellers. As we will see in the following section, the controllers of the quadcopter will demand to generate a particular T, l, m and n signals. For such a task we will need the motors to satisfy

$$\begin{bmatrix} \omega_1^2 \\ \omega_2^2 \\ \omega_3^2 \\ \omega_4^2 \end{bmatrix} = \begin{bmatrix} -k_F & -k_F & -k_F & -k_F \\ 0 & -dk_F & 0 & dk_F \\ dk_F & 0 & -dk_F & 0 \\ -k_M & k_M & -k_M & k_M \end{bmatrix}^{-1} \begin{bmatrix} T \\ l \\ m \\ n \end{bmatrix}, \tag{7.15}$$

where it can be checked that the requested inverse certainly exists.

7.2 Controllers

In this section we will present a series of controllers in order to control the attitude, the altitude and the velocity ${}^N\dot{p}$ of the quadcopter. The first two controllers will give us the tools for applying directly the formation-motion control algorithms from Chapter 6 to the quadcopter. The velocity tracking controller has been developed in order to still apply the results from Chapters 3, 4 and 5, since the output of the algorithm for single-integrators can be employed as a desired velocity signal to be tracked.

7.2.1 Attitude controller

In order to control the attitude we define first the following error signals

$$e_\phi \triangleq \phi - \phi^* \tag{7.16}$$

$$e_\theta \triangleq \theta - \theta^* \tag{7.17}$$

$$e_\psi \triangleq \psi - \psi^*, \tag{7.18}$$

where ϕ^*, θ^* and ψ^* are the desired attitude angles, for instance, generated by the system (7.10). We propose then the following controllers for the system (7.8)

$$l = -k_{p_\phi} e_\phi - (J_{yy} - J_{zz})\dot{\theta}\dot{\psi} - k_{d_\phi}\dot{\phi} \tag{7.19}$$

$$m = -k_{p_\theta} e_\theta - (J_{zz} - J_{xx})\dot{\phi}\dot{\psi} - k_{d_\theta}\dot{\theta} \tag{7.20}$$

$$n = -k_{p_\psi} e_\psi - k_{d_\psi}\dot{\psi}, \tag{7.21}$$

where $k_{\{p_\phi, p_\theta, p_\psi, d_\phi, d_\theta, d_\psi\}} \in \mathbb{R}^+$ are control gains. We then provide the corresponding stability result.

Theorem 7.4. *The origin of the attitude error signals e_ϕ, e_θ and e_ψ from the closed-loop system (7.8) with control laws (7.19)-(7.21) is globally asymptotically stable for any $k_{\{p_\phi, p_\theta, p_\psi, d_\phi, d_\theta, d_\psi\}} > 0$.*

Proof. Consider the following Lyapunov function

$$V = \frac{k_{p_\phi}}{2} e_\phi^2 + \frac{k_{p_\theta}}{2} e_\theta^2 + \frac{k_{p_\psi}}{2} e_\psi^2 + \frac{J_{xx}}{2}\dot{\phi}^2 + \frac{J_{yy}}{2}\dot{\theta}^2 + \frac{J_{zz}}{2}\dot{\psi}^2, \tag{7.22}$$

whose time derivative satisfies by including (7.19)-(7.21)

$$\begin{aligned}
\frac{\mathrm{d}V}{\mathrm{d}t} &= k_{p_\phi} e_\phi \dot{\phi} + k_{p_\theta} e_\theta \dot{\theta} + k_{p_\psi} e_\psi \dot{\psi} + J_{xx}\dot{\phi}\ddot{\phi} + J_{yy}\dot{\theta}\ddot{\theta} + J_{zz}\dot{\psi}\ddot{\psi} \\
&= k_{p_\phi} e_\phi \dot{\phi} + k_{p_\theta} e_\theta \dot{\theta} + k_{p_\psi} e_\psi \dot{\psi} \\
&+ \Big((J_{yy} - J_{zz})\dot{\theta}\dot{\psi} + l\Big)\dot{\phi} + \Big((J_{zz} - J_{xx})\dot{\phi}\dot{\psi} + m\Big)\dot{\theta} + n\dot{\psi} \\
&= -k_{d_\phi}\dot{\phi}^2 - k_{d_\theta}\dot{\theta}^2 - k_{d_\psi}\dot{\psi}^2,
\end{aligned} \tag{7.23}$$

which is clearly non-increasing in the compact set

$$\mathcal{Q} \triangleq \Big\{ e_\phi, e_\theta, e_\psi, \dot{\phi}, \dot{\theta}, \dot{\psi} : \frac{k_{p_\phi}}{2} e_\phi^2 + \frac{k_{p_\theta}}{2} e_\theta^2 + \frac{k_{p_\psi}}{2} e_\psi^2 + \frac{J_{xx}}{2}\dot{\phi}^2 + \frac{J_{yy}}{2}\dot{\theta}^2 + \frac{J_{zz}}{2}\dot{\psi}^2 \leqslant V(0) \Big\}, \tag{7.24}$$

and by invoking LaSalle's invariance principle, we can conclude the asymptotic stability of the signals $e_\phi, e_\theta, e_\psi, \dot{\phi}, \dot{\theta}$ and $\dot{\psi}$ to the origin. □

Note that the Theorem 7.4 guarantees an upper bound given by (7.24) for the attitude angles, and this uppder bound can be shaped by the gains $k_{p_{\phi,\theta,\psi}}$ while the rate of convergence can be shaped by the gains $k_{d_{\phi,\theta,\psi}}$. In other words, it helps to keep Assumptions 7.1 and 7.2 satisfied.

7.2.2 Altitude controller

In order to control the altitude of the quadcopter, from (7.10) we have to deal with the gravity g. For now we will consider that g is unknown and we will relax Assumption 7.2 by including non-linear drag forces. Therefore we want to design a control input $u \in \mathbb{R}$ for the following system derived from (7.9)

$$\begin{cases} \dot{z} &= v_z \\ \dot{v}_z &= -C_D v_z |v_z| + g + u, \end{cases} \tag{7.25}$$

where z is the altitude with respect to O_N (recalling that negative means *up*), $C_D(t) \in \mathbb{R}^+$ is a positive state-dependent time-varying drag coefficient and the control input is related to the quadcopter by $u = \frac{T}{m}$. Let us define the following error signals

$$e_z = z - z^* \tag{7.26}$$

$$e_{\xi_g} = \xi_g - g, \tag{7.27}$$

where z^* is the desired altitude and $\xi_g \in R$ is the state of an estimator for compensating the gravity with dynamics

$$\dot{\xi}_g = u_{\xi_g}. \tag{7.28}$$

We propose the altitude controller with estimator

$$u = -\xi_g - k_p\, e_z - k_d\, v_z \tag{7.29}$$

$$u_{\xi_g} = v_z, \tag{7.30}$$

where $k_p, k_d \in \mathbb{R}^+$ are positive gains, and we obtain the following closed-loop system

$$\begin{cases} \dot{e}_z &= v_z \\ \dot{v}_z &= -C_D v_z |v_z| + g - \xi_g - k_p\, e_z - k_d\, v_z \\ \dot{e}_{\xi_g} &= v_z. \end{cases} \tag{7.31}$$

Theorem 7.5. *The origin of the closed-loop system (7.31) is globally asymptotically stable for any* $k_p, k_d > 0$.

Proof. Consider the following candidate Lyapunov function

$$V = \frac{k_p}{2} e_z^2 + \frac{1}{2} v_z^2 + \frac{1}{2} e_{\xi_g}^2, \tag{7.32}$$

whose time derivative satisfies

$$\begin{aligned} \frac{\mathrm{d}V}{\mathrm{d}t} &= k_p\, e_z \dot{z} + v_z \dot{v}_z + e_{xi_g} \dot{\xi}_g \\ &= -C_f v_z^2 |v_z| + (k_p\, e_z + g - \xi_g - k_p\, e_z - k_d\, v_z) v_z + e_{\xi_g} v_z \\ &= -C_f v_z^2 |v_z| - k_d\, v_z^2, \end{aligned} \tag{7.33}$$

which is clearly non-increasing in the compact set

$$\mathcal{Q} \triangleq \Big\{ e_z, v_z, e_{\xi_g} : k_p\, e_z^2 + v_z^2 + e_{\xi_g}^2 \leqslant 2V(0) \Big\}, \tag{7.34}$$

and by invoking LaSalle's invariance principle we can conclude that the origin of the closed-loop system (7.31) is globally asymptotically stable. □

We first note that k_d is related to the rate of convergence and that k_p is related with the maximum possible values of the signals e_z, v_z and e_{ξ_g}. The estimator ξ_g in Theorem 7.5 acts as an integral controller but with the advantage that its value converges to the actual gravity. Nowadays the value of gravity can be obtained from very accurate models [2] and therefore one can use a feedforward compensation in (7.29). In such a case, one can employ the estimator ξ_g for calibrating k_F in (7.12) since $u = \frac{T}{m}$ in (7.25) and the generation of T is in open-loop.

Remark 7.6. For steering the quadcopter to a 3D position with respect to O_N, for the X and Y coordinates we can still employ the same controller as in Theorem 7.5 but without needing an estimator since gravity only is present in the Z axis.

7.2.3 Velocity controller

Since we have already decoupled the horizontal and the vertical motion of the quadcopter in (7.10), we will consider to control the *North* and $East$ velocities in ${}^N\dot{p}$ of the quadcopter and again we introduce drag forces, namely

$$\dot{v} = -C_D v ||v|| + u_v, \tag{7.35}$$

where $v \in \mathbb{R}^2$ is the stacked vector of the North and East velocities in O_N, $C_D \in R^+$ is a positive constant drag coefficient and $u \in \mathbb{R}^2$ is the control input. Note that this control signal u_v will be employed for ${}^N\ddot{p}_x$ and ${}^N\ddot{p}_y$ in (7.10). Let us define

the following error signals

$$e_v = v - v^* \tag{7.36}$$
$$e_{\xi_{C_D}} = \xi_{C_D} - C_D, \tag{7.37}$$

where $v^* \in \mathbb{R}^2$ is the desired velocity and $\xi_{C_D} \in \mathbb{R}$ is the state of an estimator for estimating the drag coefficient with dynamics

$$\dot{\xi}_{C_D} = u_{\xi_{C_D}}. \tag{7.38}$$

Consider the control law with estimator

$$u_v = \xi_{C_D} v||v|| - k_v e_v \tag{7.39}$$
$$\dot{\xi}_{C_D} = -||v|| e_v^T v, \tag{7.40}$$

that leads to the following closed-loop system

$$\begin{cases} \dot{e}_v & = -C_D v||v|| + \xi_{C_D} v||v|| - k_v e_v \\ \dot{e}_{\xi_{C_D}} & = -||v|| e_v^T v. \end{cases} \tag{7.41}$$

Theorem 7.7. *The origin of the closed-loop system (7.41) is globally asymptotically stable for any $k_v > 0$.*

Proof. Consider the following candidate Lyapunov function

$$V = \frac{1}{2}||e_v||^2 + \frac{1}{2} e_{\xi_{C_D}}^2, \tag{7.42}$$

whose time derivative satisfies

$$\begin{aligned} \frac{\mathrm{d}V}{\mathrm{d}t} &= e_v^T \dot{e}_v + e_{\xi_{C_D}} \dot{e}_{\xi_{C_D}} \\ &= e_{\xi_{C_D}} ||v|| e_v^T v - k_v ||e_v||^2 - e_{\xi_{C_D}} ||v|| e_v^T v \\ &= -k_v ||e_v||^2, \end{aligned} \tag{7.43}$$

which is clearly non-increasing in the compact set

$$\mathcal{Q} \triangleq \left\{ e_v, e_{\xi_{C_D}} : ||e_v||^2 + e_{\xi_{C_D}}^2 \leqslant 2V(0) \right\}, \tag{7.44}$$

and by invoking LaSalle's invariance principle we can conclude that the origins of e_v and $e_{\xi_{C_D}}$ are globally asymptotically stable. □

Remark 7.8. Although the Theorem 7.7 provides global stability for the velocity, we cannot forget that our whole system is based on the Assumption 7.2, i.e., sufficiently small linear speeds.

Remark 7.9. The controller in Theorem 7.7 can be extended to track a vertical velocity by incorporating the gravity g to (7.35). In such a case several options are available such as having only one estimator or two compensating drag and gravity separately.

Figure 7.3 shows the Guidance Navigation and Control (GNC) scheme for one quadrotor based on the presented results. In order to assert the stability of the whole system in Figure 7.3, it is common to assume that the Quadrotor control block in Figure 7.3 is *faster* than the Formation control block. Moreover, we also assume that the estimation of the states in the Navigation block converge to the true values even *faster* than the Quadrotor control. This estimation is done by the Inertial Navigation System (INS) [27] and it is out of the scope of this thesis.

The approach of considering different *time scales* for the GNC system is not novel at all and is widely employed in many experimental setups [41, 56]. Fortunately, the analytical results in this thesis provide means for controlling the converge rate (time scales) of the different blocks in Figure 7.3 by the tuning gains in the Formation algorithms and in the Quadrotor controllers.

7.2.4 Experimental results

In this section we briefly validate the Theorems 7.4 and 7.5 for both controlling a 3D position of the quadcopter with respect to fixed point on the ground and for calibrating k_F in (7.11) by estimating correctly the gravity g.

We fix the origin of O_N at latitude 47.255037 degrees, longitude 11.345481 degrees and 576.5 meters over the mean sea level[3]. We have set the weather conditions to the equivalent of a calm sunny day, i.e., almost no wind, 20 Celsius degrees, etc. The quadcopter have decoupled the altitude and the position control respectively. For the altitude we use the controller (7.29)-(7.30) and for the position the controller (7.29) but omitting the estimator ξ_g. The output from these controllers (desired accelerations) feed the attitude controller (7.19)-(7.21). For the attitude controller we have chosen gains $k_{p_\phi} = k_{p_\theta} = 0.75$, $k_{p_\psi} = 0.13$, $k_{d_\phi} = k_{d_\theta} = 0.0075$, $k_{d_\psi} = 0.0013$. For the altitude controller we have chosen gains $k_p = 1$ and $k_d = 1$ and for the *XY* controller the gains $k_p = 0.1$ and $k_d = 1$.

Figure 7.4a) shows the trajectory of the quadcopter starting from the origin of O_N to the desired spot ${}^N p^* = (5, -2.5, 20)$ meters. The evolution of the position can be checked in Figures 7.4b) and 7.4c). Note how the quantization of the *raw* GPS signal is noticeable. The Figure 7.4e) shows how the estimation of the gravity

[3]This position corresponds to the Innsbruck's airport in Austria

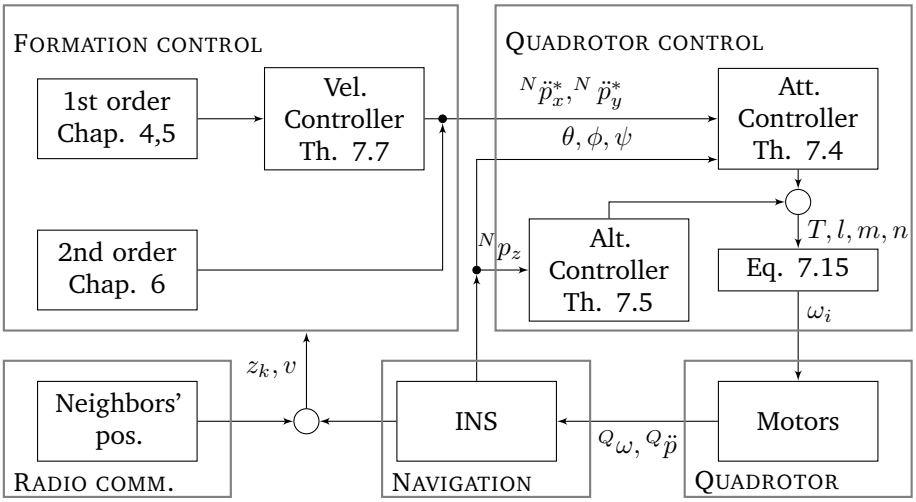

Figure 7.3: Guidance, Navigation and Control system of the quadrotor. The formation control block corresponds to the guidance system that generates the desired inertial acceleration signals for the quadrotor. One can choose among the first or second order algorithms from the Chapters 4, 5 and 6. Note that the second order algorithms do not need the extra block for controlling the velocity of the quadrotor. The quadrotor control block corresponds to the control of the altitude and attitude of the vehicle. If one desires to do 3D formation control, then ${}^N\ddot{p}_z^*$ must be provided by the Formation control block and the altitude controller is omitted. Finally, the Inertial Navigation System (INS) estimates the actual state of the quadrotor which is necessary for the formation and quadrotor controls blocks. The interpositions with respect to the neighbors of the quadrotor could be obtained by communication from the neighbors' INS or directly from on-board sensors as shown in [57].

coincides with its actual value, indicating that the calibration of k_F in (7.12) has been well done.

We will show the validation of Theorem 7.7 in the following section.

7.3 Formation control results

In order to do not overextend this chapter we will consider only three representative cases for a team of quadcopters. We will consider the team of four quadcopters placed at the Innsbruck's airport.

The first experiment will consider a team of four quadcopters with the mission of forming a regular square shape. However, we will consider that one the quadcopters has its range sensor biased with respect to the other three. As a result the final

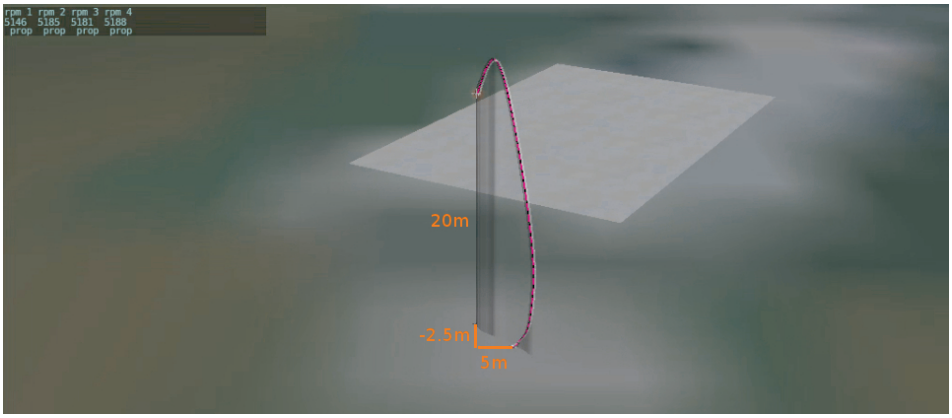

(a)

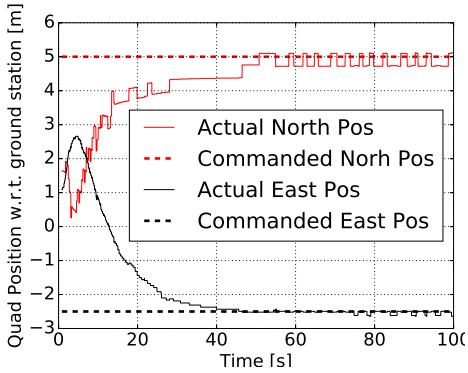

(b)

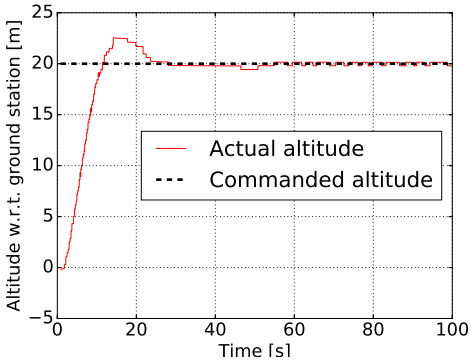

(c)

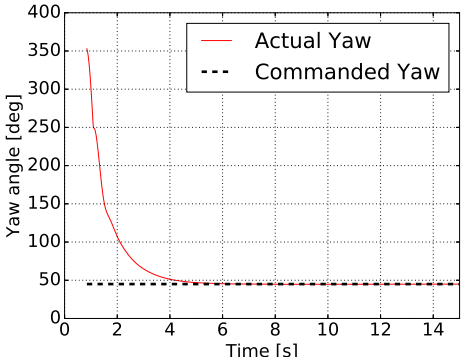

(d)

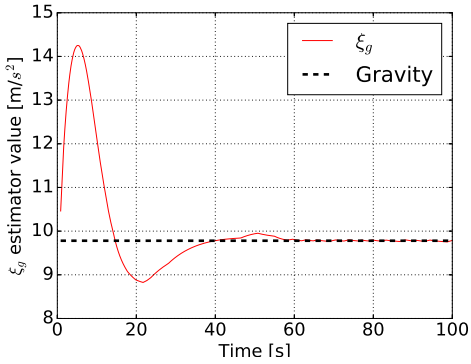

(e)

Figure 7.4: Experiment validating Theorems 7.4 and 7.5.

formation will be distorted and a steady-state motion will occur as stated in Theorem 6.4. We then apply the findings in Theorem 6.7 in order to estimate the undesired bias and to eliminate the undesired effects in the steady-state of the formation.

The second experiment, as in the Chapter 4, will consider the scenario of having four quadcopters flying in a squared formation with a prescribed orientation. This experiment will employ directly the results from the controller for second order dynamics discussed in Chapter 6 for feeding the attitude controller (7.19)-(7.21).

In the third experiment we will consider the scenario of having a team of three quadcopters intercepting and enclosing a free forth quadcopter flying with an unknown constant velocity. In this case, we will employ the results for first order dynamics from Chapter 4 for feeding the velocity tracking controller (7.39)-(7.40).

7.3.1 Square formation with biased range sensors

We first validate the results from Theorem 6.4. We consider a team of four quadcopter having as a prescribed shape a regular square with side-lenght of 50 meters. The weather conditions have been set with no wind. The sensing topology for the team of quadcopters is given by the following incidence matrix

$$B = \begin{bmatrix} 1 & 0 & -1 & 1 & 0 \\ -1 & 1 & 0 & 0 & 0 \\ 0 & -1 & 1 & 0 & 1 \\ 0 & 0 & 0 & -1 & -1 \end{bmatrix}, \tag{7.45}$$

and we set the vector of desired inter-distances to

$$d = \begin{bmatrix} 50 & 50\sqrt{2} & 50 & 50 & 50 \end{bmatrix}^T \text{meters}. \tag{7.46}$$

We induce a bias of 0.5 meters in the range sensor of quadcopter 1 with respect to the quadopter 2 in the edge $\mathcal{E}_1$. It is shown in Figure 7.5 that the quadcopters will converge to a steady-state distorted square and all of them follow a closed orbit as steady-state collective motion.

We now consider the following mismatches in the formation

$$\mu = \begin{bmatrix} -0.4 & 0.3 & 0.1 & -0.6 & 0.7 \end{bmatrix}. \tag{7.47}$$

In order to compensate them we implement the estimator in Theorem 6.10, and we set the controller gains to $c_1 = 0.02$, $c_2 = 0.02$ and $\kappa = 0.001$ and the initial conditions $\hat{\mu} = \mathbf{0}$. We show in Figure 7.6 the trajectories of the quads until they eventually stop with the desired shape once they estimated the mismatches, i.e., $\hat{\mu} = \mu$. We also show how the quadcopter 3 tracks the desired acceleration in Figure

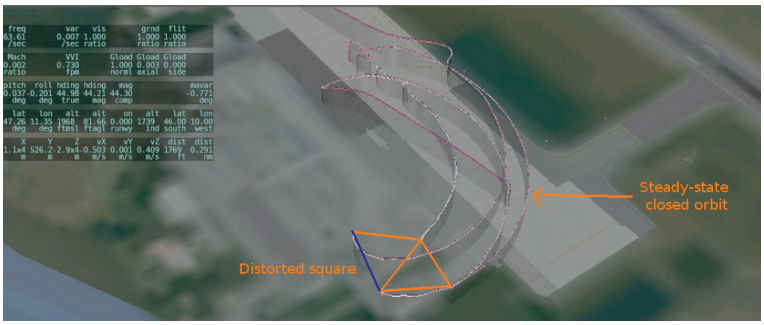

Figure 7.5: Flying formation of four quadcopters. In blue one of the vehicles has a biased sensor with respect to its neighbor. As a result, the formation will follow a steady-state collective motion and the target shape will be distorted.

7.6d). The discrepancy is due to non-modeled effects in the controller such as aerodynamic drag or centripetal forces. It is also obvious from the experiment that the centroid of the quadcopters is not static. In order to avoid a *messy* transitory, it would be advisable to start the estimators once the quadcopters are close to the prescribed target instead of from the very beginning.

7.3.2 Flying in formation with controlled heading

The mission's goal is to form a square shape with side-length of 50 meters at the same time they travel to the West with a velocity of 6 meters per second. We will consider wind from the North with an average speed of 1 meter per second. The sensing/communication topology is given by the incidence matrix (7.45) and the vector of desired inter-distances is set as in (7.46). We will consider that the heading of the formation is done by controlling ${}^{N}z_1$ by the quadcopter number 1, so we have

$$B_{or} = \begin{bmatrix} 1 & 0 & 0 & 0 & 0 \\ 0 & 0 & 0 & 0 & 0 \\ 0 & 0 & 0 & 0 & 0 \\ 0 & 0 & 0 & 0 & 0 \end{bmatrix}, \tag{7.48}$$

and combining the results from Theorems 4.9 and 6.12 we employ the following distributed control law, which will give the desired accelerations in O_N, for the quadcopters

$$u = c_1(-R(z)^T e - \overline{B}_{or} e_o) - c_2 v + c_2 \overline{A} \hat{z}, \tag{7.49}$$

where we have set $c_1 = 0.01$ and $c_2 = 0.2$, and the motion-parameters are

$$\mu = \begin{bmatrix} -6 & 0 & 0 & 0 & 6 \end{bmatrix}^T, \tilde{\mu} = \begin{bmatrix} -6 & 0 & 0 & 0 & 6 \end{bmatrix}^T. \tag{7.50}$$

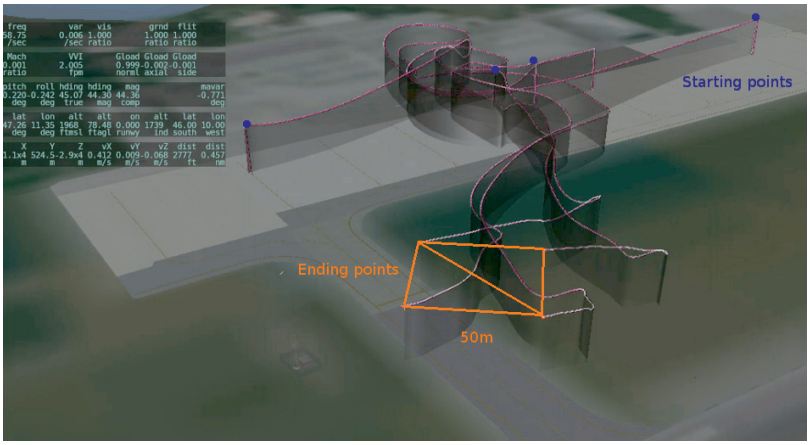

(a)

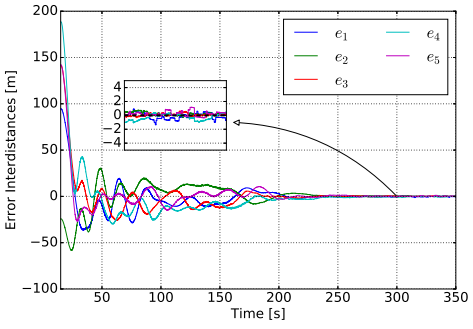

(b)

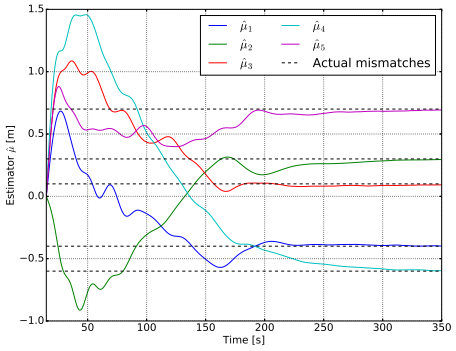

(c)

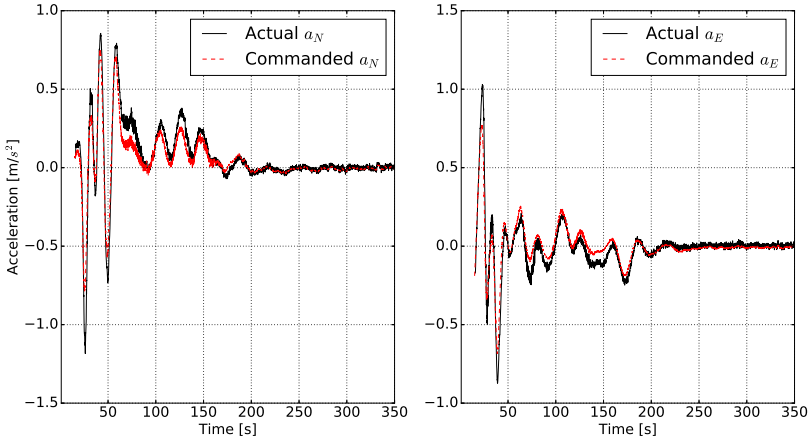

(d) Quadcopter number 3.

Figure 7.6: Flying squared formation of quadcopters estimating their mismatches.

Note that for the case of having only a desired translational velocity we have that $A_a(\mu, \tilde{\mu})$ is zero since the desired steady-state for the acceleration is zero.

We have again decoupled the vertical and the horizontal motion with 25 meters over the ground O_N as the desired altitude. We start the mission by achieving the desired altitude within the first 15 secs and then we activate the control law (7.49). The trajectories of the four quadcopters is shown in Figure 7.7a). We can observe in Figures 7.7b) and 7.7c) that the formation shape with the desired orientation is precisely achieved. In Figure 7.7e) we can see how the desired accelerations in O_N given by (7.49) for the quadcopter number 2 are tracked by employing the controller in Theorem 7.4. However two undesired effects occur. The first one, due to the wind, highlights that if all the quadcopters suffer the same translational disturbance, since the desired rigid shape is invariant to such disturbance we do not have any mean for counter-reacting it. The effect is that all the agents are travelling with a constant velocity of close to 1 meter per second to the South as we can observe in Figure 7.7d). The second undesired effect is due to the simplified model of the quadcopter and because the actual acceleration is achieved in open-loop. Since we have not taken into account effects such as aerodynamic drag, an stationary error occurs in the desired velocity. As it is shown in Figure 7.7d) we achieve a steady-state West velocity of about 5.5 meters per seconds instead of the desired 6 meters per second.

7.3.3 Tracking and enclosing a target

In this experiment we consider a team of three quadcopters initially placed at one of the parking spots of the Innsbruck's airport. The weather is a bit windy with an average of about 2 meter per second from the South. At the same time a forth quadcopter (the free target) is placed on the Airport's runway and starts to travel with a constant velocity of 1 meter per second to the West by employing the control law in Theorem 7.7. The team of three quadcopters has the mission of intercepting, tracking and orbiting the free target. We have again decoupled the vertical and the horizontal motion with 25 meters over the ground O_N as the desired altitude.

The desired 2D shape is the same as given in Figure 4.3 with $a = 50$ meters. We encode the sensing/communication topology of the system with the following matrix

$$B_d = \begin{bmatrix} 0 & 0 & 0 & 0 & 0 \\ -1 & 1 & 0 & -1 & 0 \\ 0 & -1 & 1 & 0 & -1 \\ 0 & 0 & 0 & 1 & 1 \end{bmatrix}.$$

We set the motion parameters to

$$\mu = \begin{bmatrix} 0 & 0 & 0 & -2a\gamma\sqrt{2} & 2a\gamma \end{bmatrix}^T \quad \tilde{\mu} = \begin{bmatrix} 0 & a\gamma & 0 & -a\gamma\sqrt{2} & 0 \end{bmatrix}^T,$$

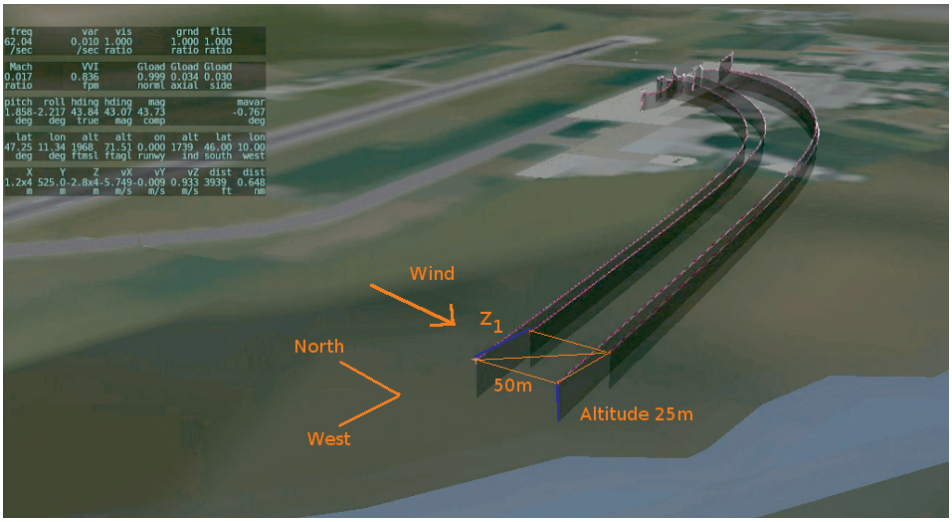

(a)

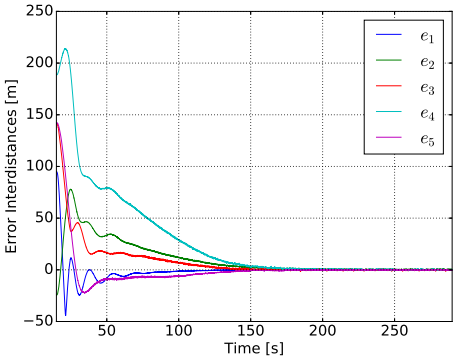

(b)

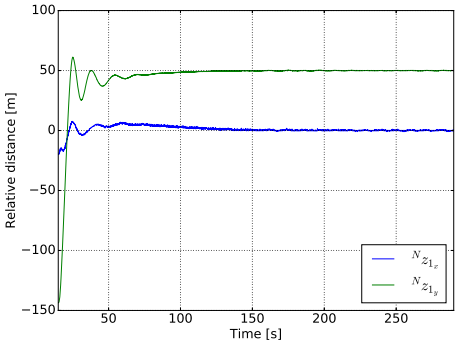

(c)

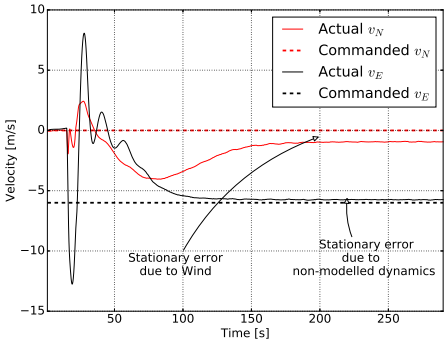

(d) Quadcopter number 2.

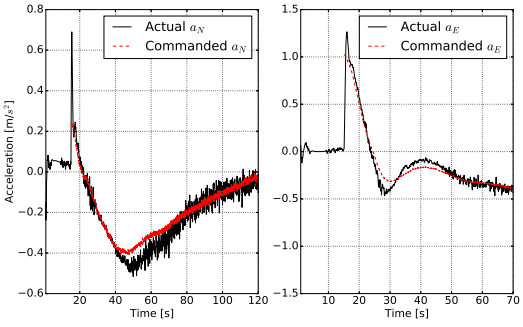

(e) Quadcopter number 2.

Figure 7.7: Flying squared formation of quadcopters with controlled heading.

where $\gamma = 0.0698$ rads/s sets the desired angular speed for the orbit motion around the target by the pursuers as it was explained in Chapter 4.4.1. The pursuers employ the following control law

$$\begin{cases} u & = -c\overline{B}_d D_{\hat{z}} e + \overline{A}(\mu, \tilde{\mu}) z + \hat{v} \\ \dot{\hat{v}} & = -\kappa \overline{B}_d D_{\hat{z}} e, \end{cases}$$

where u is employed as the desired signal for the velocity controller in Theorem 7.7. At the beginning of the mission we set $c = 0.002$ and $\kappa = 0.004$ and once the pursuers are close to the target, e.g., $||e|| < 100$, we boost the gains to ten times more in order to speed up the convergence. This is done in order to do not reach high values for the commanded velocity to the quadcopters, i.e., to satisfy Assumption 7.2.

We start the mission by achieving the desired altitude within the first 15 secs and then the pursuers go to intercept the free target. The trajectories of the quadcopters is shown in Figure 7.8a). The three pursuers achieve the desired shape with the desired angular speed around the target and estimating the target's velocity as it is shown in the Figures 7.8b), 7.8c) and 7.8d). The periodic discrepancy in the steady-state is due to the wind, which is blowing from a specific direction but the pursuers are orbiting about the target, therefore their controllers are facing a periodic disturbance. In Figure 7.8d) we can also check how the free target maintains the desired constant velocity by employing the control law (7.39)-(7.40). Finally we show how the velocity tracking controller of the pursuers is able to follow the desired signals in 7.8e).

7.4 Concluding remarks

In this Chapter we have developed a collection of simple acceleration, velocity and position tracking controllers for quadcopters. We have shown the compatibility of the estimator gradient-based and guidance controllers for second-order formations presented in Chapter 6 with the developed tracking controllers in a faithful flight simulator.

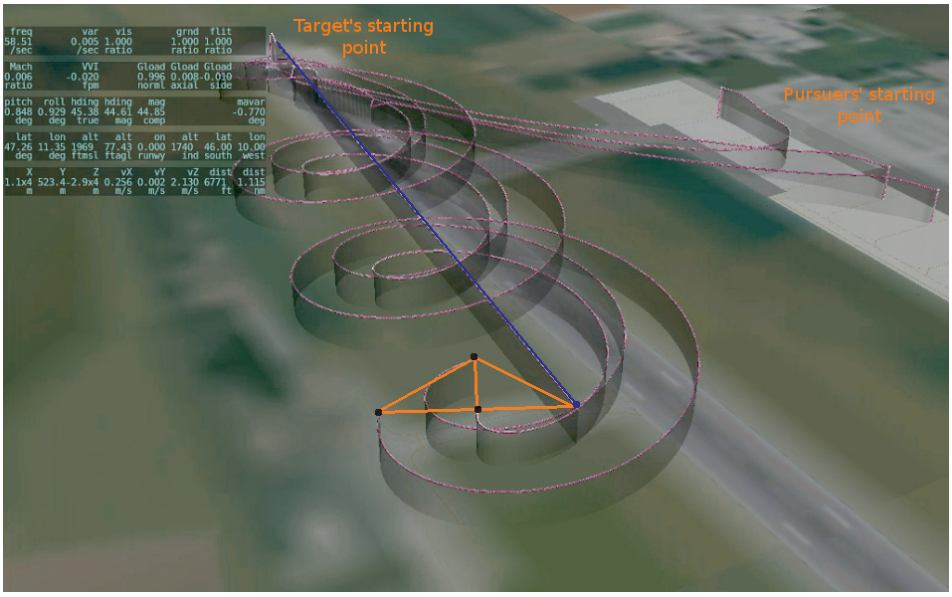

(a)

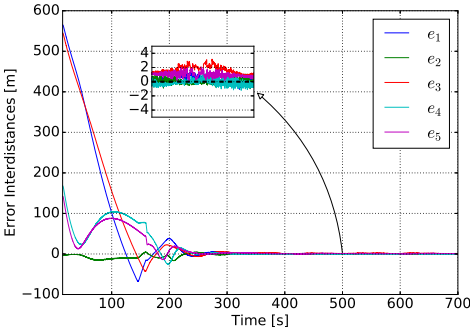

(b)

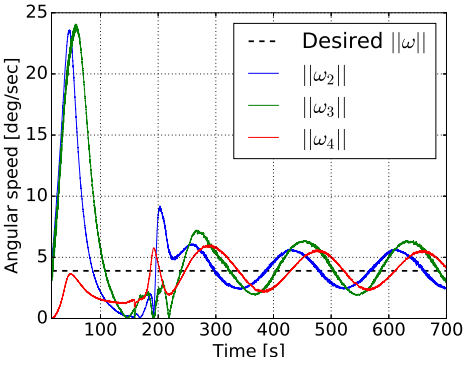

(c)

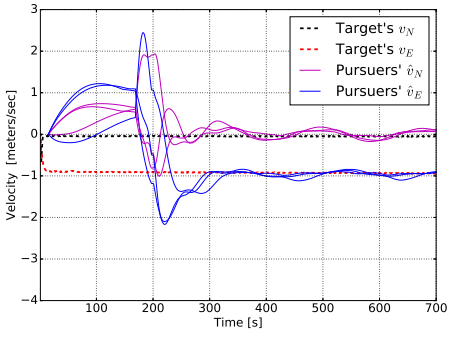

(d)

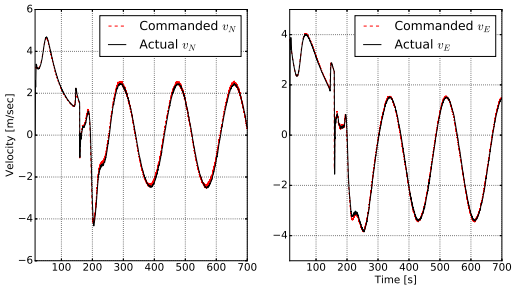

(e) Quadcopter number 2.

Figure 7.8: Three quadcopters intercept, track and orbit around a free target.

Chapter 8
Conclusions

Jones: You know, a lot of my discoveries seem like tall tales, even to me. At least there's some evidence now.

The fate of Atlantis.

We summarize in a list the main contributions of this thesis and we finally emphasize possible topics for carrying forward the presented work.

8.1 Contributions

This thesis has studied different problems in the field of distributed formation control. Hereby, we give the account of contributions and conclusions in each chapter.

- In Chapter 3 we have addressed the problem of having inconsistent measurements or mismatches in the prescribed inter-distances of neighboring agents in the gradient-based distance-based formation control setting. Such inconsistencies induce undesired effects on the formation, namely an unknown distortion in the steady-state shape and an undesired collective motion. Assuming that such inconsistencies are modelled by an unknown constant bias and a superposition of finite sinusoids with known frequency but unknown amplitude and phase, we provide a distributed algorithm, based on the internal model principle, that estimate such inconsistencies. Therefore we provide an online calibration method for the agents and we can get rid off such undesired effects. The estimators are distributed in the sense that they are executed locally in a set of agents that are called estimating agents. This estimator-based algorithm is based on the ground of two sufficient conditions, a gain in the estimator has to satisfy a lower bound and the estimating agents have to be chosen in a particular and systematic way. The addition of the estimator still preserves the exponential convergence of the original gradient-based formation controllers and does not need extra sensing. If the

deformation of the shape is not a big issue, we have provided an alternative distributed estimator-based algorithm that does not need a condition on any gain or how the estimating agents are chosen. However, with this alternative algorithm we have shown that the deformation of the steady-state shape depends on the topology of the estimating agents and therefore it can be controlled. Moreover, there is not distortion at all for the particular cases of triangular and tetrahedra formations. Finally, actual experiments with mobile robots illustrate the effectiveness of the presented algorithms.

- In Chapter 4 we have studied the problem of achieving simultaneously a desired shape with a desired motion in a formation. By exploiting the effect of having a steady-state collective motion under the presence of mismatches, we add a set of motion parameters to the prescribed distances of the autonomous agents but asserting the control of the prescribed shape of the formation. We analyze how to compute in a systematic way these distributed motion parameters in order to design a desired motion which is composed of the following superposition: a constant translational velocity and a constant rotational motion about the centroid of the formation. The desired velocity is designed with respect to a frame of coordinates fixed to the desired shape, i.e., is independent of a global frame of coordinates. One can design different trajectories with respect to a global frame of coordinates just combining different speeds for the translational and the rotational motion. These speeds are just regulated by rescaling the motion parameters by a constant. We have further shown the exponential stability of the system under these motion parameters. In the particular case of designing just a translational motion, it is possible for only one agent of the formation to control the orientation of the shape with respect to a global frame of coordinates, therefore a single leader can steer the whole formation while travelling with a controlled constant speed, and furthermore, preserving the order of the agents with respect to the direction of motion. These results enhance the popular leader-follower approach, where the followers need estimators in order to know the velocity of the leader. The results presented in this chapter are obviously free of such complexity. Another interesting application comes from taking advantage of the rotational motion. Indeed we can address the problem of enclosing and tracking a target travelling with an unknown velocity. We can assign distributed motion parameters to a team of pursuers in order to have the center of rotation at the target, whereas we can use the leader-follower approach in order to make the rest of the agents to estimate and compensate the unknown velocity of the target. We have finally shown actual experiments with mobile robots illustrating the findings of this chapter.

- In Chapter 5 we have studied the control of the scale of a rigid formation. We

first extend the recent findings in [88] about bearing rigidity theory, where a free-scaled shape is achieved by controlling the desired unit vectors in a similar way as it is done in the position-based approach. The extension consists in presenting an algorithm that allows the formation to achieve a distance-rigid shape by controlling the relative unit vectors among neighbors and at the same time by controlling only one edge a pair of agents decides the scale of the shape. We then have extended the usage of the distributed motion parameters from Chapter 4. Based again on the bearing rigidity theory, the distributed parameters can be employed not only for a controlled translation and/or spinning of the desired shape of the formation, but to control the scaling rate of the shape. We call these distributed parameters changing parameters. This is a desirable feature since the exponential convergence of the gradient-based controllers entails saturation problems to actual actuators, i.e., one should avoid step-inputs among different scales if the robots are far away from the desired scale. These distributed changing parameters allow to control precisely a time-variant scaling rate, e.g., a periodic sinusoidal one, of a scale-free shape based on distance rigidity. One of the main advantages of these morphing parameters is that they are totally compatible with the findings in Chapter 4, i.e., we can change the size of the scale of a formation while we steer it. We have finally shown actual experiments with mobile robots illustrating the findings of this chapter and their compatibility with the results from Chapter 4.

- In Chapter 6 we have analyzed the effects of having inconsistent measurements in the gradient-based formation controller for agents that are driven by second order dynamics, e.g., the Newtonian classical mechanics. We have shown that the second order dynamics case shares exactly the same ill behavior as the first order one, i.e., having an unknown distorted steady-state shape and a group collective motion composed of a constant translational and rotational velocity. We then have proceeded to develop distributed estimator algorithms in the same way as in Chapter 3 in order to estimate the inconsistencies and remove their undesired effects. As in the first order case, we have also extended and analyzed the exponential stability of the strategy of having distributed parameters in order to induce a desired motion to a multi agent system ruled by second order dynamics.

- In Chapter 7 we showed the applications of the results from Chapter 6 to a team of quadcopters flying outdoors. These popular aerial-vehicles are governed by second order dynamics and because of their mechanical construction its control can be quickly addressed. After modelling the dynamics of the quadcopter we have presented a series of tracking controllers for the position, velocity and acceleration in Earth coordinates, including a series of

estimators in order to estimate gravity of drag coefficients. We have carried out all the formation control experiments by employing a faithful flying simulator. Firstly we have shown the effectiveness of the acceleration controller by implementing the gradient-based controller to a team of four quadcopters. Secondly we have validated the reported undesired behavior in Chapter 6 when biases are present in the on board sensors of the quadcopters measuring the neighboring inter-positions. Thirdly we have validated the results from Chapter 6 for flying with a constant heading and velocity employing the acceleration tracking controller in the quadcopters. Finally we have validated the results of Chapter 4 for intercepting and tracking a target in combination of the usage of the velocity tracking controller for the quadcopters.

8.2 Further research

The main topic of this research is focused on formation control, mostly in its distance-based approach. Although in this thesis we have analyzed and proposed solutions for the practical implementation of the formation control algorithms, still several common practical issues need to be addressed in the future work. For example, a challenging problem is to consider time delays in the exchange of information. Since we were working with undirected topologies, the delay might be an issue among neighboring agents when we consider very large distances among them as in space missions. It is of interest to study what possible undesired effects in the formation may arise in the presence of delays. Another scenario is to consider time-triggered events for the acquisition of information by the agents. It seems reasonable to conjecture that the agents might not need to constantly measure local information such as inter-distances when they are far away from the prescribed behaviour. Another interesting problem in scenarios where the accuracy is a priority, is to study the effects in the formation by having quantized information. Indeed to study all these above mentioned problems at the same time will highly increase the complexity of the analysis, however, they deserve consideration as they have great practical relevance.

In order to be more specific by taking this thesis as a starting point for future works, we propose the following topics ordered by chapters.

- Chapter 3: Since the inconsistencies in the measurements of the agents are a source of undesired effects in gradient-based formation control, it is of interest to consider other measurement inconsistencies in order to address other sources of noises. The gains in the estimators of Theorems 3.1 and 3.8 require full information in order to be computed. It is desirable to extend the estimator-based algorithm for not requiring such pre-computed gain by allowing the agents to compute their own gains based on local information.

It is also interesting to analyze whether there exists a lower bound of the estimator's gains in Theorems 3.1 and 3.8, since we have shown that the given lower bound is a sufficient but not a necessary condition.

- Chapter 4: If a new agent joins a moving formation, it requires at least local communication with its neighbors in order to compute its motion parameters. It is desirable to develop an estimator algorithm for new agents in order to estimate their own motion-parameters without any communication at all. As in Chapter 3, in order to guarantee the local exponential stability, a gain requiring global information in Theorem 4.6 has to be computed. It is desirable to analyze whether the agents instead of employing such a gain, can employ a gain based only on local information.

- Chapter 5: In the case of designing a periodic scaling, all the changing parameters share the same sinusoidal signal. The first practical issue is that we require these signals to be synchronized, i.e., they have the same phase. It is desirable to implement an estimator, inspired by the internal model principle, in order to overcome such requirement.

- Chapter 6: It seems that the undesired effects of having mismatches among neighboring agents are not so dependent on the dynamics of the agents. An interesting problem is to generalize these effects to arbitrarily higher-order dynamics or more complicated ones with non-holonomic constraints.

- A combination of the results of Chapters 3 and 4 would be desirable, i.e., a combined algorithm that achieves changing-motion-control of the formation and at the same compensates possible inconsistent measurements.

Appendix

Appendix A
Mobile robots setup

The chosen platform is the wheeled robot Epuck [58]. The experimental setup consists of a team of three or four robots in a 2D area of about 2.6×2 meters. We have each robot tagged by a data-matrix on top as shown in Figure A.1. In order to apply the results from the presented theorems to the Epucks, we need to apply feedback linearization about a reference point to obtain the single-integrator dynamics. The chosen reference point is the intersection of the two solid bars of the data-matrix. There is a velocity tracking controller embedded in the robot ready for following the guidance velocity signals from the formation control algorithms. We emulate the localization sensors on board for obtaining the relative positions and distances between the robots by a camera on top of the scene. The real-time frames are processed in a PC, which estimates the relative positions and distances and transmits the corresponding information to the robots with a fixed frequency of 20Hz via Bluetooth. If a robot does not receive any information, it will *roughly* estimate the relative positions with respect to its neighbors based on its actual velocity and recent information. Since the proposed algorithms are fully distributed, each robot executes on board its control action based on the local information. The

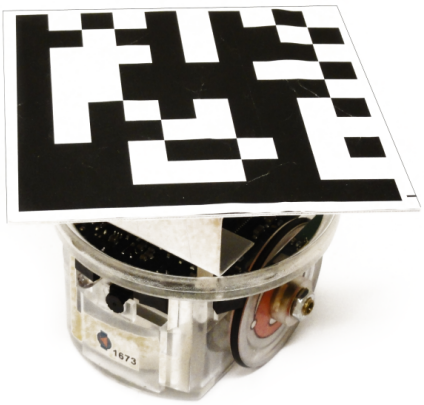

Figure A.1: Epuck robot with a data-matrix on top. The code in each data-matrix corresponds to the vertex node of the robot in the sensing graph $\mathcal{G}$.

whole image of the testing area is covered by 1280×720 pixels, where the distance between two consecutive horizontal or vertical pixels is about 2.0mm without taking into account aberrations of the camera when we are close to the borders of the image. The raw footage of the experiments reported in this thesis can be found in the playlist Robotics at `http://www.youtube.com/c/HectorGarciadeMarina`. In these videos you can also find the links to the employed source code.

Appendix B

Flight simulator X-Plane and employed quadcopter

B.1 X-Plane

The chosen platform for simulating the quadcopters is the faithful simulator X-Plane 9 [63]. This simulator has been certified by the American Federal Aviation Administration (FAA) for being used in actual pilots training. We run one instance of X-Plane per quadcopter. We have written an external software in order to read the state variables of the quadcopters from all the instances of X-Plane. These variables are then processed online in order to emulate in a realistic way, e.g. adding noises, the following on-board sensors:

- Localization system GPS. It provides reliable data about latitude and longitude in degrees up to six decimals, i.e. about half-meter of accuracy in the position. It also provides altitude over the mean sea level with an accuracy of about half-meter. It also provides velocities with respect to a navigation frame with an accuracy of about 0.5 meters per second. Updated with a frequency of 5Hz.
- 3-axis gyroscopes in order to measure the body angular velocities. Updated with a frequency of 60Hz.
- 3-axis accelerometers in order to measure the body accelerations. Updated with a frequency of 60Hz.
- 3-axis magnetometer in order to measure the Earth's magnetic field in body coordinates. Updated with a frequency of 60Hz.

The attitude angles are then estimated with a frequency of 60Hz by employing the algorithm presented by the author of this thesis in [33] which fuses GPS, gyroscopes, accelerometers and magnetometers readings.

The estimator-based and formation-motion-scaling controllers presented in this thesis are then computed in this external software in a distributed way, i.e. each quadcopter is an independent instance and computes its own control inputs using its available local data. Each quadcopter instance then sends back to X-Plane the inputs to its motors. The raw footage of the experiments reported in

Figure B.1: Quadcopter employed in the flight simulator X-Plane 9

this thesis can be found in the playlist Robotics at `https://www.youtube.com/c/HectorGarciadeMarina` along with links to the employed source code.

B.2 Technical details of the quadcopter

The employed quadcopter in X-Plane is a modified version of the one done by Jean Louis Naudin (`http://diydrones.com/profile/JeanLouisNaudin`) with the following main characteristics:

- Mass: 1.2Kg and inertia moment $J = \begin{bmatrix} 0.0075 & 0.0000 & 0.0000 \\ 0.0000 & 0.0075 & 0.0000 \\ 0.0000 & 0.0000 & 0.013 \end{bmatrix}$ Kgm^2.
- Diameter of 0.70 meters.
- Four electric brushless DC motors 2000Kv with propellers 7×5.

Bibliography

[1] P.A. Absil and K. Kurdyka. On the stable equilibrium points of gradient systems. *Systems & Control Letters*, pages 573–577, 2006.

[2] National Geospacial-Intelligence Agency. Wsg84 earth gravitational model, 2008. URL `http://earth-info.nga.mil/GandG/wgs84/gravitymod/`.

[3] National Geospacial-Intelligence Agency. World geodetic system, 2012. URL `http://web.archive.org/web/20120402143802/https://www1.nga.mil/ProductsServices/GeodesyandGeophysics/WorldGeodeticSystem/Pages/default.aspx`.

[4] B. D. O. Anderson, C. Yu, B. Fidan, and J. Hendrickx. Rigid graph control architectures for autonomous formations. *IEEE Control Systems Magazine*, 28: 48–63, 2008.

[5] John David Anderson Jr. *Fundamentals of aerodynamics*. Tata McGraw-Hill Education, 1985.

[6] Gianluca Antonelli, Filippo Arrichiello, and Stefano Chiaverini. Experiments of formation control with multirobot systems using the null-space-based behavioral control. *Control Systems Technology, IEEE Transactions on*, 17(5): 1173–1182, 2009.

[7] Ardupilot. Uav open-source project, 2007. URL `http://ardupilot.com`.

[8] L. Asimow and B. Roth. The rigidity of graphs, ii. *Journal of Mathematical Analysis and Applications*, pages 171–190, 1979.

[9] H. Bai, M. Arcak, and J. Wen. *Cooperative Control Design: A Systematic, Passivity-Based Approach*. Springer, New York, 2011.

[10] A. Belabbas, S. Mou, A.S. Morse, and B.D.O. Anderson. Robustness issues with undirected formations. In *Proc. of the 51st IEEE Conference on Decision and Control*, pages 1445–1450, Hawaii, USA, 2012.

[11] M. Belmont, J. Baker, and J. Horwood. Acoidance of phase shift errors in short term deterministic sea wave prediction. *Journal of Marine Engineering and Technology*, 2:21–26, 2003.

[12] Gerardo Beni. From swarm intelligence to swarm robotics. In *Swarm robotics*, pages 1–9. Springer, 2004.

[13] S. Bouabdallah. *Design and Control of Quadrotors with Application to Autonomous Flying*. Phd dissertation, Ecole Polytechnique Federale de Lausanne, 2007.

[14] Manuele Brambilla, Eliseo Ferrante, Mauro Birattari, and Marco Dorigo. Swarm robotics: a review from the swarm engineering perspective. *Swarm Intelligence*, 7(1):1–41, 2013.

[15] W. Burgard, M. Moors, D. Fox, R. Simmons, and S. Thrun. Collaborative multi-robot exploration. In *Robotics and Automation, 2000. Proceedings. ICRA '00. IEEE International Conference on*, volume 1, pages 476–481 vol.1, 2000.

[16] C. I. Byrnes and A. Isidori. Asymptotic stabilization of minimum phase nonlinear systems. *IEEE Transactions on Automatic Control*, 36:1122–1137, 1991.

[17] C.I. Byrnes, F. Delli Priscoli, and A. Isidori. *Output Regulation of Uncertain Nonlinear Systems*. Birkhauser, Boston, 1997.

[18] Andrea Caiti, Andrea Garulli, Flavio Livide, and Domenico Prattichizzo. Localization of autonomous underwater vehicles by floating acoustic buoys: A set-membership approach. *IEEE Journal of oceanic engineering*, 30:140–152, 2005.

[19] M. Cao, C. Yu, and B. D. O. Anderson. Formation control using range-only measurements. *Automatica*, 47:776–781, 2011.

[20] K. Cesare, R. Skeele, Soo-Hyun Yoo, Yawei Zhang, and G. Hollinger. Multi-uav exploration with limited communication and battery. In *Robotics and Automation (ICRA), 2015 IEEE International Conference on*, pages 2230–2235, May 2015.

[21] N. Chopra. Output synchronization on strongly connected graphs. *Automatic Control, IEEE Transactions on*, 57(11):2896–2901, Nov 2012.

[22] S. Coogan and M. Arcak. Formation control with size scaling using relative displacement feedback. In *American Control Conference (ACC), 2012*, pages 3877–3882, June 2012. doi: 10.1109/ACC.2012.6314988.

[23] C. de Persis and B. Jayawardhana. On the internal model principle in the coordination of nonlinear systems. *IEEE Trans. Contr. Netw. Syst.*, 1(3):272–282, 2014.

[24] ESA. Proba 3, 2016. URL `http://www.esa.int/Our_Activities/Space_Engineering_Technology/Proba_Missions/About_Proba-3`.

[25] ESA and NASA. evolved laser interferometer space antenna, 2034. URL `https://www.elisascience.org/`.

[26] E.Vos, J.M.A. Scherpen, and A.J. van der Schaft. Port-hamiltonian approach to deployment. In *Proc. of International Symposium on Mathematical Theory of Networks and Systems*, 2012.

[27] Jay Farrell. *Aided navigation: GPS with high rate sensors*. McGraw-Hill, Inc., 2008.

[28] J. Fink, N. Michael, S. Kim, and V. Kumar. Planning and control for cooperative manipulation and transportation with aerial robots. In *Proc. of the Int. Symposium of Robotics Research*, 2009.

[29] Jules Fleury, Guillaume Brunier, Emma Michaud, Edward J. Anthony, Sylvain Morvan, Philippe Dussouillez, and Antoine Gardel. High-resolution topography using SfM-photogrammetry from UAV for coastal mudflat geomorphic surveys. In EGU, editor, *EGU General Assembly 2016*, volume 18, pages EGU2016–15754, Vienna, Austria, 2016. URL `https://hal-amu.archives-ouvertes.fr/hal-01270138`.

[30] Thor I Fossen. *Guidance and control of ocean vehicles*. John Wiley & Sons, Ltd, 1994.

[31] Thor I Fossen. *Marine control systems: guidance, navigation and control of ships, rigs and underwater vehicles*. Marine Cybernetics AS, 2002.

[32] Jakob Fredslund and Maja J. Mataric. A general algorithm for robot formations using local sensing and minimal communication. *IEEE Transactions on Robotics and Automation*, 18:837–846, 2002.

[33] H. Garcia de Marina, F.J. Pereda, J.M. Giron-Sierra, and F. Espinosa. Uav attitude estimation using unscented kalman filter and triad. *Industrial Electronics, IEEE Transactions on*, 59(11):4465–4474, Nov 2012.

[34] H. Garcia de Marina, M. Cao, and B Jayawardhana. Controlling formations of autonomous agents with distance disagreements. In *Proc. of the 4th IFAC Workshop on Distributed Estimation and Control in Networked Systems*, 2013.

[35] H. Garcia de Marina, Ming Cao, and B. Jayawardhana. Controlling rigid formations of mobile agents under inconsistent measurements. *Robotics, IEEE Transactions on*, 31(1):31–39, Feb 2015.

[36] H. Garcia de Marina, B. Jayawardhana, and Ming Cao. Distributed rotational and translational maneuvering of rigid formations and their applications. *Robotics, IEEE Transactions on*, 32:684–696, June 2016.

[37] H. Garcia de Marina, B. Jayawardhana, and Ming Cao. Taming inter-distances mismatches for formation-motion control of rigid formations in second-order agents. *Automatic Control, IEEE Transactions on*, 2016. Submitted.

[38] H. Garcia de Marina, B. Jayawardhana, and Ming Cao. Precise scaling with motion control for teams of robots in rigid formations. *In preparation*, 2016.

[39] H. Garcia de Marina, B. Jayawardhana, and Ming Cao. Distributed scaling control of rigid formations. In *Proc. of 55th IEEE Conference on Decision and Control*, 2016.

[40] H. Garcia de Marina, B. Jayawardhana, and Ming Cao. On the role and compensation of distance mismatches in rigid formation control for second-order agents. In *Proc. of 10th IFAC Symposium on Nonlinear Control Systems*, 2016.

[41] J. H. Gillula, H. Huang, M. P. Vitus, and C. J. Tomlin. Design of guaranteed safe maneuvers using reachable sets: Autonomous quadrotor aerobatics in theory and practice. In *Proc. of the IEEE Int. Conf. on Robotics and Automation*, 2010.

[42] Herbert Goldstein. *Classical Mechanics*. Addison-wesley, 1951.

[43] Jing Guo, Gangfeng Yan, and Zhiyun Lin. Local control strategy for moving-target-enclosing under dynamically changing network topology. *Systems & Control Letters*, 59(10):654 – 661, 2010.

[44] U. Helmke, S. Mou, Z. Sun, and B. D. O. Anderson. Geometrical methods for mismatched formation control. In *Proc. of the 53rd Conference on Decision and Control*, pages 1341–1346, 2014.

[45] Lebrecht Henneberg. *Die graphische Statik der starren Systeme*, volume 31. BG Teubner, 1911.

[46] G. Hoffmann, S. Waslander, and C. Tomlin. Quadrotor helicopter trajectory tracking control. In *Proc. of AIAA Guidance, Navigation and Control Conference and Exhibit*, 2008.

[47] Hassan K Khalil and JW Grizzle. *Nonlinear systems*. Prentice hall New Jersey, 1996.

[48] L. Krick, M. E. Broucke, and B. A. Francis. Stabilization of infinitesimally rigid formations of multi-robot networks. *International Journal of Control*, 82: 423–439, 2009.

[49] Alex Kushleyev, Daniel Mellinger, Caitlin Powers, and Vijay Kumar. Towards a swarm of agile micro quadrotors. *Autonomous Robots*, 35(4):287–300, 2013.

[50] Ji-Wook Kwon and Dongkyoung Chwa. Hierarchical formation control based on a vector field method for wheeled mobile robots. *IEEE Transactions on Robotics*, 28:1335–1345, 2012.

[51] Ying Lan, Gangfeng Yan, and Zhiyun Lin. Distributed control of cooperative target enclosing based on reachability and invariance analysis. *Systems and Control Letters*, 59(7):381 – 389, 2010.

[52] Jonathan R. T. Lawton and Randal W. Beard. A decentralized approach to formation maneuvers. *IEEE Transactions on Robotics and Automation*, 19: 933–941, 2003.

[53] Zhiyun Lin, Lili Wang, Zhimin Han, and Minyue Fu. Distributed formation control of multi-agent systems using complex laplacian. *Automatic Control, IEEE Transactions on*, 59(7):1765–1777, 2014.

[54] A.J. Marasco, S.N. Givigi, and C.A. Rabbath. Model predictive control for the dynamic encirclement of a target. In *American Control Conference (ACC), 2012*, pages 2004–2009, June 2012.

[55] D. Mellinger. *Trajectory Generation and Control for Quadrotors*. Phd dissertation, University of Pennsylvania, 2012.

[56] Daniel Mellinger, Nathan Michael, and Vijay Kumar. Trajectory generation and control for precise aggressive maneuvers with quadrotors. *The International Journal of Robotics Research*, 31(5):664–674, 2012.

[57] Luis Merino, Johan Wiklund, Fernando Caballero, Anders Moe, José Ramiro Martinez De Dios, P-E Forssen, Klas Nordberg, and Anibal Ollero. Vision-based multi-uav position estimation. *IEEE robotics & automation magazine*, 3(13):53–62, 2006.

[58] F. Mondada, M. Bonani, X. Raemy, et al. The e-puck, a robot designed for education in engineering. In *Proc. of the 9th Conference on Autonomous Robot Systems and Competitions*, pages 59–65, 2009.

[59] S. Mou, A. S. Morse, A. Belabbas, Z. Sun, and B.D.O. Anderson. Undirected rigid formations are problematic. *IEEE Transactions on Automatic Control, to appear.*, 2016.

[60] K.K. Oh and H.S. Ahn. Distance-based undirected formation of single-integrator and double-integrator modeled agents in n-dimensional space. *International Journal of Robust and Nonlinear Control*, pages 1809–1820, 2014.

[61] Paparazzi. Uav open-source project, 2003. URL `http://wiki.paparazziuav.org/`.

[62] Myoung-Chul Park, Kyungmin Jeong, and Hyo-Sung Ahn. Formation stabilization and resizing based on the control of inter-agent distances. *International Journal of Robust and Nonlinear Control*, 25(14):2532–2546, 2015.

[63] Laminar Research. Flight simulation, 2016. URL `http://www.x-plane.com`.

[64] J.R. Riehl and Ming Cao. Formation control for cooperative containment of a diffusing substance. In *European Control Conference*, pages 1909–1914, June 2014.

[65] Matthes Rieke, Theodor Foerster, Jakob Geipel, and Torsten Prinz. High-precision positioning and real-time data processing of uav-systems. *Proceedings of the International Archives of Photogrammetry, Remote Sensing and Spatial Information Science (UAV-g 2011), Zurich, Switzerland*, 1416, 2011.

[66] Erol Şahin. Swarm robotics: From sources of inspiration to domains of application. In *Swarm robotics*, pages 10–20. Springer, 2004.

[67] K. Sakurama, S. i. Azuma, and T. Sugie. Distributed controllers for multi-agent coordination via gradient-flow approach. *IEEE Transactions on Automatic Control*, 60(6):1471–1485, June 2015.

[68] I. Shames, S. Dasgupta, B. Fidan, and B.D.O. Anderson. Circumnavigation using distance measurements under slow drift. *Automatic Control, IEEE Transactions on*, 57(4):889–903, April 2012.

[69] Roger Skjetne, Sonja Moi, Thor Fossen, et al. Nonlinear formation control of marine craft. In *Decision and Control, 2002, Proceedings of the 41st IEEE Conference on*, volume 2, pages 1699–1704. IEEE, 2002.

[70] Roger Skjetne, Sonja Moi, Thor Fossen, et al. Nonlinear formation control of marine craft. In *Decision and Control, 2002, Proceedings of the 41st IEEE Conference on*, volume 2, pages 1699–1704. IEEE, 2002.

[71] D. M. Stipanovic, C. R. Graunke, K. A. Intlekofer, and M. W. Spong. Formation control and collision avoidance for multi-agent non-holonomic systems: Theory and experiments. *International Journal of Robotics Research*, 27:107–126, 2008.

[72] Z. Sun and B.D.O. Anderson. Rigid formation control systems modelled by double integrators: system dynamics and convergence analysis. In *Proc. of the Australian Control Conference (ACC'15)*, 2015.

[73] Z. Sun, S. Mou, Brian D.O. Anderson, and A. Stephen Morse. Non-robustness of gradient control for 3-d undirected formations with distance mismatch. In *Proc. of the 2013 IEEE Australian Control Conference*, pages 369–374, 2013.

[74] Z. Sun, S. Mou, B.D.O. Anderson, and A.S. Morse. Formation movements in minimally rigid formation control with mismatched mutual distances. In *Proc of the 53rd Conference on Decision and Control*, 2014.

[75] Z. Sun, S. Mou, U. Helmke, and B. D. O. Anderson. Convergence analysis for rigid formation control with unrealizable shapes: The 3 agent case. In *Proc. of the 4th Australian Control Conference, Canberra (AUCC'14), Australia*, 2014.

[76] Z. Sun, Q. Liu, C. Yu, and B.D.O. Anderson. Generalized controllers for rigid formation stabilization with application to event-based controller design. In *Proc. of the European Control Conference (ECC'15)*, pages 217–222, 2015.

[77] Z. Sun, Q. Liu, C. Yu, and B.D.O. Anderson. Cooperative event-based rigid formation control. `http://zysun.weebly.com/research-and-publications.html`, submitted, 2015.

[78] Zhiyong Sun, Shaoshuai Mou, Brian DO Anderson, and Ming Cao. Exponential stability for formation control systems with generalized controllers: A unified approach. *Systems & Control Letters*, 93:50–57, 2016.

[79] I. Suzuki and M. Yamashita. Distributed anonymous mobile robots: Formation of geometric patterns. *SIAM J. Comput.*, 28:1347–1363, 1999.

[80] Y. Tian and Q. Wang. Global stabilization of rigid formations in the plane. *Automatica*, 49:1436–1441, 2013.

[81] Sadayuki Tsugawa, Shin Kato, and Keiji Aoki. An automated truck platoon for energy saving. In *Intelligent Robots and Systems (IROS), 2011 IEEE/RSJ International Conference on*, pages 4109–4114. IEEE, 2011.

[82] Arjan van der Schaft. Port-hamiltonian systems: an introductory survey. In *Proceedings of the International Congress of Mathematicians Vol. III: Invited Lectures*, pages 1339–1365, Madrid, Spain, 2006. European Mathematical Society Publishing House (EMS Ph).

[83] Zijian Wang and Mac Schwager. Multi-robot manipulation without communication. In *Distributed Autonomous Robotic Systems*, pages 135–149. Springer, 2016.

[84] P. Wieland, R. Sepulchre, and F. Allgower. An internal model principle is necessary and sufficient for linear output synchronization. *Automatica*, 47: 1068–1074, 2011.

[85] C. Yu, B. D. O. Anderson, S. Dasgupta, and B. Fidan. Control of minimally persistent formations in the plane. *SIAM Journal on Control and Optimization*, 48:206–233, 2009.

[86] Jing Yuan, Yalou Huang, Tong Tao, and Fengchi Sun. A cooperative approach for multi-robot area exploration. In *Proc. of IEEE International Conference on Intelligent Robots and Systems (IROS)*, pages 1390–1395, 2010.

[87] D. Zelazo, A. Franchi, and P.R. Giordano. Rigidity theory in se(2) for unscaled relative position estimation using only bearing measurements. In *Control Conference (ECC), 2014 European*, pages 2703–2708, June 2014.

[88] S. Zhao and D. Zelazo. Bearing rigidity and almost global bearing-only formation stabilization. *Automatic Control, IEEE Transactions on, to appear.*, 2016.

[89] S. Zhao and D. Zelazo. Translational and scaling formation maneuver control via a bearing-based approach. *Control of Network Systems, IEEE Transactions on, to appear.*, 2016.

Summary

This thesis addresses several theoretical and practical problems related to formation-control of rigid frameworks.

First we focus on dealing with the robustness issues of having inconsistent measurements, e.g. biases in the agents' range sensors, in the gradient-based formation-control of rigid frameworks. We propose a control strategy that eliminates such inconsistencies and at the same time we preserve the advantages of the distributed gradient control. This idea is based on placing local estimators at a subset of agents that estimate and compensate such inconsistencies. In other words this method allows the agents to calibrate their sensors locally among themselves at the same time that formation-control is running. We further extend the structure of the estimators in order to deal with broader inconsistencies. Indeed by employing the internal model principle, the estimators can handle inconsistent measurements based on a constant bias plus a finite series of sinusoids where only their frequency is known.

Second, we propose a distributed method for steering a rigid formation in a rotation and/or translation manner with respect to a frame of coordinates attached to the formation itself. By assigning motion parameters to the prescribed inter-distances of the agents one can achieve simultaneously the desired steady-state formation shape and the group motion. We further extend this result in order to solve two practical problems: the design of a constant translation of the formation with a controlled orientation with respect to a global frame of coordinates; and the tracking and enclosing of a target problem where one assigns a desired formation shape to specify how the target is enclosed and tracked by the pursuers.

Third, the simple structure of the above mentioned motion parameters opens the possibility of controlling the morphing of the formation shape. We propose a method based on distributed morphing parameters in order to control the scaling rate of a given scale-free shape. This result is compatible with steering the formation with the motion parameters, therefore the desired scaling can be achieved

simultaneously to the desired motion.

Forth, we carried out the stability analysis and effects of inconsistent measurements in a gradient-based formation-control of second-order agents' dynamics. We show that the first-order and the second-order have exactly the same non-desired consequences. We finally extend further the presented estimator-based algorithms and the motion-control by distributed motion parameters approach to the second-order dynamics case.

Finally, throughout the thesis we show practical experiments with actual mobile robots covering the developed algorithms for first-order dynamics and we have developed a series of tracking controllers for quadcopters in order to validate the estimator-based and motion-morphing-control algorithms for the second-order dynamics case.

Samenvatting

In dit proefschrift worden verschillende theorieën en praktische problemen aangekaart, gerelateerd aan formatievorming van rigide structuren.

Als eerste richten we ons op het aanpakken van de robuustheid onder invloed van onnauwkeurige metingen in formatievorming van rigide structuren met behulp van de gradiëntmethode. Een voorbeeld hiervan is de situatie waarbij de afstandssensoren van de agenten in de formatie structurele fouten maken. Wij stellen een besturingsstrategie voor die onnauwkeurigheden compenseert en tegelijkertijd het voordeel behoudt van aansturing met behulp van een gedistribueerde gradiëntmethode. Aan de basis van dit idee ligt het plaatsen van lokale schatters bij een deelverzameling van de agenten die de onnauwkeurigheden inschatten en hiervoor compenseren. Met andere woorden, deze methode stelt de agenten in staat om hun sensoren lokaal en onderling te kalibreren tijdens het vormen van de formatie. We breiden de structuur van de schatters verder uit om meerdere soorten onnauwkeurigheden te kunnen compenseren. Met behulp van het principe van het inwendig model kunnen de schatters omgaan met onnauwkeurige metingen die bestaan uit een constante afwijking plus een eindige reeks sinusoïden waarvan enkel de frequentie bekend is.

Als tweede dragen we een gedistribueerde methode aan voor het aansturen van rotatie en/of translatie in een rigide formatie ten opzichte van een lokaal referentiestelsel. Door het toewijzen van zogenaamde 'volg'-parameters aan voorgeschreven afstanden tussen de agenten kan men tegelijkertijd bereiken dat de agenten zowel een voorgeschreven formatie aannemen als een algemene groepsbeweging ondergaan. We gebruiken deze resultaten om twee praktische problemen op te lossen: het ontwerpen van een constante translatie van de formatie met een gecontroleerde oriëntatie ten opzichte van het globale referentiestelsel; en het ontwerpen van een gewenste formatie voor een groep achtervolgers om een doelwit te omsluiten en te blijven volgen.

Door de simpele structuur van de hierboven genoemde 'volg'-parameters is het

ook mogelijk om de grootte van de formatie aan te sturen. Wij stellen een methode voor die gebaseerd is op gedistribueerde transformatie-parameters met als doel om de grootte aan te sturen van schaal-vrije formaties. Gecombineerd met de 'volg'-parameters is het mogelijk om tegelijkertijd zowel de gewenste beweging als de gewenste grootte van de formatie aan te sturen.

Als vierde hebben we de stabiliteit geanalyseerd van formatievorming met behulp van de gradiëntmethode van agenten met tweede-orde dynamica onder invloed van onnauwkeurige metingen. We laten zien dat de meetfouten in de eerste-orde en tweede-orde systemen precies dezelfde ongewenste consequenties hebben. Uiteindelijk passen we de gedistribueerde 'volg'-parameters ook toe op de algoritmes gebaseerd op schatters en volgsystemen voor de tweede-orde dynamische systemen.

Door het hele proefschrift heen laten we middels praktische experimenten met mobiele robots zien hoe de ontwikkelde algoritmes werken in het geval van eerste-orde dynamica. Daarnaast hebben we een reeks volgsystemen ontwikkeld voor quadrocopters om de algoritmes gebaseerd op schatters en de 'volg'-transformatie-algoritmes te valideren voor tweede-orde dynamische systemen.